X-RAY DIFFRACTION STUDIES OF STABLE AND SUPERCOOLED LIQUID GALLIUM

Thesis by

Sergio Enrique Rodriguez

In Partial Fulfillment of the Requirements

For the Degree of

Doctor of Philosophy

California Institute of Technology

Pasadena, California

1964

(Submitted May 28, 1964)

ACKNOWLEDGEMENT

Mr. Roger W. Caputi, fellow graduate student, collaborated fully in designing, constructing, and/or disciplining the experimental equipment used in this investigation.

Professor C. J. Pings encouraged me to resume my formal education and participate in this research. His patient support of my endeavors has been monumental.

I received financial assistance from the National Science Foundation and the California Institute of Technology.

Thank you, JoAnn.

ABSTRACT

X-ray diffraction studies of stable and supercooled liquid gallium (m.p. 29.8°C.) between 0 and 50 °C. show no important dependence of internal structure on temperature. Atomic radial distribution functions were determined for 0, 10, 20, 29.5, 30, 40, and 50 °C. from diffraction data to S = 11 Å^{-1}. Diffraction data was obtained in reflection geometry with Ag K-alpha radiation, scintillation counter, and pulse-height analyzer. The sample was contained in a sealed plastic cell with transparent walls. A supporting assembly provided temperature control within 0.1°C. and a transparent plastic X-ray window which permitted visual inspection of the sample surface. Arguments are presented in favor of normalizing scattered intensities to independent scattered intensity at high S values. The method of inversion is based on a single, piecewise polynomial approximation to the scattering function i(S) for each temperature.

CONTENTS

INTRODUCTION

This investigation traced the structure of a liquid phase from temperatures above the melting point into the metastable supercooled state. The structural characteristics of liquids near points of phase transition, particularly the melting point, are of special importance to the general understanding of the liquid state. Most molecular theories or models for liquids speculate on the similarity of the liquid state to the solid or gaseous states of matter. The comparisons arise because both solids and gases yield to fundamental interpretations as completely regular or disordered molecular aggregations, while ordinary liquids, resembling solids for high internal cohesion and gases for lack of rigidity, seem to require an intermediate description. In 1934 Andrade(1) visualized liquids near the melting point as collections of crystalline groupings; in 1958 Eyring(2) proposed identifying solid-like and gas-like structures in a liquid. It appears that the liquid state has continued to elude a distinctive description, if one exists. For ordinary liquids, identification with the solid state is perhaps the stronger because the change in such properties as density and energy content is relatively smaller for melting than for vaporization. This circumstance, for instance, has led to a

variety of lattice models for the liquid state in which each molecule is confined to a small volume as it would be in the solid. Therefore, studies of liquid behavior near the melting point are specially significant. In the case of liquid structure it is conceivable that substantial changes occur as the liquid passes into the unstable supercooled region. The structure of the supercooled phase may be more solid-like than that of the stable phase, or show a different temperature dependence. These possibilities were investigated here by determining the structure of liquid gallium, which melts near 30°C., in the temperature range from 0°C. to 50°C.

Liquid structure means, in this case, the description of molecular configuration which is obtained by interpreting the scattering of X rays from the phase of interest. Such interpretations of scattered X rays, neutrons, or electrons constitute the most direct experimental measure of anything which may be called liquid structure. The description obtained is in terms of a radial density distribution which yields the number of molecules as a function of distance from any reference molecule on a time and space average. It is readily appreciated that such a function does not constitute a complete description of structure. Rather, because of the averaging process, it is of a statistical nature, intermediate between a detailed microscopic and a macroscopic description of the fluid. The radial

distribution tells which intermolecular distances are preferred in the liquid but not how this preference came about, that is, what regions of space or extents of time may be occupied by gas-like or solid-like structures. For the understanding of equilibrium properties the gross description seems wholly adequate but for visualizing transport properties the more detailed description would seem necessary.

The metal gallium presents a convenient opportunity for the investigation of a liquid phase above the melting point and in the supercooled condition. The metal melts at about 29.8°C.(3), just above room temperature, and supercools readily. Turnbull(4) supercooled "bulk" specimens of gallium to about -25°C.; Briggs (5) supercooled "small" drops of gallium to -28°C.; Defrain(6) supercooled 6-gram (1 cc) masses of gallium cleaned with hydrochloric acid to -40°C. and untreated samples to as low as -22°C. This extreme willingness to supercool in comparison to other metals is ascribed to the peculiar structure of gallium in the solid state. Gallium crystallizes to a complex, open structure (7) considerably different from the close-packed structure of most other metals(8). From one point of view(9)(10), the arrangement of atoms in most liquid metals approximates a close-packed structure and the transition to a significantly-different arrangement such as that of crystalline gallium would be difficult, thus providing for the tendency to supercool. Turnbull(5,10)

defends the theory that freezing is ordinarily catalyzed by foreign particles and that such accidental catalysts are likely to be cubic or hexagonal in structure, thus promoting the freezing of most metals rather than that of gallium. The experimental basis for this opinion is that many metals can be supercooled extensively by subdividing the liquid so that a substantial portion is relatively free of nucleation catalysts. Either way, the reason for this outstanding property of gallium lies with its crystalline structure. However, from the point of view of heterogeneous nucleation any liquid metal could be studied in the supercooled region. The advantage of gallium lies not so much with a unique physical property as in minimizing complexity of the experimental conditions required. Ease of supercooling may not be the only outstanding effect of complex crystalline structure on the solid-liquid transition of gallium. A study of the melting of gallium(12) indicated that melting does not occur sharply but extends over a temperature range of perhaps $0.1^{\circ}C.$ in a manner which could be associated with the crystalline structure.

The choice of a specific substance for the study of liquid structure limits the general significance of the results to liquids in the same class, in this case the liquid metals. From the comments above, gallium may not even be a representative member of the class of liquid metals. On the other hand, results

of liquid structure determinations to date indicate considerable uniformity for metals in their liquid state. Gallium itself, due probably to the convenient melting point, was included in a pioneer experiment by Menke(13) on the determination of liquid structure by X-ray diffraction. Subsequently, liquid structure has been determined by diffraction methods for many metals(14)(15). Most of these determinations included one or two temperatures somewhat above the melting point of the substance. Recent determinations such as that of Kruh(16) on mercury and Furukawa(17) on tin have included a sequence of temperatures above the melting point, thus showing the effect of temperature on structure.

The interpretation of some of these results placed considerable emphasis on similarities between spacings and coordination numbers indicated by the liquid structure and the corresponding values for the crystal. In summary(18) such correlations seem to hold for the close-packed metals but fail for metals having complex crystal structure such as bismuth, antimony, and gallium. These loose-packed or open structures collapse on melting to give higher coordination and the density increases. For example, gallium which may be assigned a coordination of seven in the crystal is said to have eleven nearest neighbors in the liquid(19), while silver changes coordination from twelve to ten neighbors upon melting(20). This alteration in structure has been related (18)(21) to changes in other properties such as thermal and

electrical conductivities which are said to increase on melting for the loose-packed metals, again in contrast with the behavior of the close-packed metals. This last extension of the argument may not be appropriate unless the possibility of anisotropic properties in the solid is taken into account. For gallium, Powell(22) determined a considerable anisotropy in the crystalline conductivities. If this anisotropy is taken into account by presuming a polycrystalline solid, the electrical conductivity is then found to decrease on melting as with most metals. However, it may still be advanced that, where structure is concerned, the metals tend toward similarity on melting. This fact alone may be a substantial clue as to the essentially different nature of the liquid state.

In contrast to what may be supposed there are no extensive studies on the dependence of equilibrium or transport properties of liquid gallium on temperature near and below the melting point. Spells(23) determined the viscosity from the melting point up to 1100^{o}C. However, no particular attention was paid to the behavior close to the melting point, while the supercooled region was deliberately avoided in view of the danger to the experimental device from the expansion of gallium upon freezing. Accurate data on properties like viscosity near the melting point can be of value in deciphering liquid structure. Measurements(24) on the continuity of properties through the freezing point for

various liquids led to the conclusion that molecular aggregations must occur in supercooled liquids. The viscosity of tin near the freezing point was interpreted(25) in terms of the existence of aggregates or clusters of atoms. Such interpretations do not imply anticipation of the freezing phenomenon since the configurations of aggregates which may be present in the liquid need not correspond to the crystal structure of the solid. Neither would the presence of these aggregates be refuted by an "uncrystalline" radial density distribution as the latter is but a time and space average which could come about through a large variety of detailed behavior.

Since the analysis which relates the scattering of X rays to liquid structure has been given by a number of authors(26)(27), only a summary need be presented here. It is possible to describe the scattering in terms of the distribution of electrons, atoms, molecules, or any other aggregate which is presumed or known to exist as a unit in the liquid phase. For the case at hand, the basic scattering unit may be taken as an atom. If it is assumed that the scattering properties of an individual atom are always the same, regardless of the state of aggregation, the choice of an atom as the unit of interest is immaterial to the correctness of the analysis. A scattering parameter and a scattering function are defined by

$$S = 4\pi \frac{\sin\theta}{\lambda} \qquad (1)$$

$$i(S) = \frac{(I_{coh}/NI_o) - f^2}{f^2} \qquad (2)$$

2θ is the angle between the incident X-ray beam and the direction along which scattered radiation is observed. λ is the wavelength of the incident radiation. I_{coh} is the coherent intensity scattered by the liquid, i.e. the scattering which occurs without change in wavelength. I_o is the incident intensity. N is the number of atoms which are scattering. f is the atomic scattering factor which already accounts for the interference effects of electron distribution within the atom. The term f^2 gives the coherent intensity scattered by an independent atom in a dimensionless "electron unit" the scattering by a classical electron per unit intensity of the same incident radiation. Its use in equation (2) implies that the individual atoms in the liquid perform as when they are alone. The scattering function i(S) represents the scattering per atom due to interactions among atoms, that is, in excess of f^2, expressed in terms of this independent scatter.

The scattering function may be related to the distribution of atoms in the liquid by

$$i(S) = \int_0^\infty 4\pi R^2 [\rho(R) - \rho_o] \frac{\sin(SR)}{SR} \, dR \qquad (3)$$

$\rho(R)$ is the average density of other atoms at radius R from any arbitrarily chosen reference atom. ρ_o is the macroscopic or average over-all density of the liquid. The term $\frac{\sin(SR)}{SR}$ of the integrand in equation (3) represents the interference portion of the scattering by two atoms separated by distance R if the pair thus formed assumes all possible orientations with respect to the primary beam with equal probability. Except for the presence of the macroscopic density ρ_o, the integral of (3) is simply a summation of pair interactions for the reference atom. It can be shown(26) that the introduction of the density ρ_o has no appreciable effect on the scattering function defined by (3) except at extremely small angles which are not ordinarily accessible to the experiment. Conversely, the scattering function in (3) is incorrect to the extent of an integral which represents scattering from the entire specimen as a unit and is negligible in the experimental range of interest.

The integral limit of equation (3) extends to infinity on the premise that the local neighbor density $\rho(R)$ approaches the average density ρ_o at large values of R owing to the absence of long-range order in the liquid. It is then possible to apply the Fourier integral theorem and obtain the density distribution as an inversion of the scattering function

$$4\pi R\left[\rho(R)-\rho_o\right] = \frac{2}{\pi}\int_0^{S_m} Si(S)\sin(RS)\,dS \qquad (4)$$

The integral limit in equation (4) is S_m rather than infinity because the typical experiment cannot approach infinite values of the scattering parameter S. Therefore, the integration is carried out to the highest significant value available, thus introducing a truncation error in the resulting radial density distribution.

Granted the validity of the assumptions which lead to these relations, there is only one radial distribution which can be obtained within given experimental limits. However, the outright inversion given by equation (4) is not the only way of deducing radial distribution from the scattering data. From equation (3) or a similar relation for the scattered intensity a direct interpretative approach could be taken in which suitable combination of density and radius are sought to satisfy the scattering behavior. Such an approach gives greater range to the imagination and permits more varied conclusions to be drawn from the data. However, an entire continuum of frequencies contributes to the observed scattering function. It cannot be reasonably expected that a likely interpretation does represent the complete interaction of frequencies involved.

In the early work by Menke(13) gallium was studied at 18°C. and at 45°C. Significant differences were observed in the scattering functions for these two temperatures which upon inversion led to entirely similar radial distributions. Hendus(19) exper-

imented on gallium at only 20°C., the results showing broad agreement with those previously obtained by Menke. An interesting feature of the scattering function i(S) in both studies is the asymmetry of the first and largest scattering maximum which shows a hump or shoulder on the high-angle side. The review article by Furukawa(14) refers to unpublished work which also indicates the existence of this distortion. In a direct interpretation of structure from equation (3) this feature of the scattering function suggests specially close neighbors. However, the radial distributions obtained by complete inversion do not show such neighbors distinctly, the distance in question falling within the first broad coordination shell. With regard to supercooling, an investigation similar to the present one was carried out by Dorsch and Bemrose(28) on water. From direct interpretation of the data it was concluded that the structure of supercooled water became progressively more ice-like as the temperature was lowered. No complete inversions were calculated.

EXPERIMENTAL

General

A basic consideration in the design of the scattering experiment involves the geometrical relationship of the sample to the incident beam and the directions in which scatter will be measured. With respect to the fundamental scattering process described by equations (2) and (3) the geometry is of no significance. However, the reduction of experimental scattering to the intensity in the scattering function requires a series of corrections, as for sample absorption and scattering by sample enclosure. The experimental arrangement has to take into account how these corrections are to be carried out and what effect they will have on the accuracy of the results. For liquids in general there are two basic geometries for the measurement of X-ray scattering, a "reflection" method in which the incident and scattered rays are on the same side of a liquid surface, a "transmission" method in which the scattering is observed on the generally opposite side of the sample from the incident beam.

In the case of metals, which are mostly strong absorbers for the usual incident frequencies, the reflection method amounts to scattering from a liquid layer on the order of 0.001 inches thick since the incident radiation has been almost completely

absorbed in passing to this depth. For many gross purposes such a layer amounts to a surface but from the molecular viewpoint it is sufficiently thick to represent conditions in the bulk phase. It follows that a reflection type of experiment can be undertaken from a free surface of the liquid which, by suitable design of experimental conditions, can be made the only contributor to the observed scattering. On the other hand, in the case of the transmission method, a sufficiently thin sample of the metal must be contained within the scattering area. A portion of the observed scattering corresponds then to the sample enclosure and must be eliminated by correction. The possibility of avoiding such a correction in the reflection method is a highly significant advantage which has led to its adoption by most investigators of metals. An exception is the work of Muller and Hendus(29) on antimony using relatively hard tungsten radiation.

Disadvantages of the reflection method lie with the necessity of controlling the position of a free liquid surface, freeing it of lower-density impurities, and correcting for scatter from the vapor above the surface. This last factor was of no importance in the case of gallium which has an entirely negligible vapor pressure at the temperatures of interest. According to Speiser and Johnston(30) the vapor pressure of gallium is but 0.001 mm Hg at 1000°C. On the other hand, the

hardest available radiation was silver K-alpha and expansion of gallium on freezing presented the danger of damaging a thin-walled container suitable for the transmission technique. Hence, the reflection method was selected.

Experimental measurements were carried out on a Norelco X-ray diffractometer(34) with fixed X-ray source. Scattered radiation was measured by means of a movable scintillation counter mounted on a Norelco goniometer. A schematic diagram of the reflection geometry is shown in Figure 1. The liquid surface coincides with the goniometer axis. A slit in front of the X-ray source determines an incident beam which makes a relatively shallow angle with the surface. Scatter slits ahead of the counter define the scattered beam to be measured. This combination rotates about the goniometer axis, thus determining various scattering angles 2θ in the vertical plane. Both incident and scattered beams are collimated in the axial direction by Soller slits. Scattered power at each angular position is determined from the number of counts registered in a given time or viceversa.

The primary radiation was silver K-alpha (0.561Å) provided by a Norelco (32118) X-ray tube operated at about 40 kilovolts and 11 to 13 milliamperes. The high-voltage generator was powered by a Norelco (42232) Voltage Regulator having a rated stability of 0.05%. The original intent was to use molybdenum

K-alpha (0.711Å) radiation which allows reaching a sufficiently-low value of the scattering parameter S at a larger angle of scatter than silver K-alpha. This consideration is fairly important in the reflection method because small angles of scatter require small angles of incident and scattered rays with the liquid surface. The possibility of error due to misalignment increases as these angles become shallower. However, molybdenum radiation was not used because the fluorescence radiation excited from the gallium dominated the scattered radiation and could not be successfully eliminated. The basic reason for this difficulty lies with the poor energy discrimination of the scintillation counter. Even with the beta filter and additional aluminum filters ahead of the counter, it was impossible to discriminate sufficiently against the softer fluorescence radiation. The fluorescence is also excited in the case of silver K-alpha radiation but, with the shorter primary wavelength, the unwanted radiation is essentially eliminated by the filtering action of the gallium itself and the beta filter ahead of the counter.

Sample containment

The experimental assembly described below consists of two main parts, an inner cell which actually contains the gallium and an outer jacket which provides support and temperature control. The inner cell has the manifold functions of providing for control

of the liquid level, maintaining the pure gallium under sealed conditions, permitting visual observation of the liquid surface, and providing for the low-absorption passage of incident and scattered radiation. The design and features of this cell have been reported in the literature(31); some details of construction are shown in Figure 2. The cell is basically a hollow cylinder about an inch in diameter and three-quarters inch long made from methyl-methacrylate plastic (Lucite or Plexiglas). The plastic material was chosen for several reasons. In the first place, gallium reportedly alloys with most ordinary metals (3)(32). Secondly, the plastic is a remarkably competent material which is easily machined providing simultaneously for mechanical strength and transparency to X rays. For example, the thin (0.008 inch) window of this cell, which does not represent a lower limit, has a transmission of about 95% for molybdenum radiation and 99% for silver radiation.

Finally, the window can be made optically transparent by polishing, thus permitting inspection of the liquid surface. The principal contamination to be expected is the formation of the oxide which causes the surface of gallium to lose its characteristic brightness in favor of a dull grayish appearance. In its oxidation behavior the metal resembles aluminum(33) forming a very thin layer of the oxide which then prevents further contamination. If such a layer is truly of molecular thickness,

it would not interfere appreciably with the scattering behavior of the sample. Thus, an adequate sample could be presumed from taking sufficient precautions in the initial loading. Visual inspection serves to certify that a clean surface does obtain during the course of an experiment.

An obvious drawback of the plastic material for general purposes is that it cannot withstand high temperatures as it begins to soften at about 70°C. However, the range of temperatures considered for this experiment were below this point. As far as cooling of the plastic is concerned, there seem to be no serious limitations.

As seen in Figure 2, one end of the cell contains an eccentric cylindrical well of approximately the same length and half the diameter of the main cell reservoir. The purpose of this well is to provide the necessary amount of control over the position of the liquid level. In its operating position the axis of the cell is aligned with the horizontal axis of the goniometer and the cell and eccentric well are approximately half-full of the liquid. A rotation of the cell away from this central position will cause liquid to flow into or out of the well, thus lowering or raising the level of the liquid in the main part. With the dimensions given and the cell approximately half-full, almost 0.002 inches of change in level are obtained per degree of rotation which is adequate to adjust the surface

to the goniometer axis. At the opposite end of the cylindrical cell a filling hole is provided. This passage terminates with a tubing extension which is used to effect a vacuum seal once the cell has been loaded.

The entire cell is constructed of three pieces of the plastic. Two of these comprise the cell itself and are shoulder-joined as shown in Figure 2. The third is the tubing extension which is butted onto the end of the cell. These joints were bonded with ethylene dichloride solvent. The pieces for the main body of the cell are machined from cast rod, the filling extension is commercial 3/8-inch o.d. tubing which was found to give a better vacuum seal by heating than a comparable piece bored from cast material.

Figure 2 shows that the exterior of the cell at the edges of the central thin wall or X-ray window is finished in a series of two steps. The inner of these gives the thin, polished window some protection against accidental scratches. The higher steps serve for seating split brass rings which limit and define the width of the working beams. The actual operating region is only about 0.45 inches along the axis of the goniometer as indicated in the figure.

External assembly

The features of the external or supporting part of the experimental arrangement are shown in Figure 3, a vertical section along the axis of the goniometer, and in Figures 4 and 5, photographs of the complete assembly mounted on the goniometer. This outer shell of equipment provides a centering support for the inner cell, cooling by fluid circulation and electrical heating, and a vacuum space between the X-ray window (W_2 in Figure 3) of the inner cell and an outer X-ray window (W_1). This space has the dual purpose of giving insulation and preventing the condensation of moisture along the path of radiation at the colder temperatures. This jacket was also constructed almost entirely of the plastic which provided thermal compatibility with the inner cell and a favorable combination of strength and weight. The entire assembly could be held on a single shaft running through the center of the goniometer.

In order to keep the main experimental area clear, the inlet and outlet (CC) of the cooling jacket are both on the side away from the goniometer. The flow of the coolant is asymmetric, the fluid passing to the other side of the window and returning to the outlet via passages (CP) which are located just below the inner cell. The heater wire is wound onto two separate sleeves (HS) which slip over either end of the inner cell. These two sections are series-connected, also below the window of the inner

cell, by means of springs which fit over taper pins forced into the edges of the heater sleeves. In this manner the coolant-fluid and heater-wire crossover connections within the jacket do not interfere with the useful angular range.

The principal structural units of this jacket are the outer shell (S) pieces on either side of the X-ray window region. These are thick plastic rings partly hollowed by a series of holes parallel to the axis. The units fit snuggly around the cooling jacket and are internally fluted to provide for pumping out and decrease friction in assembly and thermal conduction while still providing rigid centering. Between these end pieces is the outer X-ray window (W_1), a plastic hoop about 0.018 inches thick and 4 inches in diameter with heavier edges which fit closely over the end pieces(S). The thin or window portion is uniform within 0.001 inches over the entire circumference so that there is no significant change in transmission with scattering angle. This outer window is also polished on both sides to transparency so that the sample may be inspected without dismounting the assembly. The overall transmission of both inner and outer X-ray windows is about 89% for molybdenum K-alpha radiation and about 96% for silver K-alpha radiation.

At their ends away from the X-ray window the two outer sections (S) fit into accurately recessed plates of larger diameter. One of these (P_1) is used to bolt the entire unit onto a brass

hub which is in turn mounted on a shaft passing along the goniometer axis. The vacuum seal between these plates and the shell pieces is effected by O-rings. The seal between the latter and the X-ray window is obtained by applying high-vacuum grease along the shoulder joint. The end plate (P_2) on the side away from the goniometer has a central opening which admits the cooling jacket. A second plate (P_3) with a hub provides coolant inlet and outlet connections (CC) and a vacuum connection (VC) at right angles to the goniometer axis. This plate also seats against an O-ring and leaves a central opening sufficient for the inner cell and heater sleeves. Vacuum closure of this entry is provided by a smaller plate (P_4) and O-ring. Through this final plate are led the external electrical connections by means of tight-fitting taper pins (E_2), and the thermocouple wires through a small-diameter hole (E_1) packed with grease. In operation the entire affair is held together by atmospheric pressure when the vacuum is established. Under these conditions the plastic hoop which forms the outer X-ray window supports a total load of some three-hundred pounds in addition to atmospheric pressure in the radial direction.

Figure 4 is a photograph of the diffractometer arrangement showing the X-ray tube turret at the left and counter arm on the right of the sample assembly. The coolant lines are not shown but the jacket connections may be seen at the upper near

end. The thermocouple, heater, and vacuum leads to the jacket can be seen. The springs hooked to the edges of the flanges (P_1 and P_2) provide temporary support when the vacuum is not operational. Figure 5 was taken from the counter side, looking downward at the sample area. The slot which passes radiation to and from the sample, the inner cell and sample, and other details are seen through the outer window of the jacket. As these photographs show, the sample assembly is a fairly compact unit mounted entirely on the goniometer. It is easily rotated for adjustment of the liquid level. The entire unit can be removed from the goniometer, as for alignment checks, without disturbing the connections or the internal arrangement.

Temperature

The principal measuring thermocouple is copper-constantan mounted on a thin, curved copper plate which fits snuggly to the underside of the thin-shelled inner cell. This arrangement provides for a relatively large conducting area across the thin but poorly conducting plastic. Since the surface temperature is of primary interest, calibrating runs were made against thermocouples which actually dipped into the surface of a mercury sample. The difference between the central surface and underside thermocouple increased monotonically with the difference between room and cell temperatures. At -10^{o}C. the

surface temperature was about 0.1°C. higher than that recorded at the outer plate. Variations in temperature at the surface were estimated from the readings of two surface thermocouples. For all temperatures of interest, the temperature was uniform within 0.05°C. across the entire surface. For gallium which has greater thermal conductivity than mercury(5) the corrections were proportionately decreased. A distilled-water-ice bath monitored by a resistance thermometer was used as thermocouple reference. Measurements of emf were made with a Leeds and Northrup Wenner potentiometer.

Temperatures below room conditions were obtained by circulating cold nitrogen gas to cool the cell some 5°C. below the desired point and then warming with the electric heater. Temperatures above room conditions were reached with the heater alone. For temperature control the heater was operated by a Leeds and Northrup C.A.T. Control unit. The controlling signal for this unit was the difference between the cell thermocouple and an adequately-set reference emf provided by mercury batteries and divider circuit having drift of less than one microvolt per day. The experimental temperatures were constant within 0.05°C., and the reported surface temperatures are believed significant within ±0.10°C.

Gallium sample

After assembly of the inner cell all internal surfaces were thoroughly scoured and cleaned and the cell was then kept in a vacuum desiccator for an extended period of time. Immediately prior to filling, a vacuum of less than one micron was maintained in the cell for over a day. This procedure was followed to clean the inside surfaces from absorbed oxygen and water which would tend to oxidize the gallium after loading the cell. In the filling procedure the end of the filling tube was provided with a plastic three-way stopcock which allowed for either maintaining the cell under vacuum or allowing gallium to flow down from a temporary storage vessel above the cell. An excess of gallium was melted and allowed to stand warm in this upper container for a period of about an hour with the intention of floating oxides or other matter to the top of the liquid. The required amount of gallium was then allowed to flow down into the cell. Pumping on the cell was resumed and a vacuum seal effected at the filling tube by slowly warming a short section with a small heating coil until the tube collapsed.

Gallium samples of 99.9999% purity were obtained from the Aluminum Company of America. Two cells were filled in the manner described with approximately 32 grams (5.3 cc) of gallium which, allowing for the curvature of the liquid surface near

the walls, was sufficient to fill this cell to the axis. Preliminary runs for each of these cells at about the melting point of gallium indicated that the diffracted intensity pattern was essentially the same for both. In subsequent work, however, only one of these samples was utilized as the vacuum seal on the other was believed to be, and eventually proved to be, defective.

Upon first loading a cell the clean gallium does not wet the clean plastic and a very pronounced surface curvature is obtained near the cell walls. After weeks of residence in the cell, small amounts of oxide or some other impurity were observed on the surface of the gallium. This material collected near the cell walls, leaving the center free and clean so that subsequent diffraction would not be affected. Owing to this contamination and/or allowing the cell to remain undisturbed for some time, the gallium tended to wet the walls more, thus flattening the surface to some extent and making its curvature a less-critical consideration. This wetting phenomenon may agree with the observation of Boyer(35) and Briggs(5) who concluded that wetting of glass and other surfaces by gallium was due to formation of the oxide.

Supercooling tests on the gallium revealed a pronounced "thermal-history" effect, that is, the amount of supercooling obtainable depended on the highest temperature reached since

the last occurrence of freezing. A considerable increase in the extent of supercooling was obtained by prewarming the metal to about 45 or 50°C., but warming beyond this point, to about 60°C., did not significantly decrease the lowest temperature attainable in the liquid form. This behavior agrees with an observation by Turnbull(36) that for a gallium sample the thermal history effects were not significant beyond warming to some 20°C. above the melting point. The lowest temperature reached in repeated supercooling attempts was -5°C., rather than the anticipated -20°C.(4)(5)(6). On the heterogeneous-nucleation viewpoint of the freezing phenomenon, this limitation of the supercooled range could have resulted from the large volume of the sample or the microscopic character of the cell wall(10).

During the course of these tests an attempt was made to measure the actual melting point of the sample in the cell as permitted by the available thermocouple system. The technique consisted of inducing the gallium to freeze and, while freezing was in progress, minimizing the temperature difference between the thermocouple underneath the sample and a thermocouple recording the temperature of the plastic near the sample. The stable temperature thus recorded by the gallium-sensing thermocouple was then a reasonable estimate of the melting point. The value obtained was 29.8°C. which agrees well with published values for the expected accuracy of this measurement. This

result provided simultaneous evidence for the identity and condition of the gallium and reliability of the thermocouple system.

Alignment

The alignment of the goniometer to obtain a 0^{o} reference line followed the standard procedure given by the manufacturer. The sample to X-ray anode and sample to scatter slit distances, not critical in this experiment, were respectively 7.0 and 6.1 inches. The angle α between the incident beam and the horizontal was measured with the aid of the parafocusing system of the goniometer. A bubble level was placed on a flat steel bar held on the powder specimen holder of the goniometer. With the bar horizontal as indicated by the level, the diffraction angle read by the goniometer corresponds to twice the desired angle. The procedure was repeated with various reversals of the steel bar and bubble level to average out their imperfections. The angle of incidence was $4.80 \pm .02^{o}$. The absolute value is of no special significance provided it is sufficiently small to permit reaching the desired lowest angle of scatter. The height of the slit defining the incident beam was 0.045 inches so that the incident beam extension on the horizontal plane was somewhat greater than the inner-cell diameter, thus irradiating the entire sample surface.

Centering of the liquid level was based on the following principles. The intersection of the incident beam and the beam defined by the scatter slits determine the volume within the inner cell which can contribute to the scattering. As the liquid level is raised or lowered, the scattering volume will move into the liquid or into the space above the liquid. Either way, scattered intensity decreases so that a maximum is observed with the liquid near the central position. The sharpness of this maximum depends on the relative height of the beams. This test was repeated many times with various slit combinations and at various scattering angles. A setting of particular interest was $2\theta = 9.6^{o}$, twice the angle of incidence, where both beams make the same angle with the horizontal and the effects of surface curvature are balanced.

In performing these tests sufficient time had to be allowed to insure a stable surface at each setting. Due to variable wetting of the cell wall, the gallium was sluggish in reaching equilibrium. Temporary bulging of the surface can lead to false intensity maxima and hysteresis effects as the surface is made to rise and fall by rotating the cell assembly. In repeated settings the position of the level was generally reproducible within about 5^{o} of rotation corresponding to about ± 0.005 inches uncertainty in the vertical position of the surface.

Experimental corrections

Having established the experimental geometry and radiation, the experimental scatter may be related to the coherent intensity which is necessary for the evaluation of the scattering function in equation (2). The problem is twofold. In the first place, correction must be applied for all experimental factors which differ from the basic scattering process described by equations (2) and (3). Secondly, the conerent intensity thus obtained must be expressed in the intensity units of the independent scatter term f^2 in order to form the scattering function. This last requirement is a problem of normalization which will be taken up in discussing the analysis of data. That is, having established all other necessary corrections, the coherent intensity is left related to the experimental power up to one unknown constant factor.

The necessary experimental corrections are common to most X-ray diffraction investigations. The simplest of these is for background signal or observed counting rate when no scatter is being measured. This amounts to a subtraction from all scattering signals and is not related to the scattering experiment itself but rather to the detecting system. The other corrections arise from the geometry of the experimental situation and are dependent on the angle of scattering. There is an absorption correction required by the fact that for any volume element of

the liquid the total path through the liquid of incident and scattered radiation depends on the angle of observation. Qualitatively, the smaller the scattering angle, the longer the path through the liquid and stronger the absorption. Another correction which could be termed for "field of view" relates to the amount of the liquid which can contribute scattering into the counter at any particular angle. The scatter slits define a beam which takes in decreasing amounts of the liquid surface as the angle of observation increases. Finally, there is the usual polarization correction. Assuming a completely unpolarized incident beam, the electric field components in the scattering plane, i.e. normal to the goniometer axis, contribute decreasingly to the scattered intensity as the angle of observation increases.

These effects do not describe all the experimental deviations. In addition, a portion of the observed scatter will be incoherent or Compton modified radiation which produces no interference effects and is scattered at reduced energies. Owing to this angle-dependent decrease in energy, all absorption effects occurring after the scattering process discriminate against the modified scatter. Corresponding adjustments must be made on the corrections which apply to coherent scattering. Lastly, the modified scatter is subject to the usual Breit-Dirac correction for electron recoil.

The necessary expressions for these corrections are derived and discussed in Appendix I. Required experimental values are given in Table I. In summary, the coherent intensity may be related to the experimental scattered power as follows:

$$\frac{I_{coh}}{NI_o} = AE_{XC} - F_{MC} \tag{5}$$

A, defined by equation (I-11) of Appendix I in terms of experimental parameters, is the normalizing factor to be discussed later. E_{XC} is a corrected experimental power given by

$$E_{XC} = \frac{\sin\alpha' + \sin\varphi}{1+\cos^2 2\theta} (E_X - E_B) \tag{6}$$

where 2θ is the scattering angle, α' is the angle of incidence to the surface, $\varphi = (2\theta - \alpha')$ is the angle of the scattered beam with the surface. E_X is the actual experimental measurement of counting rate, and E_B is the background signal. F_{MC} is a corrected modified scatter per atom given by

$$F_{MC} = \frac{F_M}{B^2} \frac{\sin\alpha + \sin\varphi}{B^a \sin\alpha + \sin\varphi} e^{-(B^b-1)\mu_D t} \tag{7}$$

F_M is the independent modified scatter per atom. B is the ratio of modified to incident wavelength given by equation (I-14) of Appendix I in terms of angle and incident wavelength. The con-

stant exponents a and b of B yield the ratios of modified to incident absorption coefficients for the sample and beta filter respectively, $\mu_D t$ is the product of primary absorption coefficient and thickness for the filter.

All factors of F_M in equation (7) represent relative reductions in the observed modified scatter, and all decrease with angle from unity at 0^o. The factor $1/B^2$ is the Breit-Dirac correction, the trigonometric ratio represents the adjustment for sample absorption, and the exponential term represents absorption discrimination at the beta filter which, for the radiation utilized, is the only important absorber in the path of scattering to the counter crystal. The over-all importance of these corrections depends on the relative magnitudes of coherent and modified scatter. For silver K-alpha primary radiation and $2\theta = 60^o$ which was the useful experimental limit, the Breit-Dirac correction amounts to 0.5% of the coherent scatter, the sample absorption to 0.2%, and the filter absorption to 1.8%. Thus, the filter effect was most important, while discrimination by the sample is relatively negligible and was included for generality. Since the effect of all these corrections is generally small, it is not necessary that they be established very accurately.

Departures from ideality resulting from surface oscillations and curvature, angular beam apertures, and misalignment of the

liquid surface are discussed in Appendix I. These lead mainly to errors in the corrections for sample absorption and field of view which are strongly dependent on the beam angles with the surface of the liquid. The angular amplitude of surface oscillations was estimated from the reflection of a light beam by a mercury sample mounted on the goniometer. These oscillations were on the order of tenths of one degree and did not provide a significant effect. The extent of deviation from the horizontal due to surface curvature was estimated analytically. Curvature effects were made negligible by limiting the maximum length (across the goniometer axis) of the scattering surface contained by the scattered beam to about 0.3 inches. With this restricted scattering length, the effective angular spread of the beams gives negligible correction deviations.

The principal possibility of error is in setting the liquid surface to the goniometer axis. A deviation introduces a correction error which is most important at high angles where sample absorption is lowest and chiefly determined by the shallow angle of incidence to the surface. For the estimated uncertainty of $\pm$ 0.005 inches in the vertical position of the surface, the error is about 1% at large angles.

Scatter detection

Scattered radiation was detected by means of a scintillation counter and pulse-height analyzer combination. The required high-voltage supply, amplifier, analyzer, timer, counter, and printer were 8000 series units of the Nuclear Chicago Corporation. The detector itself was assembled in the laboratory using a Harshaw Type HG, 0.1-inch thick NaI(Tl) crystal, a Dumont 6291 multiplier phototube, a high-voltage cascade base constructed from circuit drawing B2-1845 of Philips Electronics Inc., and preamplifier unit made according to circuit drawing 2943 of Franklin Electronics Inc.

Considerable effort was expended in reducing the noise-counting rate of the counter to levels sufficiently low in comparison with the intensities to be measured. The desired performance was obtained through careful assembly of circuits, good electrical contacts and insulation in the high-voltage base of the phototube, and adequate electric and magnetic shielding of the phototube. For example, it was ascertained that a low noise level could not generally be obtained unless the pin base and receptacle of the phototube were very carefully cleaned of dirt and moisture. Electric shielding was provided by a suitably-grounded copper sheath around the phototube, and magnetic shielding by a Dumont Mumetal shield. The noise level was also reduced by providing lead-sheet shielding around the

periphery and front of the tube except for the minimal crystal area left open for counting. The noise level thus obtained appeared to be quite stable in the main but did drift on occasion to higher stable values which were sometimes impractically high. It was found that low levels could usually be restored by reassembling the phototube to the high-voltage base. This area seems to be a surprisingly sensitive source of noise problems, the more precautions taken to protect it from contamination, the better the performance of the device. It is also possible that wind currents or temperature gradients created by the temperature control system of the laboratory contributed to erratic noise levels. At least, the stability was apparently aided by protecting the counter from this hazard. Investigation of these fairly low level noise effects is a time-consuming operation which could not be carried to completion. The reason is that noise-counting rates are subject to the usual statistical uncertainties and, since the counting rate is low by definition, it becomes impractical to amass sufficient counts for judging the effects of a particular alteration. Therefore, once a major reduction of the noise level had been achieved and this level was acceptable, the problem was not specifically pursued.

In addition to the basic noise of the scintillation counter, a number of other sources of background signal had to be eliminated. The use of isolation transformers on the entire counting

train eliminated counts associated with the use of other electrical equipment in the laboratory. Several key switches and relays used in the operation of automatic counting-cycle and goniometer-stepping devices had to be shielded or kept clean or protected by means of capacitors in parallel in order to prevent the introduction of spurious counts. The output pulse of the amplifier was carefully adjusted and periodically checked to insure that secondary pulsing would not make the analyzer accept counts of excessive energy. Another source of background signal is the incidental scatter from slit mountings and other parts of the goniometer. These were ferreted out by trial and error and eliminated through proper shielding of the detector. Still another source of unwanted signal are the "escape" counts(39) caused by high-energy quanta which lose a portion of their energy through fluorescence of iodine in the scintillator crystal and appear lower on the energy scale of the analyzer. These can only be controlled by limiting the maximum voltage of the X-ray tube.

Spectrum

The scintillation counter was operated at 700 volts with approximately 50,000X amplifier gain. Figure 5 gives the analyzer pulse amplitude distribution of scatter by gallium with silver K-alpha radiation and 0.003-inch palladium beta filter

in front of the counter. The angle of scatter is $2\theta = 12.75^{o}$ which corresponds approximately to the first intensity peak and gives a negligible modified-scatter component. The analyzer distribution conforms fairly well to the Gaussian which would be obtained for a pure K-alpha line(39). An operating window was chosen from 30 volts to 80 volts on the analyzer scale. This width permitted neglecting counting losses from energy displacement of the modified scatter. The background signal corresponding to this window was normally about 0.05 counts/second but did drift for some experimental runs to as much as 0.17 counts/second. For comparison, the weaker experimental signals were on the order of one count per second.

Figure 6 gives a LiF-crystal spectrum of the incident radiation with the 30-80 volt analyzer window. This semi-quantitative spectrum shows considerable radiation components on either side of the K-alpha lines centered at about 16.08^{o}. The long tail of softer radiation is filtered out by the gallium itself. The high-energy side is sharply limited by the absorption edge of the palladium beta filter. An estimated 50% of the scattered radiation will lie within ±1% of the central K-alpha energy and practically all within ±10%.

Measuring program

In addition to the natural decline in coherent intensity, the experimental deviations combine to reduce scatter considerably with increasing angle. The sample absorption effect, which favors scattering at the higher angles, is overcome by the decreasing field of view of the scattered beam. It was impractical to observe the entire angular range of interest with a fixed set of scatter slits as the time necessary for accurate counting became excessively large. Hence, a program of changing to larger scatter slits as the angle increased was adopted. The angle at which these slit changes could take place was partly determined by the available slit combinations and the beam height permitted by scattering-surface limitations previously discussed.

Table II gives a summary of the slit combinations used with the corresponding angular ranges, approximate relative powers, and angular resolutions. The program of slit changes amounts to a compromise between the intensity and resolution. The latter is favored since the angular breadth increases as the sum of slit heights whereas the power received increases with their product. Since the slits of the combinations are of comparable height, the power received by a combination is not uniform across the entire beam. The angular resolution given in Table II is the average between the total angular aperture and the aperture of the central region of uniform intensity.

The general features of the scattering functions are in agreement with this program since the sharper changes in intensity with angle, requiring the better resolution, will occur at the smaller angles. Furthermore, lack of monochromatization implies of itself a loss in resolution in terms of the scattering parameter S as this number increases. In view of the decreasing resolution, and the general disappearance of features in the scattering function with increasing angle, the angular increment between experimental points is also increased at each slit change as indicated in Table II.

Changes in the scatter slits imply a change in the normalizing constant applicable to each angular range. This is apparent in the definition of A given by equation (I-11) which includes as factors the average solid angle subtended at the surface of the sample. Hence, each modification of the scatter slits requires establishing a ratio between normalizing constants, that is, an internormalization which will adjust the intensity of the combinations to a common basis. Since the scatter slit settings are not exactly reproducible, each set at each temperature included a substantial angular overlap with the adjoining ranges, as shown by Table II, thus redetermining the adjusting ratio. There follows that the angular ranges of the various slit combinations need not be taken at the same incident intensity provided this intensity is steady for each range. The

incident intensity factor of the constant A then forms part of the internormalizing ratio.

The regions of overlap between slit combinations tend to match on total counts because the increasing slit size is accompanied by an increase in angular increment and hence fewer points. The general rule for computing the adjusting ratio for slit changes was to compare each point of the wider-spaced run with its angular counterpart and the average of the two adjoining points in the closer-spaced run. The exception to this rule was at the overlap of the first and second slit combinations where the smaller number of counts correspond also to the wider angular spacing and only the matching angles were compared. Correspondingly, in the analysis of data all points of an overlap are given equal weight excepting again the first overlap where only the points of the second run are used. In the overlap of fixed-time runs, the slit adjusting ratio was calculated by first adding the corrected intensities for the points in each run and then forming the ratio, thus weighting the points roughly according to number of counts. In the overlap of fixed-count runs the individual ratios were averaged, and in the overlap of fixed-time with fixed-count the average of both methods was utilized. These adjusting ratios do not appear as such in the analysis as they are logically absorbed into the different normalization constants A of the angular ranges.

Modification of the scatter slits is part of the larger issue of determining the counting times or counting cycles required to define the scattering function. This complex problem has no precise practical answer because of experimental limitations on slit dimensions, fixed count cycles, and time in general. The proper goal of the experiment is determining the scattering function i(S) with sufficient and uniform accuracy for the inversion given by equation (4). Since the entire scattering function i(S) participates in each inversion, its success is determined by the accuracy of the experimental points in combination with their spacing, i.e. by the curve-determining properties of the experimental points. Other factors being equal, the sharper features of the scattering function occurring at low angles demand closer point spacing and less individual accuracy than the almost-featureless region at high angles. The latter can only be measured accurately with poor resolution and yet is of particular importance for the normalization process. These considerations are in general agreement with the systematic changes in resolution and angular increment already discussed.

The principal counting error arises from the random distribution of the quanta in time(40). A given counting rate is only reproducible within a Gaussian distribution of standard deviation given approximately by the square root of the number

of counts recorded. For the primary purpose of obtaining the coherent intensity of the scattering function, this counting error is enlarged by the background correction, which also has a distributed error, and by the subtraction of the modified scatter contribution. Last but not least, any deviations in the scattering function are amplified by the factor S appearing in the inversion integral. The probable absolute error in the scattering function i(S) may be related to the principal counting error by

$$\Delta i(S) > \frac{0.67}{C^{\frac{1}{2}}} \left[1+i(S)\right] \qquad (8)$$

where C is the number of counts, the factor 0.67 corresponds to the 50% band of the Gaussian distribution, and the inequality comes from neglecting background and modified scatter in the right hand member. In the present case where background and modified scatter are not too large in relation to the coherent intensity, this expression yields a fair estimate of the effects of total counts on the definition of the scattering function.

It appears by inspection of equation (8) that the deviations of i(S) depend somewhat peculiarly on the magnitude of the function itself. A single fixed-count strategy, for example, would not provide for a uniform definition of the function. Where the i(S) function is changing rapidly, through the first and

perhaps the second maxima, the method of fixed-time counting would be more appropriate for uniform i(S) definition. In the lowest angular range where i(S) is near -1 few counts are required, while the increase at the first maximum can amplify the counting error twofold. Such considerations, plus the factor S of the inversion integral, were roughly taken into account in selecting the counting method summarized in Table II. In general, the first portions of the scattering function were obtained in fixed time and the latter portions in fixed count. Thus, the 10,000 counts provided near S = 10 Å^{-1}, in contrast to the 4,000 counts near S = 5 Å^{-1}, recognize the increasing importance of the factor S in the inversion. However, some 5,000 counts are still provided at S of only 2.5 Å^{-1} where the scattering function is large.

With the provision for internormalization, the angular ranges of Table II were not necessarily taken in sequence. X-ray generation was allowed to stabilize for at least one-half hour prior to scanning each range. Each scan was automatic; data printout after each counting cycle provided a signal which stepped the counter arm to its next position. A step programmer allowed for a variety of angular increments. The background signal was determined at the beginning and end of each scan. Ordinarily, the change in background was slight. In a few instances where the background increased to relatively high or

erratic counting rates the runs were discarded. In other cases showing significant increases, it could be ascertained from experience and observation that the change had occurred gradually while recording data. Background signal was assigned to each data point by linear interpolation on a point basis between the initial and final estimates.

Investigation

Diffracted intensity measurements were taken with the gallium at temperatures of 0.0, 10.0, 20.0, 29.5, 30.0, 40.0, and 50.0 ^{o}C. Almost exactly the same scanning plan was followed in all cases. Each temperature run took about three days to complete. The lowest temperature of supercooling which could be reached in several attempts was about -5^{o}C. No measurements were made below 0^{o}C. Tables V contain the counting data for the various angular ranges at each temperature. The first two columns give the angle of scatter 2θ and the counts or time recorded for the indicated counting mode. The background range applicable to each case is shown. The remaining columns of Tables V give the normalized, corrected total scatter AE_{XC} , coherent scatter I_{coh}/NI_{o} , and scattering function i(S) of equations (5) and (2) for each data point. These three quantities depend on the normalizing constant and independent scatter values to be discussed.

All temperature runs were taken to an angular maximum of

2θ about 100° or S = 17.2 Å^{-1} and the run at 30°C. to $2\theta = 133^{\circ}$ or S = 20.5 Å^{-1}. However, only the data to $2\theta = 60^{\circ}$ was utilized in the inversions. The data beyond this point is questionable because an expected effect failed to materialize. As the angle increases past $2\theta = 64^{\circ}$ the Compton modified scatter due to the K-beta line of the incident beam is displaced to energies below the absorption edge of the palladium beta filter. The improved transmission for this component should cause a relatively pronounced increase in scattering. This behavior was not observed, possibly because the effect was masked by a too-broad incident spectrum. It is doubtful that the high-S data could have been retained for the inversion in any case. By S = 10 Å^{-1} the amplitude of the scattering function is approaching experimental errors, and experimental corrections (Appendix I) become less reliable with increasing angle. These uncertainties are made more serious by the factor S of the inversion integral and the increasing contribution of modified scatter.

DATA ANALYSIS

Normalization

Combination of equations (2) and (5) gives the scattering function in terms of the experimental scatter as

$$i(S) = \frac{1}{f^2}\left[AE_{XC}-(f^2+F_{MC})\right] \qquad (9)$$

where E_{XC} and F_{MC} are corrected functions defined by equations (6) and (7). In order to obtain numerical values, there still remains to evaluate the constant A defined in equation (I-11). This constant cannot be directly calculated with any reliability due to the number and complexity of its factors, particularly the absolute intensity on the surface of the liquid and the scatter-slit parameters. Therefore, this constant is usually evaluated by an indirect or normalizing procedure requiring that the scattering function i(S) conform to some known property. Two normalizing criteria are popular(14). One of these is based on the fact that i(S) must vanish for very large values of S corresponding to the disappearance of all interference effects as given by equation (3). The second uses the requirement that radial density distribution must vanish at the position of the central reference atom to obtain an integral condition on the

scattering function. Both approaches are subject to truncation errors as they are not rigorously applicable except for information approaching an infinite range in S.

The first of these methods was selected here on the basis of arguments given in Appendix II. It is shown that both methods converge in the limit of no truncation. For the case of finite truncation, however, the second or integral method invokes a condition which is not truly pertinent to the experiment itself. The vanishing of i(S) at high S for the first method is used here in the precise form

$$i(S_m) = 0 \tag{10}$$

where S_m is the highest value of S for the function i(S) to be inverted. It is shown that this condition is necessary for a density distribution exhibiting no long-range order in the liquid. Specifically, the resulting coordination number of atoms at a long distance from the reference atom will be given by $-\frac{2}{\pi} S_m i(S_m)\cos(S_m R)$. Thus, unless $i(S_m)$ is made exactly zero, the distribution of neighbors will show constant-amplitude regularity at large distances. It was precisely the absence of such regularity that permitted extending the integration limits of equation (3) to infinity. This consideration does not prove that equation (10) is the only permissible normalizing condition.

The long-range order resulting from any other reasonable normalization procedure can be viewed as the necessary consequence of truncating at finite S_m. However, the argument does give an added physical basis to the normalizing approach represented by equation (10).

Independent scatter

For the evaluation of the scattering functions, and hence the normalizing constant, it is necessary to provide data on independent scattering as a function of S, namely f^2, the coherent scatter, and F_M, the modified or incoherent scatter, of an independent atom. Both of these are expressed in standard "electron units," as multiples of the intensity scattered by a single classical electron per unit incident intensity. Values of the atomic scattering factors for gallium have been calculated by Freeman(41). In the case of silver K-alpha radiation on gallium these factors require an appreciable dispersion correction for the K absorption edge. The corrected value of f^2 is given by(42)

$$f^2 = (f_0 + \Delta f'_K)^2 + (\Delta f''_K)^2 \qquad (11)$$

where f_0 applies to very high frequencies in comparison to the K edge, and $\Delta f'_K$, $\Delta f''_K$ are constants which correct for the proximity of the K-edge absorption frequency to the frequency

of the incident radiation. The necessary constants for correction were obtained from Cromer(43). No quantum-mechanical estimates of the modified scatter F_M are available for gallium. Freeman(44)(45) gives values for the nearby elements copper (atomic number 29) and germanium (atomic number 32). In the absence of any specific information for the independent scatter by an element, values are usually based on the Thomas-Fermi approximation to electron distribution(46). This approximation leads to independent modified scatter which is a continuous function of the atomic number. It was thought adequate and preferable to obtain the modified scatter for gallium by simple linear interpolation on atomic number within the small range between copper and germanium. A summary of all the data used in evaluating the independent scattering terms is given in Table III. In assigning independent scatter to the specific experimental values of S, the tabulated data was interpolated to the abscissa of interest by an exact Lagrangian fit to the nearest four points.

Inversion

Having established the complete relation between experimental scatter and the scattering functions, there remains to perform the inversion given by equation (4). The required operation differs from an ordinary numerical integration in an important

respect. Only the i(S) part of the integrand is given by discrete numerical values, the remaining factors, S and sin(RS), are known analytically. Therefore, it seems desirable to obtain a functional approximation to i(S) which permits performing the actual integration analytically. This requirement is satisfied by any polynomial approximation to the scattering function. It is not necessary, of course, that the polynomial or other function approximate i(S) over the entire range. It is sufficient to obtain a piecewise approximation in which the coefficients of the approximating polynomials vary from region to region of the O-to-S_m inversion range. The over-all integral can then be obtained as the sum of the corresponding integrals for each of the regions approximated. This general approach has a large theoretical and practical advantage in that the inversion for any value of the radius utilizes exactly the same approximation. The inversion process is then consistent for all values of the radius, and it is unnecessary to re-evaluate the integrand at discrete points for each value of the radius. The approximation accomplishes essentially a substitution of the known points by a set of parameters for the approximating function in order to simplify the process of integration.

As mentioned previously, a polynomial is an adequate choice for a piecewise integrable approximating function. There can be no precise rule for selecting the order of this polynomial

or the manner in which it is to be fitted to data. In particular, there is no need to require that the approximating polynomial pass exactly through all points. The only general rules which seem applicable are that the deviation of experimental points from the polynomial should not exceed the experimental errors, and that the approximating process should not give excessive relative weight to any data points.

In this particular application of the piecewise approach, a third-order polynomial was fitted to the data by an ordinary least-squares procedure. The method of integration is shown in Appendix III. The third order appeared sufficiently high to allow for the fitting of data over substantial S range including inflection points and fairly sharp extrema. Each cubic was fitted to five or more equally weighted points thus providing a smooth representation of the data within the estimated experimental accuracy. Having subdivided the experimental S range into a number of panels, the most basic procedure would have been to fit the cubic approximation for each panel to the points within that panel. This process, however, can lead to substantial discontinuities in i(S) at the boundaries between panels. As shown in Appendix III, such first-order discontinuities lead to corresponding constant amplitude ripples in the density distribution at large radius. This effect is analogous to the oscillations caused by a non-zero value of $i(S_m)$, as discussed

above. However, in the latter case the oscillations are adjusted to zero by the normalizing constant whereas this constant has little influence on the intermediate discontinuities.

Since the disappearance of long-range order was a basic premise of the normalizing process, the elimination of first-order discontinuities in the piecewise representation of i(S) is needed for consistency. To provide continuity, the polynomial representing each panel was fitted not only to the points within the panel but also to the points on either side up to the mid-points of the adjoining panels. Further, each polynomial was constrained to pass through the i(S) value given by the preceding (in S) polynomial at the common boundary. This manner of fitting the data retains equal weighting of all points except for the end panels of the experimental range. Since each successive polynomial is made to pass through some given point, only three coefficients of the cubic are disposable in fitting the data. However, with the overlapping described, this constraint is relatively mild as the discontinuities otherwise obtained would be quite small. Excessive continuity from panel to panel does tend to destroy the essential premise that different approximations apply within each panel. This consideration is neutralized by the fact that overlapping was not accomplished by increasing the number of points fitted with each polynomial but rather by decreasing the size of the panels.

Details

Final values of i(S) for polynomial fitting were based on normalization strictly in accordance with equation (10), using the smooth approximation to i(S) at S_m, the truncation point. This process is relatively simple as the value of $i(S_m)$ varies linearly with the constant A. The procedure actually yields the normalization constant A for the angular range which includes S_m. Constants for the other angular ranges at the particular temperature then follow from the adjusting ratios previously discussed. These values of A are given in Tables V and were used to evaluate the tabulated functions of interest at each data point. Points below $2\theta = 8^o$ for the first angular range, and below $2\theta = 11^o$ for the second, were discarded as the alignment corrections were questionable. Points above $2\theta = 11^o$ in the first range were discarded in favor of the higher accuracy values of the second range in fitting the polynomials. At all other overlaps, the points of each angular range were given equal weight.

The chosen truncation point is about $S_m = 11.0$ Å^{-1} but, more precisely, $S_m = 7\pi/2$ Å^{-1}. This precise value has no important significance, but merely provides a convenient choice of radius increment for developing the inversions. The consideration here is that the inversion will contain $2\pi/S_m$ Å as the minimum period component. To reveal all the vagaries of the

inversion, a general radius increment of about $\pi/2S_m$ Å must be chosen which corresponds to extrema of the minimum period. This rule of selection, in combination with the chosen value of S_m leads to radius increment which is a rational fraction (1/7) of one Ångstrom and facilitates plotting. Much finer values must be used to define the first coordinate maximum where the density distribution varies rapidly. Through this region the basic R increment was subdivided to 1/28 Å.

Coefficients for the piecewise cubic representations of i(S) at each temperature are given in Tables VI. Exactly the same selection of panels was used for each temperature. In order to increase the precision of the least-squares fitting routine and the reproducibility of smooth i(S) values, the polynomials were not based on the coordinate S itself but on its increment from the lower boundary of each panel. For example, for a panel extending from S_1 to S_2, the cubic is expressed in powers of $(S-S_1)$. Hence, the constant coefficient in each cubic is actually the value of i(S) at the lower boundary of the panel. As indicated by the coefficients, the approximation i(S) = -1 was used for the first panel, between S = 0 and 1.5 $Å^{-1}$, which contains no data. This approximation was suitable for the i(S) functions observed. Some similar approximation must be made in all liquid-structure determinations as the angular range does not ordinarily extend to 0^o where, in fact, the scattering is

not described correctly by equation (3).

The computational arrangement followed is summarized in Appendix III. All calculations were performed on the I.B.M. 7090 computer at the California Institute of Technology.

Results

Figure 8 shows actual experimentally-derived values of the scattering function i(S) and the smoothing approximation for the $0^{o}C$. investigation, as an example of the approximating method. Figure 9 is a plot of the corresponding inversion results for the function $4\pi R^2\left[\rho(R)-\rho_o\right]$ at $0^{o}C$. The smooth approximations to i(S) for all temperatures are shown in Figure 10. Figure 11 shows graphical curves of $4\pi R^2\left[\rho(R)-\rho_o\right]$ for all the temperatures.

The radial distribution function g(R) correlates the probability that two atoms will be distance R apart to the density of the liquid(47). In terms of radial neighbor distribution $\rho(R)$ and average atom density ρ_o, the radial distribution function is given by

$$g(R) = \frac{\rho(R)}{\rho_o} \qquad (12)$$

Figure 12 gives graphical curves of the radial distribution functions obtained for the temperatures investigated. These

are based on ρ_o values interpolated from those in Table I which derive from the stable liquid densities given by Wagner and Gitzen(3). Since the density variation is relatively small over the temperature range of interest, this extension of density behavior to the supercooled liquid should be adequate. The low-R region below the first crossing of zero by g(R) is not shown. The extreme oscillations and negative values of the calculated function in this region are physically meaningless (Appendix III).

CONCLUSION

This investigation reveals almost no change in the structure of liquid gallium over the 0 to 50 °C. temperature range, including 30° of supercooling. This constancy of structure is evident in the scattering functions shown in Figure 10 and more so in the distributions of Figures 11 and 12. Principal points of the scattering and inversions are also summarized in Table IV.

Tabulated for i(S) are the coordinates of the first, second, and third maxima, and the "shoulder" on the asymmetric high-S side of the first peak. These were obtained from the smoothed representations of Figure 10. The first maximum is sharp within 0.02 Å^{-1}, the second considerably broader but identifiable within 0.05 Å^{-1}, the third is within 0.1 Å^{-1} although selected much more accurately for Table IV. A fourth maximum is apparent in Figure 10 but it is too broad and poorly defined to warrant specification. The position of the first-peak shoulder, amounting to a sudden increase in slope, is definable within 0.05 Å^{-1} by linear extension of the adjoining curve segments. Within the limits of definition the S ordinates of the three features are essentially invariant with temperature. The corresponding i(S) values show significant variations with no very clear trend. First-maximum values are particularly subject to counting and smoothing errors.

The colder temperatures show somewhat sharper i(S) features, the change seemingly occurring with the first 10^{o} of supercooling.

The tabulated maxima for the radial distribution function follow from curves as shown in Figure 12. The first maximum is sharply defined to within 0.02 Å, the second less-so to within 0.05 Å, and the third within no less than 0.1 Å. These features are not significantly affected by temperature or supercooling. The colder temperatures again show slightly sharper definition with the change occurring early in the supercooled range. The general aspects of the structure appear to be insensitive to variations in the scattering function. This is particularly exemplified by the i(S) curve for 29.5^{o}C. in Figure 10 which is substantially different from the others through the main peak but leads to no important differences in structure.

The remaining information in Table IV concerns the coordination function $4\pi R^2\rho(R)$ giving the average number of atoms for an infinitesimal spherical shell at distance R from any atom in the liquid. This distribution is obtained from the $4\pi R^2[\rho(R)-\rho_o]$ inversion results shown in Figure 11 by adding the contribution of the average density ρ_o. The R value reported as the zero of the coordination function corresponds to the distance of closest approach by two atoms in the liquid. This ordinate was defined as the lowest R for which the coordination is always positive. For lower R the calculated function shows negative values and

oscillations which may be seen in the distributions in Figure 11. This behavior has no physical significance since the region immediately about the center of a reference atom cannot be occupied by any others and the coordination should be zero up to the distance of closest approach. The spurious behavior of the calculated function may be ascribed to the inversion process (Appendix III) and is therefore ignored.

Coordinates for the first peak of the function $4\pi R^2 \rho(R)$ are also given in Table IV. This feature is sharply defined to within 0.02 Å. The location does not agree exactly with the first peak of the radial distribution function g(R) because of the additional R^2 dependence of the coordination function. Similarly, the first coordination maximum occurs at somewhat higher R than the corresponding maximum of the $4\pi R^2[\rho(R)-\rho_o]$ distribution in Figure 11. This coordination maximum is the only one which occurs. The remaining maxima of $4\pi R^2[\rho(R)-\rho_o]$ do not carry over as such to the coordination function because they are relatively small by comparison with the average density term. This fact is apparent from the very small second and third peaks shown by the radial distribution functions.

Coordination numbers for this first and only peak are given by three methods of definition(14)(15). Method A postulates that the true high-R flank of the first peak is symmetric with the low-R side. Hence, the area of the coordination curve

between the distance of closest approach and the maximum is multiplied by two. Method B takes the coordination number as that included up to the high-R minimum setting off the first peak. This minimum is rather broad and the corresponding R not readily defined. A fixed value of 3.6 Å was used in all cases. Method C depends on extrapolating the high-R side of the first peak to zero. This operation is poorly defined, the peak was extended to about 4.0 Å on the high-R side in reasonable fashion so that the residual coordination appeared as a continuation of the remaining high-R distribution.

The integrations involved in calculating coordination numbers consist basically of two parts, a uniform ρ_o density contribution depending solely on the defining R limits, and a deviation from uniformity given by integration of the $4\pi R^2\left[\rho(R)-\rho_o\right]$ curves of Figure 11. In all methods, the uniform density term is much more important than the structural part. For example, the value 10.8 for method B at 50°C. consists of 8.5 atoms from integration of ρ_o and 2.3 atoms from integration of $\left[\rho(R)-\rho_o\right]$. Thus, these coordination numbers are quite sensitive to the manner in which the peak is defined or limited. As methods B and C do not yield precise limits, the corresponding coordination is uncertain to several tenths and is ordinarily rounded to the nearest atom. Method A, at least in this case, does yield a precise value since the distances of nearest

approach and maximum are sharply defined.

Method A is thus the most likely to provide an objective indication of variation in coordination. Table IV shows a significant decrease in this coordination estimate as temperature increases. However, this method uses the strictest possible interpretation of the nearest-neighbor group. It presumes by definition that the members of this group can occupy space toward or away from the reference atom with equal probability. Both methods B and C, though imprecise, seem more objective in their definition. These also show some trend with temperature but the variation is too small to be considered significant.

It is not possible to give a compact estimate of the reliability of the distribution results. Errors in the measurement of scatter, normalization, truncation, and fitting of data can contribute in a complex manner to the inversion results. Lack of monochromatization is not a specially significant source of error. The effect of a spread in scattered energies is to give an S-proportional spread in the S values contributing to the scatter. There results a loss of resolution and a general damping of extrema of the i(S) function important only at the higher S values. Provided that the incident energies are reasonably well centered about the primary value, the over-all effect is simply a hastening of the approach to independent scatter or i(S) = 0. Lack of monochromatization may then be

likened to a progressive truncation or built-in modification function. There results a loss in definition of the high-frequency components of the radial distribution but no marked distortions.

The experimental corrections discussed in Appendix I should not lead to more that 1% uncertainty in coherent scatter or 0.01 in i(S) at high S. The normalization process by itself is a similar source of error. From the discussion in Appendix III and the amplitude of the i(S) curves at high S, the normalizing constant is probably reliable within 2% or 0.02 in i(S) at high S. Equally or more important are the internormalization or adjustments required by the successive slit changes as errors in these tend to displace a particular section of the i(S) curve. Similarly, serious counting errors in relation to the point spread or where the fitting of i(S) is somehow sensitive to individual points can cause spurious oscillations in the inversion.

From the inversion integral in equation (4) there follows that false components of the $4\pi R^2[\rho(R)-\rho_o]$ inversion would have amplitudes of $S\Delta i(S)$ order of magnitude, where $\Delta i(S)$ is the displacement of the i(S) curve. Considering that the inversion range is 0 to 11 Å^{-1} in S, and that deviations of a few hundreths in i(S) are likely, error features of several tenths atoms/Å can be expected. Therefore, point values of the radial distribution such as reported in Table IV are subject

to considerable uncertainty. Further, the variety of small humps which distort the distributions of Figures 11 and 12 must be disregarded. This is particularly obvious in cases like the small maximum just beyond the principal one shown by the 40°C. inversion and not by the other distributions. By comparison, the extended bulge which precedes the second peak, as shown specially by the curves of Figure 12, seems significant in being a consistent feature. However, this detail must also be suspected as it is of small magnitude and its recurrence may simply reflect consistency in the treatment of data.

The position of the i(S) features agrees quite well with the values reported by Hendus(19) at 20°C.: S = 2.50 Å^{-1} for the first maximum, 3.12 for the shoulder, and 4.86 for the second peak. However, the curve given for coherent intensity indicates considerably sharper i(S) features than those obtained here, the first maximum being about 1.7 and the second about 0.7. No explanation for this discrepancy can be given without more detailed knowledge of that technique. That investigation employed crystal-monochromated copper K-alpha radiation, and film camera to S about 8 Å^{-1}. It is doubtful that any differences in monochromatization, resolution, or normalization could lead to such wide difference in the i(S) amplitudes. Hendus' inversion for the radial distribution function shows maxima of about 2.75 at 2.7 Å, 0.15 at 5.6, and 0.1 at 8.2.

The low-R side of the first peak descends sharply to zero at 2.4 Å. This g(R) curve has an overly-smooth appearance and may be idealized(14). The amplitudes are again considerably larger than the ones obtained here and, in addition, the maxima are displaced, particularly the first maximum which is a well-resolved feature. These differences may be due in part to the higher truncation value of S_m = 11 $Å^{-1}$ used in this investigation. For the coordination curve Hendus reports a first maximum at 2.77 Å or about 0.1 Å less than observed here. The reported coordination number of 11 by method C is in agreement with the present estimates.

The i(S) curves presented by Menke(13) show better agreement with the present values as to general amplitude. However, the g(R) inversion curve has an extremely pronounced first maximum of near 3.5. Hendus(19) estimates that the corresponding coordination number would be 14 or 15. In the scattering function shown by Menke for 18°C. the high-S shoulder of the first peak is actually resolved into a separate maximum. This behavior is not shown by Hendus and failed to materialize in this investigation. In fact, Table IV indicates that the position and height of this shoulder remain essentially invariant with temperature. Furukawa(14) alludes to unpublished data showing a decrement of this shoulder with temperature but over the more extended range of 23 to 192°C.

The first-peak shoulder distortion of these i(S) curves indicates a more complex distribution of distance in the liquid than for a simple principal peak. However, this complexity is insufficient to cause distinct features in the broad structure given by the inversion process. Additional structural details can be obtained(17) by separating the main peak into two component peaks. The smaller would correspond to the distorting shoulder. A separate inversion for this artificial peak then yields its structural interpretation. Since the separation is arbitrary, it is doubtful that the significance of the results warrant carrying out the precise inversions. A rough estimate of the meaning of this shoulder can be obtained by direct interpretation of the scattering function.

Equation (2) states that the function i(S) is a superposition of sin(RS)/RS components having amplitudes proportional to the local coordination $4\pi R^2 \rho(R)$. The ρ_o may be ignored for this concept by a reversal of the argument which led to its original introduction. Peaks in i(S) can then be roughly ascribed to high densities near values of R corresponding to maxima in sin(RS)/RS. The first such maximum of interest occurs at approximately RS = $5\pi/2$. Thus, the main i(S) maximum at S = 2.51 Å^{-1} corresponds to R of about 3.1 Å which is not too far different from the principal distance of 2.9 Å returned by the complete inversion. Since the shoulder occurs at S of about

3.1 Å^{-1}, the corresponding R would be 2.5 Å. The two peaks which presumably compose the principal i(S) peak may be imagined to be of similar shape. However, the shoulder feature is only about one-third the height of the principal maximum. There follows that the larger of the two postulated maxima is essentially that of i(S) itself while the shoulder corresponds to a smaller peak representing a much-smaller coordination number perhaps one-ninth as large. The total coordination is somewhere between 8 and 11 atoms. Thus, it appears that the actual distribution in the liquid may consist of about one atom at 2.5 Å and 7 to 10 atoms at about 3.1 Å.

This crude estimate is abetted by the fact that a similar situation prevails in the crystalline gallium(7). Each gallium atom in the crystal has a nearest neighbor at 2.48 Å and six others at distances from 2.69 to 2.79 Å. The near distance corresponds to the strongest bonding so that a Ga-Ga complex appears to be the structural unit(48). Conceivably this molecular association carries into the liquid phase. As mentioned previously this possibility cannot be supported or denied by the complete inversion. The coordination for a molecular neighbor is much smaller and not too much closer than the entire first coordination shell.

In any event the structure of the liquid is relatively unaffected by supercooling. A very close inspection of the

inversion results shows some slight sharpening of structural features at the lower temperatures. This behavior is vaguely reflected in a corresponding increase of the coordination number. It also appears that any structural changes brought on by supercooling may occur shortly below the melting point rather than progressively as temperature decreases. However, the possible structural changes are much too small to be resolved quantitatively by an investigation of this type.

APPENDIX I

EXPERIMENTAL CORRECTIONS

The corrections which relate coherent scattering to experimental scattering are first obtained for an almost-ideal experimental situation. In this case, the incident and scattered beams in Figure 1 are assumed to consist of nearly-parallel rays at the liquid surface, the surface is flat and at the goniometer axis. The possible effects of actual experimental conditions are then considered independently. All intensities (I) are in quanta of the incident radiation per unit time and area. Correspondingly, the experimental measurement (E), a power quantity, is in quanta per unit time or, more specifically, counts/second received by the detector. The subscripts 1,2,... represent various approximations to this experimental scatter. Coordinate designations are given in Figure 1.

From equation (1) of the text, the coherent scattering by any volume element of the liquid is given by

$$I_{coh} = I_o N f^2 \left[i(S)+1 \right] = I_o N F(S) \qquad (I\text{-}1)$$

I_o is the intensity incident at the volume element. N is the

number of atoms it contains. F(S) summarizes the interference effects of electron distribution within individual atoms and the configuration of atoms in space. F(S) is a dimensionless function which may be said to have "electron units" in that the scattered intensity is expressed as a multiple of the scattering per unit incident intensity by a classical electron. It is F(S) which must be evaluated to obtain i(S) from equation (1) of the text.

The first consideration in relating (I-1) to experimental scatter is that the latter represents scattering contributions from various volume elements. The experimental scatter is thus given by an integral over the participating volume of the sample of uniform density ρ_o.

$$E_1 = \rho_o \int_V \omega r_1^2 I_o F(S)\, dV \qquad (I-2)$$

ω is the solid angle subtended by the experimental scatter slits at distance r_1 from a particular volume element and $\rho_o dV$ is the number of atoms in an element. For perfectly collimated beams the area ωr_1^2 and parameter S are invariant throughout the volume. Hence,

$$E_1 = \rho_o \omega r_1^2 F(S) \int_V I_o dV \ . \qquad (I-3)$$

Equation (I-3) cannot apply strictly to any actual experiment. The simplification will be retained with the assumption that

slit resolution is sufficiently fine to ignore variations in F(S) throughout the volume or that the average value of F(S) is acceptable. The factor ωr_1^2 then corresponds to an average for the particular slit configuration in relation to the sample.

The angles between the surface and the incident and scattered beams are respectively α and φ. In reaching a depth z the incident radiation will travel distance $z/\sin\alpha$ through the liquid while the scattering will travel distance $z/\sin\varphi$ before emerging from the liquid. Using the exponential absorption rule, the experimental scatter is given by

$$E_2 = \rho_o \omega r_1^2 F(S) I_{oo} \iiint e^{-\mu\left(\frac{1}{\sin\alpha} + \frac{1}{\sin\varphi}\right)z} \, dxdydz \qquad (I\text{-}4)$$

I_{oo} represents the presumably-uniform intensity incident at the liquid surface. μ is the absorption factor. Integration over length L on x, width W on y (the goniometer axis), and from the surface z = 0 of the liquid to some depth z yields

$$E_2 = \rho_o \omega r_1^2 F(S) I_{oo} \frac{WL}{\mu}\left(\frac{\sin\alpha\sin\varphi}{\sin\alpha+\sin\varphi}\right)\left[1-e^{-\mu z\left(\frac{\sin\alpha+\sin\varphi}{\sin\alpha\sin\varphi}\right)}\right] \qquad (I\text{-}5)$$

For relatively strong absorbers the exponential term decreases rapidly with depth. In the case of gallium μ is about 480 per inch(38) for Ag K-alpha radiation. For α about 5^o and φ about 90^o (minimum absorption) the exponential reduces to 0.001 at depth of about 0.0012 inches. Since the actual liquid specimen

is much deeper, the exponential term can be neglected. Practically all the observed scattering comes from a thin surface layer so that all appreciably deep samples can be considered infinitely deep. The observed scatter is then

$$E_2 = \rho_o \omega r_1^2 F(S) I_{oo} \frac{WL}{\mu} \left(\frac{\sin\alpha \sin\varphi}{\sin\alpha + \sin\varphi}\right) \qquad (I\text{-}6)$$

This simplification is very useful since the scattering may be considered as a surface effect for gross geometric purposes.

A further absorption correction is required by the passage of scattered radiation through the X-ray windows, atmosphere, and beta filter before reaching the counter. The absorption along this path is, by design, essentially invariant so that this correction amounts to an angle-independent factor D.

$$E_3 = \rho_o \omega r_1^2 F(S) I_{oo} \frac{WL}{\mu} \left(\frac{\sin\alpha \sin\varphi}{\sin\alpha + \sin\varphi}\right) D \qquad (I\text{-}7)$$

The width W of the scattering surface is not ordinarily a function of angle as it is determined by the constant-width beams or, in the present case, defined by the brass-ring shields of the inner cell. The spacing between these is about 0.450±0.001 inches in the angular region of interest and the width W may be considered constant. The length L, however, is determined by the angle between the liquid surface and the beam having the lesser

spread on the liquid surface. In this experiment the incident beam took in the entire surface of the specimen and the scattering length L was controlled by the scattered beam height. If H is the height of this beam at the liquid surface, the length of scattering surface is given by

$$L = \frac{H}{\sin \varphi} \tag{I-8}$$

and equation (I-7) becomes

$$E_4 = \rho_o \omega r_1^2 F(S) I_{oo} \frac{W}{\mu} \left(\frac{\sin \alpha}{\sin \alpha + \sin \varphi}\right) DH \tag{I-9}$$

This relation now contains a correction for absorption and field of view depending on the scattering angle through $\varphi = (2\theta - \alpha)$. In the "parafocusing" version of this experiment the angle α is maintained equal to φ by rotating the X-ray source about the goniometer axis thus making the angular factor of (I-9) a constant and eliminating the need for this correction.

The usual correction for polarization must be applied to the classical electron scattering which is the reference unit of these expressions. Assuming unpolarized incident radiation, the intensity at angle 2θ is reduced by a factor $(1+\cos^2 2\theta)/2$ and the experimental scatter is

$$E_5 = \rho_o \omega r_1^2 F(S) I_{oo} \frac{W}{\mu} \left(\frac{\sin \alpha}{\sin \alpha + \sin \varphi}\right) DH \left(\frac{1+\cos^2 2\theta}{2}\right) \tag{I-10}$$

The angle-independent factors may be combined into an over-all constant 1/A giving

$$A = \frac{2}{\rho_o \omega r_1^2 I_{oo} DWH \sin\alpha} \tag{I-11}$$

$$E_5 = \frac{F(S)}{A} \frac{1+\cos^2 2\theta}{\sin\alpha + \sin\varphi} \tag{I-12}$$

The modified or incoherent portion of the experimental scatter may be evaluated by the same scheme. At a volume element

$$I_{mod} = \frac{I_o N F_M(S)}{B^2} \tag{I-13}$$

In this case the function $F_M(S)$ does not contain interference terms but is simply the independent modified scatter per atom which is known in principle, as with f^2 its counterpart in coherent scattering. The factor $1/B^2$ is the special Breit-Dirac correction which allows for the effect of electron recoil on the observed intensity(49)(50). It is not included with $F_M(S)$ as it is not dependent on the scattering parameter S alone. Rather, B is the ratio of modified to incident wavelength given by(51)

$$B = \frac{\lambda_M}{\lambda} = 1 + k \frac{\sin^2\theta}{\lambda} \tag{I-14}$$

where k (approximately 0.04852 Å) is a fundamental constant

corresponding to the maximum change in wavelength for backward scatter.

The absorption by the sample is treated as in the case of coherent scatter except that, owing to the reduction in energy on scattering, a different absorption coefficient applies in the liquid after scattering. For the same reason, the absorption along the path to the counter will be different for the modified scatter. On the other hand, the slit resolution, scattering length L, and polarization factor are exactly the same as for coherent scatter. The modified scatter observed experimentally is then

$$E_{M_1} = \frac{\rho_o \omega r_1^2 F_M(S) I_{oo} W}{B^2} \frac{\sin\alpha}{\mu_M \sin\alpha + \mu \sin\varphi} D_M H \frac{1+\cos^2 2\theta}{2} \qquad \text{(I-15)}$$

The dependence of μ on wavelength may be approximated by a simple exponential law(53)

$$\frac{\mu_M}{\mu} = \left(\frac{\lambda_M}{\lambda}\right)^a = B^a \qquad \text{(I-16)}$$

where the exponent a is characteristic of the sample. The modified scatter may be written in terms of the constant A. Combining (I-11) with (I-15) and using the relation given in (I-16) yields

$$E_{M_1} = \frac{F_M(S)}{AB^2} \frac{1+\cos^2 2\theta}{B^a \sin\alpha + \sin\varphi} \frac{D_M}{D} \qquad \text{(I-17)}$$

The distinction between D_M and D, the different transmissions of modified and coherent scatter along the path to the counter, is caused almost entirely by the beta filter. Transmission through the air and the beryllium and aluminum foils protecting the scintillator crystal is practically complete. The transmission by the two plastic X-ray windows is about 98% for the Ag K-alpha energy so that discrimination is negligible in comparison with the beta-filter effect. Considering the filter only

$$\frac{D_M}{D} = \frac{e^{-\mu_{DM}t}}{e^{-\mu_D t}} = e^{-\left(\frac{\mu_{DM}}{\mu_D} - 1\right)\mu_D t} \qquad \text{(I-18)}$$

Subscript D refers to absorption factors in the filter, and t is the filter thickness. Applying the exponential law with exponent b to the variation of these absorption factors with wavelength gives from (I-17)

$$E_{M_1} = \frac{F_M(S)}{AB^2} \frac{1+\cos^2 2\theta}{B^a \sin\alpha + \sin\varphi} e^{-(B^b-1)\mu_D t} \qquad \text{(I-19)}$$

A final expression for the total experimental counting rate can now be obtained by adding (I-17) to (I-12) and adding the background counting rate E_B.

$$E_X = E_B + \frac{1}{A} \frac{1+\cos^2 2\theta}{\sin\alpha + \sin\varphi} \left[F(S) + \frac{F_M(S)}{B^2} \frac{\sin\alpha + \sin\varphi}{B^a \sin\alpha + \sin\varphi} e^{-(B^b-1)\mu_D t} \right] \qquad \text{(I-20)}$$

Solving for F(S) and combining with (I-1) gives the coherent intensity term required by equation (1) of the text.

$$F(S) = \frac{I_{coh}}{NI_o} = A \frac{\sin\alpha + \sin\varphi}{1+\cos^2 2\theta} (E_X - E_B) - \frac{F_M(S)}{B^2} \frac{\sin\alpha + \sin\varphi}{B^a \sin\alpha + \sin\varphi} e^{-(B^b-1)\mu_D t} \qquad (I\text{-}21)$$

Deviations of the experiment from this idealized situation are caused by surface oscillations and curvature, beam divergence, and incorrect centering of the liquid surface. These small deviations affect mostly the angles α and φ between each beam and the surface in the scattering plane. Furthermore, since the scattering occurs essentially from the liquid surface, the scattering angle 2θ is not determined by goniometer alignment alone but depends also on the accuracy of the surface centering procedure.

The angles α and φ enter the experimental scatter, as in equation (I-9) through a factor

$$Q = \frac{\sin\alpha}{\sin\alpha + \sin\varphi} \qquad (I\text{-}22)$$

It can be assumed that this factor would apply at the center of the goniometer when and if the surface happens to be in its equilibrium horizontal position at that location. The effect of small deviations may then be estimated from an expansion of the

factor Q in terms of these deviations. In the case of surface oscillations and curvature, deviations in α and φ are related by

$$\delta\varphi = -\delta\alpha \tag{I-23}$$

since a change in surface inclination has opposite effects on the two angles. As the effects in question are basically symmetrical about the central reference situation, first-order terms in Q will integrate out and make no net contribution. If Q is represented by the limited expansion

$$Q = Q_o(1 + c_1\delta\alpha + c_2\overline{\delta\alpha}^2) \tag{I-24}$$

the average value of Q in a range of α variation from $-\Delta\alpha$ to $+\Delta\alpha$ is given approximately by

$$Q_{av} = Q_o(1 + \tfrac{1}{3}c_2\overline{\Delta\alpha}^2) \tag{I-25}$$

where the last term is an estimate of the error. Such second-order errors may be expected to be small. Expansion of Q using (I-23) shows that the largest error occurs for φ near 90^o and is given by

$$\frac{\Delta Q_{av}}{Q_o} = \frac{\overline{\Delta\alpha}^2}{3\sin\alpha} \tag{I-26}$$

In this experiment the angle α was about 5^{o} so that the angular factor in (I-26) is in excess of 10.

Surface oscillations were observed with a specially mounted open mercury sample which reflected a thin light beam, over a long optical path, onto a screen. The angular amplitude of the oscillations was typically a few tenths of one degree and never exceeded on degree. The corresponding error estimate given by (I-24) is then less than 0.1% so that this deviation may be safely neglected.

No simple, reliable measurement of surface curvature was obtained and the effect was evaluated by approximate analysis. Considering only curvature in the scattering plane, the surface is described by the equation

$$\rho_o g z = \gamma \left[1 + \left(\frac{dz}{dx}\right)^2 \right]^{-\frac{3}{2}} \left(\frac{d^2 z}{dx^2}\right) \qquad \text{(I-27)}$$

where γ is the surface energy of the liquid. The left side of (I-27) represents the pressure of the liquid column and the right side the surface stress at a point of the surface. This equation neglects principally the curvature of the liquid surface at z = 0. It is applicable only to an infinite surface but may be integrated to give a relation between the slope of the surface and distance from the cell wall (x_w)

$$\ln \Delta\alpha \quad - \text{const} = -\left(\frac{\rho_o g}{\gamma}\right)^{\frac{1}{2}} |x_w - x| \qquad \text{(I-28)}$$

The unspecified constant is a combination of terms depending on the angle of contact at the wall. This angle of contact is difficult to estimate. It is initially quite large for a freshly-loaded cell or when the surface equilibrium is disturbed. However, the angle decreases considerably after the liquid has resided in the cell for some time and/or the surface is allowed to stabilize at a given cell position. The behavior is possibly due to the formation of slight amounts of oxide which collect near the wall and increase wetting (5)(35). Assuming an intermediate non-wetting value of 135^{o} for the angle in the liquid between the surface and the wall, the constant in (I-28) is about 0.084. For gallium the quantity $(\rho_o g/\gamma)^{\frac{1}{2}}$ is about 7.25 per inch(3). At a distance of 0.3 inches from the wall equation (I-28) gives $\Delta\alpha$ of about 0.05 and (I-26) an estimated maximum error of 1%. The experimental cell had a diameter of about one inch so that this estimate corresponds to an allowed experimental length L of 0.4 inches. The target area was kept well inside these limits, largely inside 0.3 inches, by proper selection of scatter slits (Table II). Since the infinite-surface approximation increases the error estimate, the effect of surface curvature can be neglected.

The deviations in α and φ due to beam divergence or angular aperture are also symmetrical about the central values. For a small displacement δx along the horizontal, the deviations

are now related by

$$\delta x = - \frac{r_0 \delta\alpha}{\sin\alpha} = \frac{r_1 \delta\varphi}{\sin\varphi} \qquad \text{(I-27)}$$

where r_0 and r_1 are distances from the goniometer axis to the anode and to the center of the scatter slit combination. Using this relation, a second-order expansion of Q on δx gives a maximum error, again at high angles, of

$$\frac{\Delta Q_{av}}{Q_o} = \frac{\overline{\Delta x}^2}{6 r_1^2} \qquad \text{(I-28)}$$

where Δx is the spread of the scattering length on either side of the center. Since r_1 was of the order of 6 inches and Δx was limited to less than 0.2 inches by surface curvature considerations, this error is wholly negligible. In the direction along the goniometer axis the beams are well collimated by the Soller slits and no appreciable experimental deviation can result.

Deviations arising from misalignment of the liquid surface with the center of the goniometer are non-symmetrical. Furthermore, deviations in α and φ are related to vertical displacements δz by

$$\delta z = \frac{r_0 \delta\alpha}{\cos\alpha} = \frac{r_1 \delta\varphi}{\cos\varphi} \qquad \text{(I-29)}$$

so that, in contrast with the prior effects, the changes in α and φ do not tend to compensate. A first order expansion of the factor Q gives

$$\frac{Q}{Q_o} = 1 + \frac{r_1 \cos^2\alpha \sin\varphi - r_0 \cos^2\varphi \sin\alpha}{r_0 r_1 \sin\alpha(\sin\alpha + \sin\varphi)} \qquad \text{(I-30)}$$

The linear coefficient is seen to be zero if $r_1 = r_0$ and $\alpha = \varphi$, hence another advantage of a moving-anode technique. In the present case the largest error will occur at high angles or at extremely low angles with the surface. Using $\varphi = 90^0$ gives

$$\frac{\Delta Q}{Q_o} = \frac{\cos^2\alpha}{r_0 \sin\alpha(1+\sin\alpha)} \delta z \qquad \text{(I-31)}$$

On the basis of repeated tests with the leveling procedure described in the text, it is estimated that the liquid surface coincided with the goniometer axis to about ±0.005 inches. Since r_0 was about 7 inches and α about 5^o, the maximum error given by (I-31) is 0.8%.

The vertical position of the surface is also affected by curvature in the plane (y,z) of the goniometer axis. In this direction, the walls are also much nearer to the scattering area. An estimate in the manner previously employed for surface curvature gives a maximum relief of 0.020 inches between the edge of the scattering area and the highest point of the

surface (of infinite extent where the equations are concerned). The average relief, however, is only 0.002 inches. Further, this effect is second-order as it may be expected to place high and low regions of the surface above and below the goniometer axis. The effect is negligible by comparison with the leveling procedure itself.

Finally, the error in level position implies an error in 2θ the scattering angle. In the case of small surface oscillations or curvature, the angle 2θ is not affected, while for beam divergence only the resolution is affected (Table II). However, since the scattering is a surface effect, a displacement of the surface from the goniometer axis will cause a corresponding displacement in scattering angle from that given by the goniometer. The true scattering angle is given by the actual sum of α and φ so that by (I-29) the change in 2θ is

$$\delta(2\theta) = \delta(\alpha+\varphi) = \left(\frac{\cos\alpha}{r_0}+\frac{\cos\varphi}{r_1}\right)\delta z \qquad \text{(I-32)}$$

This deviation will be largest at small angles. For the estimated inaccuracy of ±0.005 inches in level position, the deviation is at worst 0.1° corresponding to as much as 1% error in the estimate of the scattering parameter at the lowest angles. By comparison, errors in scattering angle due to goniometer alignment or from manipulation of slits are unimportant.

APPENDIX II

NORMALIZATION

Normalization refers to evaluating the constant A of equation (5) in the text. Two approaches have been proposed(14) which will be denoted as method 1 and method 2. Method 1 is usually described vaguely as requiring that i(S) approach zero for large values of S. Here, a precise definition will be taken, namely

$$i(S_m) = 0 \qquad \text{(II-1)}$$

where S_m is the highest value of S to be considered. Method 2, advanced by Krogh-Moe(53), requires

$$\int_0^{S_m} S^2 i(S)\, dS = -2\pi^2 \rho_o \qquad \text{(II-2)}$$

The derivation of these conditions is not the primary concern here. Method 1 arises from the expectation that interference effects must disappear for very large values of S, as shown by equation (3) of the text. Method 2 derives from requiring that the radial density $\rho(R)$ given by equation (4) approach zero as the radius goes to zero, and implies separate knowledge of the average atom density ρ_o. The principal question is the

selection of one of these methods for numerical purposes.

Since the normalization constant A acts directly on the experimental scatter, the normalizing conditions should be compared in terms of this quantity. The scattering function is given by equation (2) of the text as

$$i(S) = \frac{1}{f^2}\left[\frac{I_{coh}}{NI_o} - f^2\right] \qquad \text{(II-3)}$$

The coherent intensity is related to the experimental scatter by equation (5) of the text

$$\frac{I_{coh}}{NI_o} = AE_{XC} - F_{MC} \qquad \text{(II-4)}$$

where AE_{XC} and F_{MC} represent the experimental and modified intensities corrected for experimental conditions. It follows that

$$i(S) = \frac{AE_{XC} - I_{IC}}{f^2} \qquad \text{(II-5)}$$

where $$I_{IC} = f^2 + F_{MC} \qquad \text{(II-6)}$$

I_{IC} represents the coherent-and-modified independent scatter per atom which is subtracted from the corrected experimental intensity to obtain the interference effects.

Method 1 can be expressed as

$$\frac{A_1 E_{XC}(S_m) - I_{IC}(S_m)}{f^2(S_m)} = 0 \qquad \text{(II-7)}$$

$$A_1 E_{XC}(S_m) = I_{IC}(S_m) \qquad \text{(II-8)}$$

The last equation conveys the normalization idea, that the experimental scatter is adjusted to equal the independent scatter at large values of S.

Method 2 becomes

$$\int_0^{S_m} \frac{S^2}{f^2} (A_2 E_{XC} - I_{IC})\, dS = -2\pi^2 \rho_o \qquad \text{(II-9)}$$

$$A_2 \int_0^{S_m} \frac{S^2}{f^2} E_{XC}\, dS = \int_0^{S_m} \frac{S^2}{f^2} I_{IC}\, dS - 2\pi^2 \rho_o \qquad \text{(II-10)}$$

This last relation shows an important characteristic of method 2. At fairly high values of S_m the value for the constant A_2 is ordinarily insensitive to the liquid density. In the right-hand integral the ratio (I_{IC}/f^2) must be at least unity, as shown by equation (II-6), so that the integral must be of the order of S_m^3.

$$\int_0^{S_m} \frac{S^2}{f^2} I_{IC} dS \geq \frac{S_m^3}{3} \qquad \text{(II-11)}$$

At $S_m = 10\ \text{Å}^{-1}$, for example, the right-hand integral of (II-8) would be at least $333/\text{Å}^3$. On the other hand, the atomic density ρ_o of gallium is about 0.053 atoms/Å^3 so that the corresponding term of (II-10) would amount to only $1.0/\text{Å}^3$. Thus, the borrowed density ρ_o has ever-decreasing influence on the normalization constant and none whatever in the limit of infinite S_m or complete information. It seems improper to introduce the density ρ_o, or a condition having to do with this density, in normalizing. Rather, this density is in principle determinable from complete data.

Equation (II-10) may also be written as

$$A_2 = \frac{\int_0^{S_m} \frac{S^2}{f^2} I_{IC}\, dS}{\int_0^{S_m} \frac{S^2}{f^2} E_{XC}\, dS} - \frac{2\pi^2 \rho_o}{\int_0^{S_m} \frac{S^2}{f^2} E_{XC}\, dS} \qquad \text{(II-12)}$$

In the limit of very large S_m equation (II-12) yields

$$\lim_{S_m \to \infty} A_2 = \frac{I_{IC}(S_m)}{E_{XC}(S_m)} = A_1 \qquad \text{(II-13)}$$

where the second equality follows from (II-8). The two normalization methods converge in the limit of very-high truncation S_m and are then equally justified. However, the convergence is strictly a consequence of a high S_m which puts preponderant

weight on the terminal values of the integrands involved in method 2 and renders the ρ_0 negligible. Thus, with increasing completeness of information, the improving values of method 2 approach those given by method 1. It may be said that method 1 tends to exactness and method 2 tends to method 1. Stating the converse would be ridiculous as 1 is the simpler and more basic in its definition. For finite values of S_m, method 2 still puts some weight on all data. The discrepancy between the two normalization constants then reflects the composite effects of truncation and experimental error.

The implications of method 2 on the physical nature of the radial density distribution are apparent in the original premise that $\rho(0)$, the density of neighbor atoms at radius zero, must vanish. However, it is not usually recognized that method 1 would be required by the important condition that $4\pi R^2 [\rho(R)-\rho_0]$ must vanish at large radius. This function, an "excess differential coordination number," will be abbreviated as

$$O(R) = 4\pi R^2 [\rho(R)-\rho_0] \qquad \text{(II-14)}$$

Combining equations (3) and (4) of the text in terms of the function O(R) gives

$$\frac{O(R)}{R} = \frac{2}{\pi} \int_0^{S_m} \int_0^{\infty} \frac{O(R')}{R'} \sin(SR')\, dR' \sin(SR)\, dS \qquad \text{(II-15)}$$

where R' distinguishes the variable for integration on radius and O(R') is interpreted as the true radial function. Performing the integration on S gives

$$\frac{O(R)}{R} = \frac{2}{\pi} \int_0^{\infty} \frac{O(R')}{R'} \left[\frac{\sin S_m(R-R')}{2(R-R')} - \frac{\sin S_m(R+R')}{2(R+R')} \right] dR' \qquad \text{(II-16)}$$

This expression is a special case of the general folding described by Waser and Schomaker(54) as the result of modifying some true i(S) with an arbitrary multiplying function. Multiplying both sides of (II-16) by R and taking the limit for large R gives

$$O(\infty) = \frac{2}{\pi} \int_0^{\infty} \frac{O(R')}{R'} \left[\frac{\sin S_m(R-R')}{2} - \frac{\sin S_m(R+R')}{2} \right] dR' \qquad \text{(II-17)}$$

This limit is justified in the range of large R' by the assumption that O(R') truly vanishes at large R' in the liquid. Since

$$\frac{\sin S_m(R-R')}{2} - \frac{\sin S_m(R+R')}{2} = -\sin(R'S_m)\cos(RS_m) \qquad \text{(II-18)}$$

equation (II-17) becomes

$$O(\infty) = -\frac{2}{\pi} \cos(RS_m) \int_0^{\infty} \frac{O(R')}{R'} \sin(R'S_m)\, dR' \qquad \text{(II-19)}$$

By equation (3) of the text and the definition in (II-14) the

integral of (II-19) is $S_m i(S_m)$, hence

$$O(\infty) = -\frac{2}{\pi} S_m i(S_m) \cos(S_m R) \qquad \text{(II-20)}$$

Equation (II-20) indicates that unless $i(S_m)$ is exactly zero the coordination number has a constant amplitude oscillation for large radius. Therefore, method I can be interpreted as the requirement of no long-range order in the liquid.

From these considerations method 1 is to be preferred. Both approaches seem equally justified on physical grounds. However, the physical implications of method 1 are particularly pertinent to the experiment. On the other hand, method 2 comes about through a requirement which is actually redundant in the limit of large S_m truncation.

Method 1 can also be selected on a practical basis. The actual result of inverting i(S) information is the function $R[\rho(R)-\rho_o]$. This result is divided by R to obtain $[\rho(R)-\rho_o]$ thus tending to amplify the low R errors in the original inversion. Method 2 adjusts $\rho(R)$ to its proper value zero at R = 0 but has little relative effect elsewhere, being but a derivative condition. The behavior of $[\rho(R)-\rho_o]$ remains ordinarily so distorted at low radius (Appendix III) that it is excluded from representations in any case. At the other extreme, the function $R^2[\rho(R)-\rho_o]$ multiplies the inversion by R thus

amplifying truncation errors in the high-radius range. Method 1 tends to eliminate the highest-frequency ripples which affect a relatively long range in R as the distribution peaks in liquids damp down rapidly. Thus, method 1 in some form is often selected(14) on the basis of the appearance of the inversion.

These arguments do not imply that method 1 is the only good normalizing process. For a normalizing constant that does not satisfy (II-1), the resulting large radius oscillations can be simply taken as a necessary consequence of finite truncation. Supposing A_0 is the true unknown constant, the scattering function for any other constant A is related to the true scattering function $i_0(S)$ by

$$i(S) = \frac{A}{A_0} i_0(S) + \left(\frac{A}{A_0} - 1\right) \frac{I_{IC}(S)}{f^2(S)} \qquad \text{(II-21)}$$

which follows from (II-5). Supposing $i_0(S_m)$ is not necessarily zero, a finite value of $i(S_m)$ and the corresponding long-range density oscillations given by (II-20) have two components, a valid portion corresponding to truncation of $i_0(S)$, and a mathematical addition arising from incorrect normalization. Method 1, which makes $i_1(S_m)$ zero, pretends that at high S_m the second contribution would be more important. The long-distance oscillations, whether arising from truncation or incorrect normalization, constitute an error in the inversion. Therefore, the elim-

ination of this oscillation in method 1 does not of itself introduce significant error. The actual error of normalization appears in the factor A_1/A_0 which would multiply the true function $i_0(S)$ according to equation (II-21).

Setting (II-21) to zero at S_m gives the normalizing constant of method 1 as

$$\frac{A_1}{A_0} = \frac{\frac{I_{IC}(S_m)}{f^2(S_m)}}{\frac{I_{IC}(S_m)}{f^2(S_m)} + i_0(S_m)} \qquad \text{(II-22)}$$

As would be expected, the larger the independent scatter in comparison to interference, the closer the approximation. The error in normalization can be obtained from (II-22) and an estimate of the largest possible amplitude of $i_0(S_m)$. However, there seems to be no definitive way of obtaining such an estimate from fundamental considerations. The possible amplitude of $i_0(S_m)$ must be based on inspection of the general i(S) behavior with the likelihood of decreasing amplitude oscillations.

APPENDIX III

INVERSION CALCULATION

These derivations are for a third-order polynomial as the piecewise approximating function described in the text. Extension to higher-order polynomials or even other integrable functions should follow without difficulty.

The S range of interest is divided into N-1 panels by boundary values $0, S_1, S_2, \ldots S_N$. All the experimental i(S) data to be inverted lies between S_1 and S_N. The chosen truncation value S is near the upper end of the range, $S_{N-1} < S_m \leq S_N$. For the nth panel, $S_{n-1} \leq S \leq S_n$, an incremental S coordinate is defined by

$$s = S - S_{n-1} \tag{III-1}$$

and the approximating cubic expression by

$$i_n(s) = \sum_{k=0}^{3} c_{k,n} s^k \tag{III-2}$$

The notation $i_n(S)$ indicates the analytical approximation to i(S) in the restricted range of the nth panel. The shortened coordinate s was adopted to increase numerical precision in the

least-squares fit and, for the same reason, retained in performing the inversion.

The inversion formula is given by equation (4) of the text. However, primary interest is on the function $4\pi R^2[\rho(R)-\rho_o]$ describing the "excess" coordination number for a differential shell, which may be given as

$$O(R) = 4\pi R^2[\rho(R)-\rho_o] = \frac{2}{\pi}\int_0^{RS_m} Si(S)\sin(RS)\, d(RS) \qquad \text{(III-3)}$$

The contribution to this integral by the nth panel is

$$O_n(R) = \frac{2}{\pi}\int_{RS_{n-1}}^{RS_n} (S_{n-1}+s)\, i_n(s)\sin(RS)\, d(RS) \qquad \text{(III-4)}$$

Defining

$$h_n(s) = \frac{2}{\pi}(S_{n-1}+s)i_n(s)$$

$$h_n(s) = \frac{2}{\pi} S_{n-1} i_n(s) + \frac{2}{\pi} s\, i_n(s)$$

$$h_n(s) = \frac{2}{\pi} S_{n-1} \sum_0^3 c_{k,n} s^k + \frac{2}{\pi} \sum_0^3 c_{k,n} s^{k+1} \qquad \text{(III-5)}$$

the expression for $O_n(R)$ becomes

$$O_n(R) = \int_{RS_{n-1}}^{RS_n} h_n(s)\sin(RS)\, d(RS) \qquad \text{(III-6)}$$

A generalized indefinite integral for expressions of type (III-6) is readily obtained by parts

$$O(R) = - h(s)\cos(SR) + \frac{h'(s)}{R}\sin(SR) + \frac{h''(s)}{R^2}\cos(SR) - \frac{h'''(s)}{R^3}\sin(SR) - \frac{h^{iv}(s)}{R^4}\cos(SR) + \ldots \qquad \text{(III-7)}$$

The primes denote derivatives with respect to the argument. This layout of the integral continues to as many derivatives as necessary. In the present case the approximating function is a cubic in s or S which is augmented by a factor s or S in the integral, as shown by (III-5), so that no derivatives beyond the fourth need be considered. Expressions for the derivatives in terms of the polynomial coefficients follow from equation (III-5) and will not be given explicitly here. Evaluation of the contribution $O_n(R)$ follows from introducing the corresponding $h_n(s)$ and limits in (III-7)

$$\begin{aligned} O_n(R) = &- h_n(s_n)\cos(S_nR) + \frac{h_n'(s_n)}{R}\sin(S_nR) + \frac{h_n''(s_n)}{R^2}\cos(S_nR) \\ &- \frac{h_n'''(s_n)}{R^3}\sin(S_nR) - \frac{h_n^{iv}(s_n)}{R^4}\cos(S_nR) \\ &+ h_n(0)\cos(S_{n-1}R) - \frac{h_n'(0)}{R}\sin(S_{n-1}R) - \frac{h_n''(0)}{R^2}\cos(S_{n-1}R) \\ &+ \frac{h_n'''(0)}{R^3}\sin(S_{n-1}R) + \frac{h_n^{iv}(0)}{R^4}\cos(S_{n-1}R) \quad . \end{aligned} \qquad \text{(III-8)}$$

In (III-8), $s_n = S_n - S_{n-1}$ is the length of the nth panel. An exception occurs for the last panel. Since S_m is not necessarily equal to S_N, the integral limits s_N and S_N are replaced by $s_m = S_m - S_{N-1}$ and S_m.

The complete function O(R) is to be obtained by adding all panel contributions. Equation (III-8) shows that for each panel boundary S_n there will be terms contributed by the adjoining nth and (n+1)th panels, except for the outer bounds at S = 0 and $S = S_m$. To incorporate these into a general summation over the boundaries S_n, a 0th panel ($S<0$) and an (N+1)th panel ($S>S_m$) are invented for which all coefficients are zero.

$$c_{k,0} = 0 \quad , \quad c_{k,N+1} = 0 \tag{III-9}$$

This (N+1)th panel can be identified with truncation of data at $S = S_m$. The function O(R) is then

$$O(R) = -\sum_{0}^{N}\left[h_n(s_n)-h_{n+1}(0)\right]\cos(S_nR)$$

$$+\frac{1}{R}\sum_{0}^{N}\left[h'_n(s_n)-h'_{n+1}(0)\right]\sin(S_nR) \quad +\frac{1}{R^2}\sum_{0}^{N}\left[h''(s_n)-h''_{n+1}(0)\right]\cos(S_nR)$$

$$-\frac{1}{R^3}\sum_{0}^{N}\left[h'''_n(s_n)-h'''_{n+1}(0)\right]\sin(S_nR) \quad -\frac{1}{R^4}\sum_{0}^{N}\left[h^{iv}_n(s_n)-h^{iv}_{n+1}(0)\right]\cos(S_nR) \; . \tag{III-10}$$

In (III-10) $S_0 = 0$, $S_N = S_m$, $s_N = S_m - S_{N-1}$ and the bracketed coefficients are given in terms of the polynomial coefficients by differentiating equation (III-5).

The combination of terms expressed by equation (III-10) was the one actually used in computation except for consecutive factoring or nesting of (1/R) factors. This combination seems advantageous in that, aside from bounded trigonometric terms, each value of R enters at the end of the calculation in a numerically-consistent manner.

By earlier stipulation, there is no experimental data for the 1st panel and the corresponding approximating function must be assumed. For this investigation it was considered adequate to put $S_1 = 1.5\ \text{Å}^{-1}$ and

$$i_1(s) = -1 \qquad \text{(III-11)}$$

whereby the corresponding polynomial coefficients are $c_{0,1} = -1$ and the rest are zero as shown in Tables VI.

With equation (III-10) the entire inversion spectrum on R has been replaced by selected frequencies, both sine and cosine, corresponding to the chosen panel boundaries. This substitution does not constitute a loss of information. It was accomplished on the premise that the approximating functions $i_n(s)$ did represent the scattering function within experimental

accuracy. Thus, the distribution of frequencies with relatively complicated amplitudes in (III-10) is actually an intermediate inversion step.

Equation (III-10) reveals some essential features of the inversion method and the inversion itself. These features are of general validity because any inversion calculation must use some similar approximating scheme for i(S). Errors in the measuring, normalizing, fitting, and computation must appear in the h(s) amplitudes of (III-10). The (1/R) factors suggest that such errors will be amplified at small values of R, in keeping with the general observation that distributions obtained in this manner are usually distorted in that range. Furthermore, the fluctuations caused by these errors will be most noticeable for the higher frequencies and may have the general appearance of a true truncation error.

Towards large values of R, on the other hand, these error contributions will be damped. The function O(R) itself will ultimately vanish except for the leading term in (III-10). The amplitudes in this term are simply

$$-\left[h_n(s_n)-h_{n+1}(0)\right] = -\frac{2}{\pi} S_n\left[i_n(S_n)-i_{n+1}(S_n)\right] \qquad \text{(III-11)}$$

Thus, these amplitudes are proportional to the discontinuities in the approximating functions at panel boundaries, including

the discontinuity at the truncation point S_m. This last observation is in agreement with the conclusions concerning normalization reached in Appendix II. The discontinuity at S_m is set to zero by the method of normalization, but the intermediate discontinuities, which are strictly due to experimental and approximating errors, are barely affected in the process. However, the ultimate disappearance of long-range order requires that the leading term of (III-10) be zero, and, in keeping with the normalization argument, the discontinuities should be eliminated.

This consideration led to the method of overlapped fitting described in the text. The approximating polynomial $i_n(s)$ for a panel was fitted to the points within the panel and the adjoining half panels. It was further required that

$$i_n(0) = c_{0,n} = i_{n-1}(s_{n-1}) \qquad \text{(III-12)}$$

Thus, the leading coefficient of a polynomial is determined by the preceding polynomial and no first-order discontinuities occur.

NOMENCLATURE

A - normalization constant

a - absorption variation exponent for sample

B - modified/incident wavelength ratio

b - absorption variation exponent for the beta filter

C - counts

c - coeffieient

D - sample-to-counter transmission factor

E - detected power (counts/second)

f - atomic scattering factor

F - scatter function

g - radial distribution function

H - scattered beam height at sample

h - function in inversion calculation

i - interference scattering function

I - radiation intensity (quanta/time-area)

k - maximum wavelength modification

L - scattering length of liquid surface

N - number of atoms, number of inversion panels

O - coordination function

Q - angle-dependent correction factor

R - radius from reference atom

S - scattering parameter

s - incremental S within inversion panel

t - beta-filter thickness

W - scattering width of liquid surface

Greek

α - angle of incident beam to liquid surface

γ - surface energy

2θ - angle of scatter

λ - wavelength of radiation

μ - absorption coefficient

ρ - liquid density (atoms/volume)

Subscripts

B - background signal

C - corrected

coh - coherent

D - sample-to-counter absorbers (beta filter)

I - independent

M - modified

mod - modified

m - truncation value of S

X - experimental

o - average density or incident radiation

REFERENCES

1. E. N. da C. Andrade, "A theory of the viscosity of liquids," Phil. Mag. 17, 497 and 698 (1934).
2. H. Eyring, T. Ree, N. Hirai, "Significant structures in the liquid state," Proc. Natl. Acad. Sci. 44, 683 (1958).
3. G. H. Wagner, W. H. Gitzen, "Gallium," J. Chem. Ed. 29, 162 (1952).
4. D. Turnbull, "The subcooling of liquid metals," J. App. Phys. 20, 817 (1949).
5. L. J. Briggs, "Gallium: thermal conductivity, supercooling; negative pressure," J. Chem. Phys. 26, 784 (1957).
6. A. Defrain, I. Epelboin, M. Erny, "Sur la surfusion du gallium," Comptes Rendus 248, 1486 (1959).
7. B. D. Sharma, J. Donohue, "A refinement of the crystal structure of gallium," Z. Krist. 117, 293 (1962).
8. L. Pauling, General Chemistry, 2nd ed., p. 492, W. H. Freeman, San Francisco (1953).
9. F. C. Frank, "Supercooling of liquids," Proc. Roy. Soc. A215, 43 (1952).
10. J. H. Hollomon, D. Turnbull, "Nucleation," Prog. Met. Phys. 4, 333 (1953).
11. D. Turnbull, "Formation of crystal nuclei in liquid metals," J. App. Phys. 21, 1022 (1950).

12. J. Jack, F. Sebba, "The melting of gallium," Trans. Far. Soc. 50, 226 (1954).

13. H. Menke, "Rontgeninterferenzen an Flussigkeiten," Phys. Z. 33, 593 (1932).

14. K. Furukawa, "The radial distribution curves of liquids by diffraction methods," Rep. Prog. Phys. 25, 395 (1962).

15. R. F. Kruh, "Diffraction studies of the structure of liquids," Chem. Rev. 62, 319 (1962).

16. R. F. Kruh, G. T. Clayton, C. Head, G. Sandlin, "Structure of liquid mercury," Phys. Rev. 129, 1479 (1963).

17. K. Furukawa, B. R. Horton, J. Hamor, G. I. Williams, "The structure of liquid tin," Phil. Mag. 8, 141 (1963).

18. B. R. T. Frost, "The structure of liquid metals," Prog. Mct. Phys. 5, 96 (1954).

19. H. Hendus, "Die Atomverteilung in den flussigen Elementen Pb, Tl, In, Au, Sn, Ga, Bi, Ge und in flussigen Legierungen des Systems Au-Sn," Z. Naturf. 2a, 505 (1947).

20. O. Pfannenschmid, "Atomverteilung in flussigen Quecksilber, geschmolzenem Silber und Gold," Z. Naturf. 15a, 603 (1960).

21. O. Kubaschewski, "The change of entropy, volume, and binding state on melting," Trans. Far. Soc. 45, 931 (1949).

22. R. W. Powell, "The electrical resistivity of gallium and some other anisotropic properties of this metal," Proc. Roy. Soc. A209, 525 (1951).

23. K. E. Spells, "The determination of the viscosity of liquid gallium over an extended range in temperature," Proc. Phys. Soc. London 48, 299 (1936).

24. N. N. Greenwood, R. L. Martin, "Discontinuities in the physical properties of supercooled liquids," Proc. Roy. Soc. A215, 46 (1952).

25. E. McLaughlin, A. R. Ubbelohde, "Prefreezing phenomena in molten metals," Trans. Far. Soc. 56, 988 (1960).

26. R. W. James, The Optical Principles of the Diffraction of X Rays, 2nd ed., Chap. IX, G. Bell and Sons, London (1958).

27. G. Fournet, "Etude de la structure des fluides et des substances amorphes au moyen de la diffusion des rayons X," Handbuch der Physik, Vol. XXXII (1957).

28. R. G. Dorsch, B. Bemrose, "X-ray diffraction study of the internal structure of supercooled water," *N.A.C.A. Technical Note 2532 (October 1956).*

29. H. K. F. Muller, H. Hendus, "Die Atomverteilung in flussigen Antimon," Z. Naturf. 12a, 896 (1957).

30. R. Speiser, H. L. Johnston, "Vapor pressure of inorganic substances. IX Gallium," J. Am. Chem. Soc. 75, 1469 (1953).

31. S. E. Rodriguez, C. J. Pings, "Cell for X-ray diffraction studies of absorbing liquids," Rev. Sci. Instr. 33, 1469 (1962).

32. Communication from Aluminum Company of America (Dec. 1960).

33. Communication from Aluminum Company of America (March, 1949).

34. W. Parrish, E. A. Hamacher, K. Lowitzch, "The Norelco X-ray diffractometer," Philips Tech. Rev. 16, No.4, 123 (1954).

35. S. Boyer, "Gallium-in-quartz thermometer graduated to 1000°C.," Ind. Eng. Chem. 17, 1252 (1925).

36. D. Turnbull, "Kinetics of heterogeneous nucleation," J. Chem. Phys. 18, 198 (1950).

37. B. D. Cullity, Elements of X-Ray Diffraction, Appendix 3, Addison-Wesley Publishing, Reading (1956).

38. Internationale Tabellen zur Bestimmung von Kristallstrukturen, pp. 577-578, Gebruder Borntraeger, Berlin (1935).

39. W. Parrish, T. R. Kohler, "Use of counter tubes in X-ray analysis," Rev. Sci. Instr. 27, 795 (1956).

40. W. Parrish, "X-ray intensity measurements with counter tubes," Philips Tech. Rev. 17, No. 7-8, 206 (1956).

41. A. J. Freeman, "Atomic scattering factors for spherical and aspherical charge distributions," Acta Cryst. 12, 261 (1959).

42. R. W. James, reference 26, p. 152.

43. D. T. Cromer, "Anomalous dispersion corrections computed from relativistic Hartree-Dirac-Slater wave equations," Unpublished.

44. A. J. Freeman, "A study of the Compton scattering of X-rays: Ne, Cu^{+}, Cu and Zn^{++}," Acta Cryst. 12, 274 (1959).

45. A. J. Freeman, "X-ray incoherent scattering functions for non-spherical charge distributions: N, N^-, C^-, O, O^+, O^{++}, O^{+++}, F, F^-, Si^{++++}, Si^{+++}, Si, and Ge," Acta Cryst. 12, 929 (1959).

46. W. Heisenberg, "Uber die inkoharente Streuung von Rontgenstrahlen," Phys. Z. 32, 737 (1931).

47. T. L. Hill, Statistical Mechanics, p. 185, McGraw-Hill, New York (1956).

48. L. Pauling, "Atomic radii and interatomic distances in metals," J. Amer. Chem. Soc. 69, 542 (1947).

49. R. W. James, reference 26, p. 463.

50. A. H. Compton, S. K. Allison, X Rays in Theory and Experiment, 2nd ed., p. 235, D. van Nostrand, Princeton (1935).

51. R. B. Leighton, Principles of Modern Physics, p. 433 and App. A, McGraw-Hill, New York (1959).

52. A. H. Compton, S. K. Allison, reference 50, p. 533.

53. J. Krogh-Moe, "A method for converting experimental X-ray intensities to an absolute scale," Acta Cryst. 9, 951 (1956).

54. J. Waser, V. Schomaker, "The Fourier inversion of diffraction data," Rev. Mod. Phys. 25, 671 (1953).

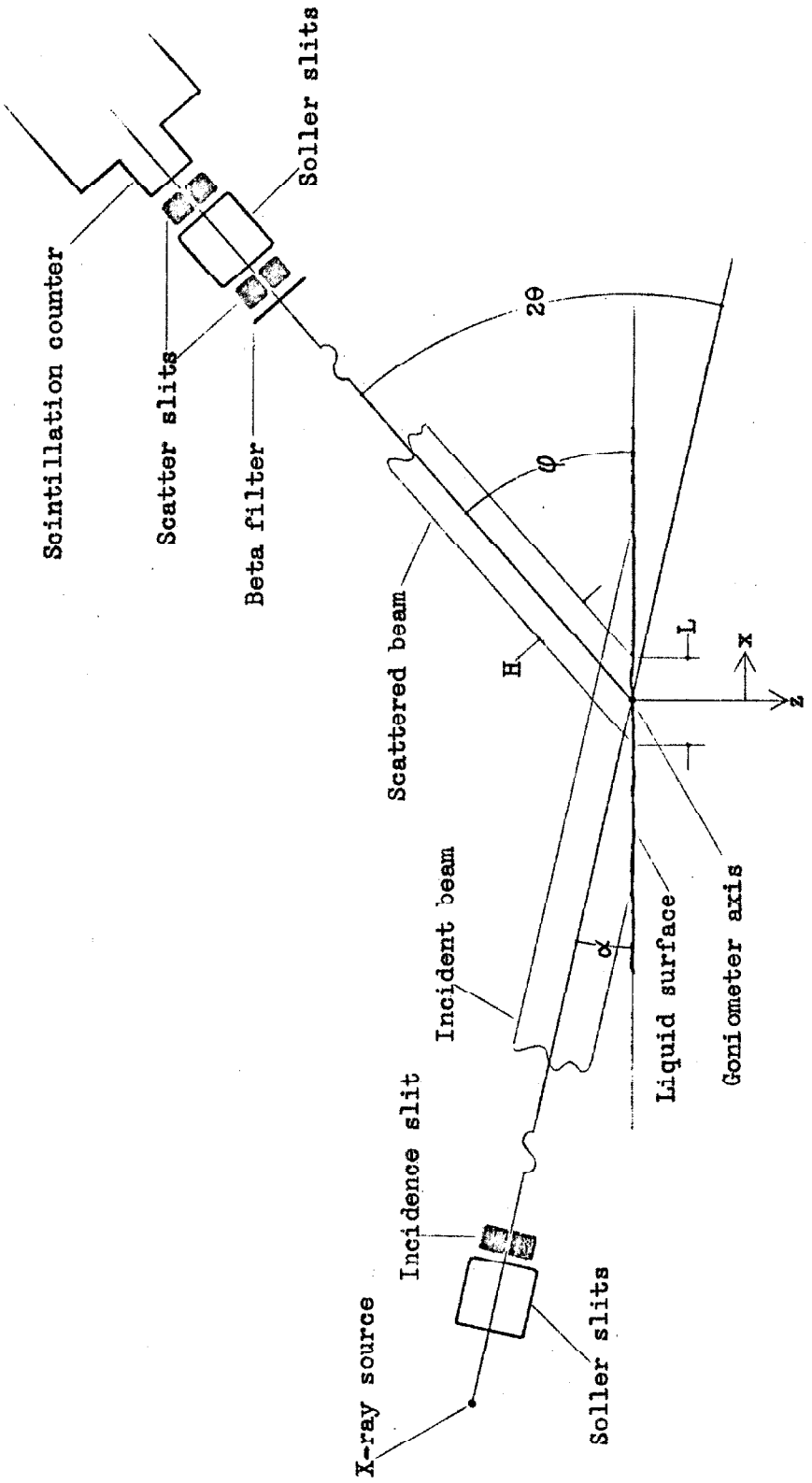

Figure 1. Diagram of diffraction scheme.

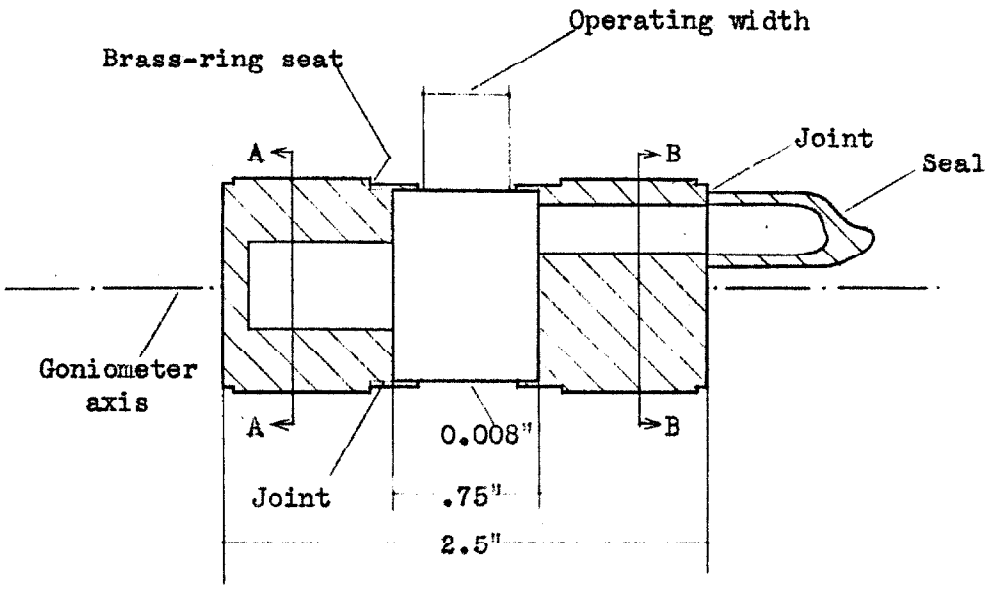

Vertical section along goniometer axis
seen from X-ray source side.
Cell shown empty.

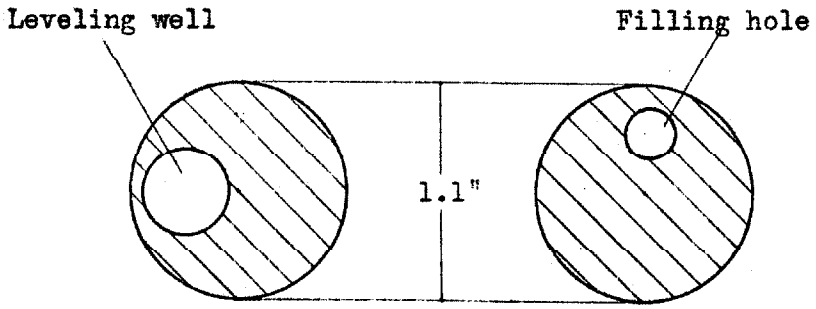

Figure 2. Inner sample cell.

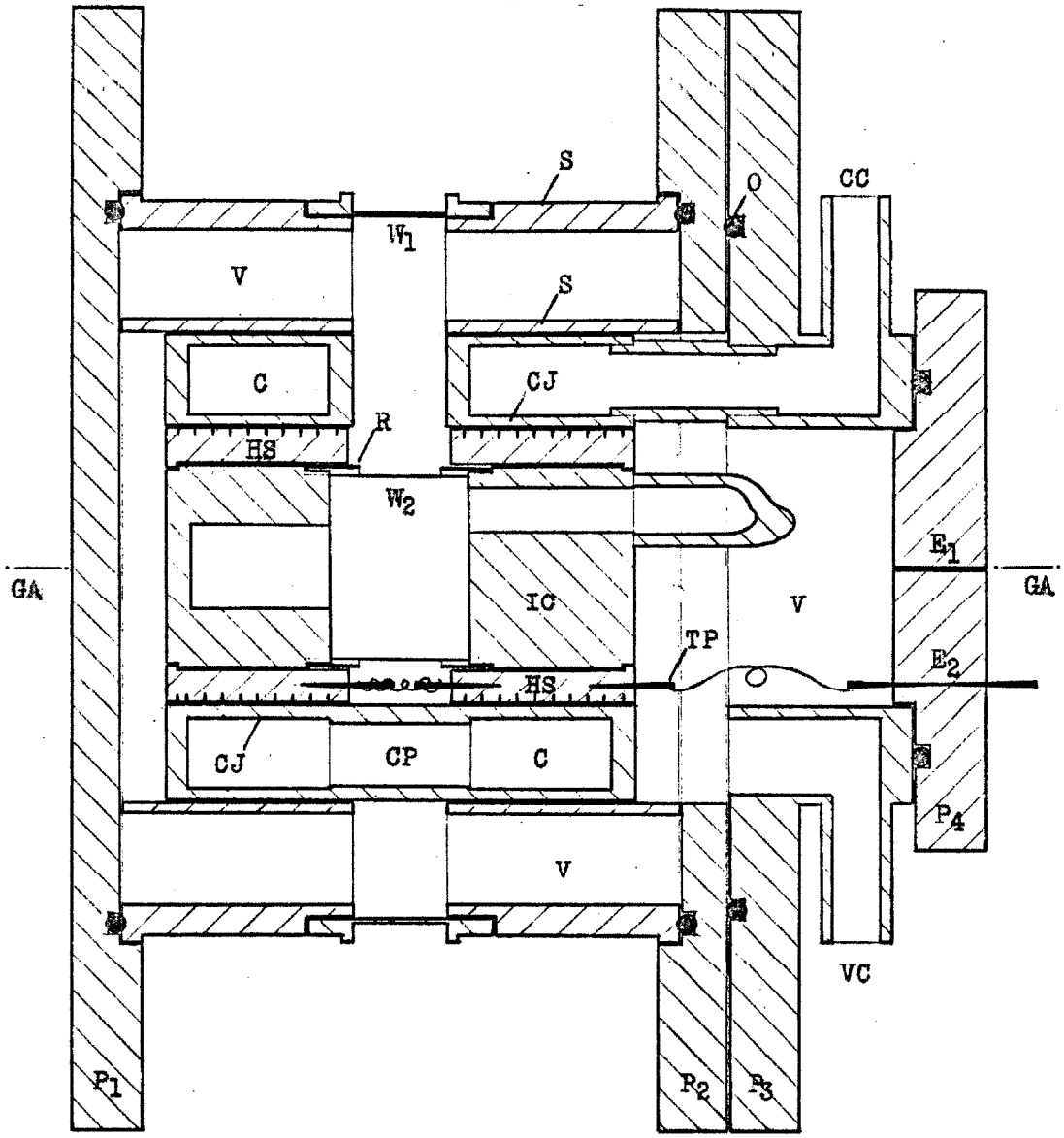

GA - Goniometer axis
IC - Inner cell
W_1, W_2 - X-ray windows
R - Brass ring
S - Outer shell
P_1, P_2 - End plates
O - O-ring
V - Vacuum
C - Coolant
CJ - Coolant jacket
P_3 - Coolant jacket plate
CC - Coolant connections (2)
CP - Coolant passages (2)
HS - Heater sleeves
TP - Taper pins (2)
P_4 - Entry plate
E_1 - Thermocouple entry
E_2 - Heater leads

Figure 3. Sample-containing assembly. Actual size. Vertical section seen from X-ray source side.

Figure 4. General view of diffraction arrangement.

Figure 5. Sample assembly. View along scattering plane from detector side.

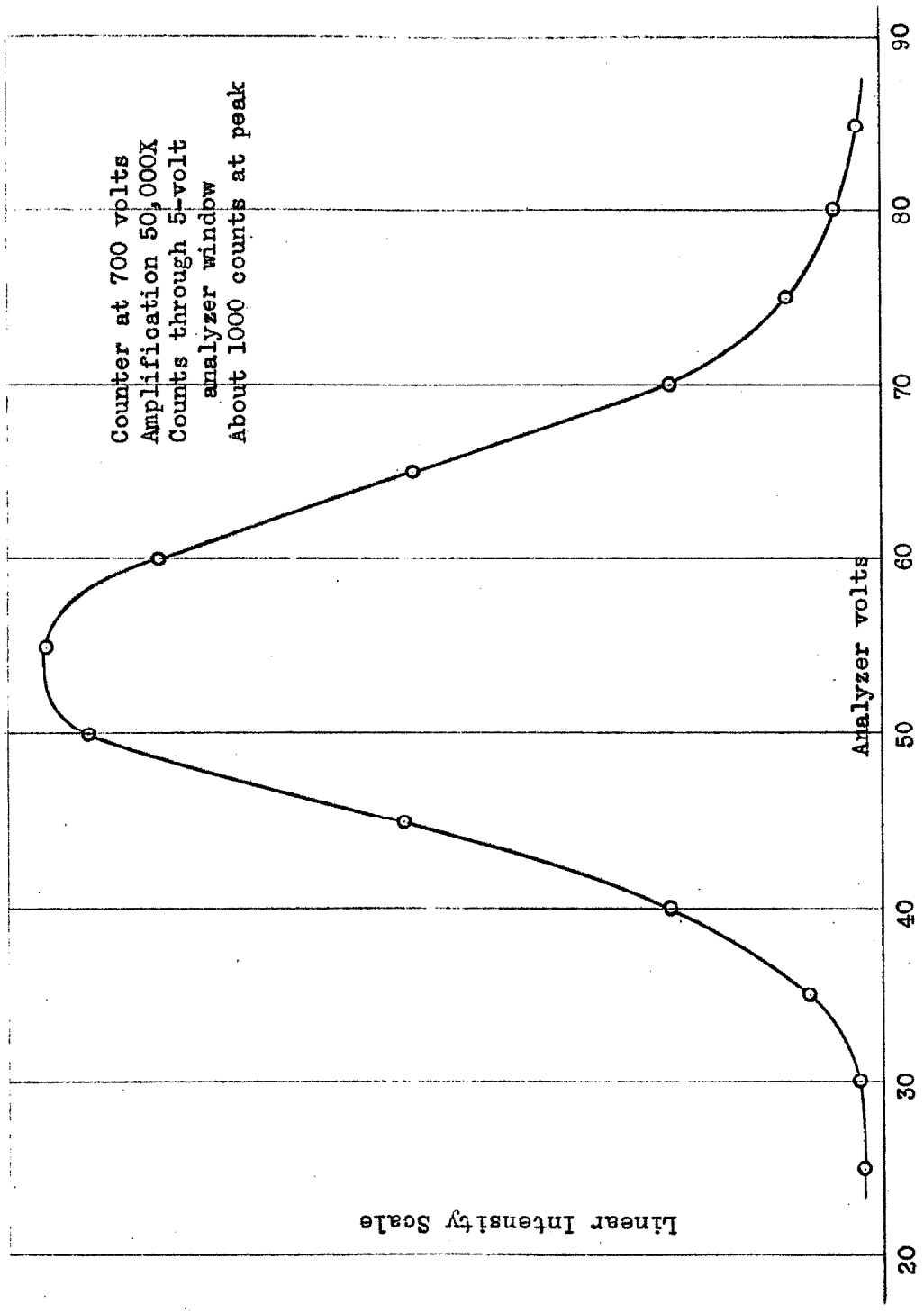

Figure 6. Analyzer pulse-amplitude distribution of scatter by Gallium at 2θ=12.75°.

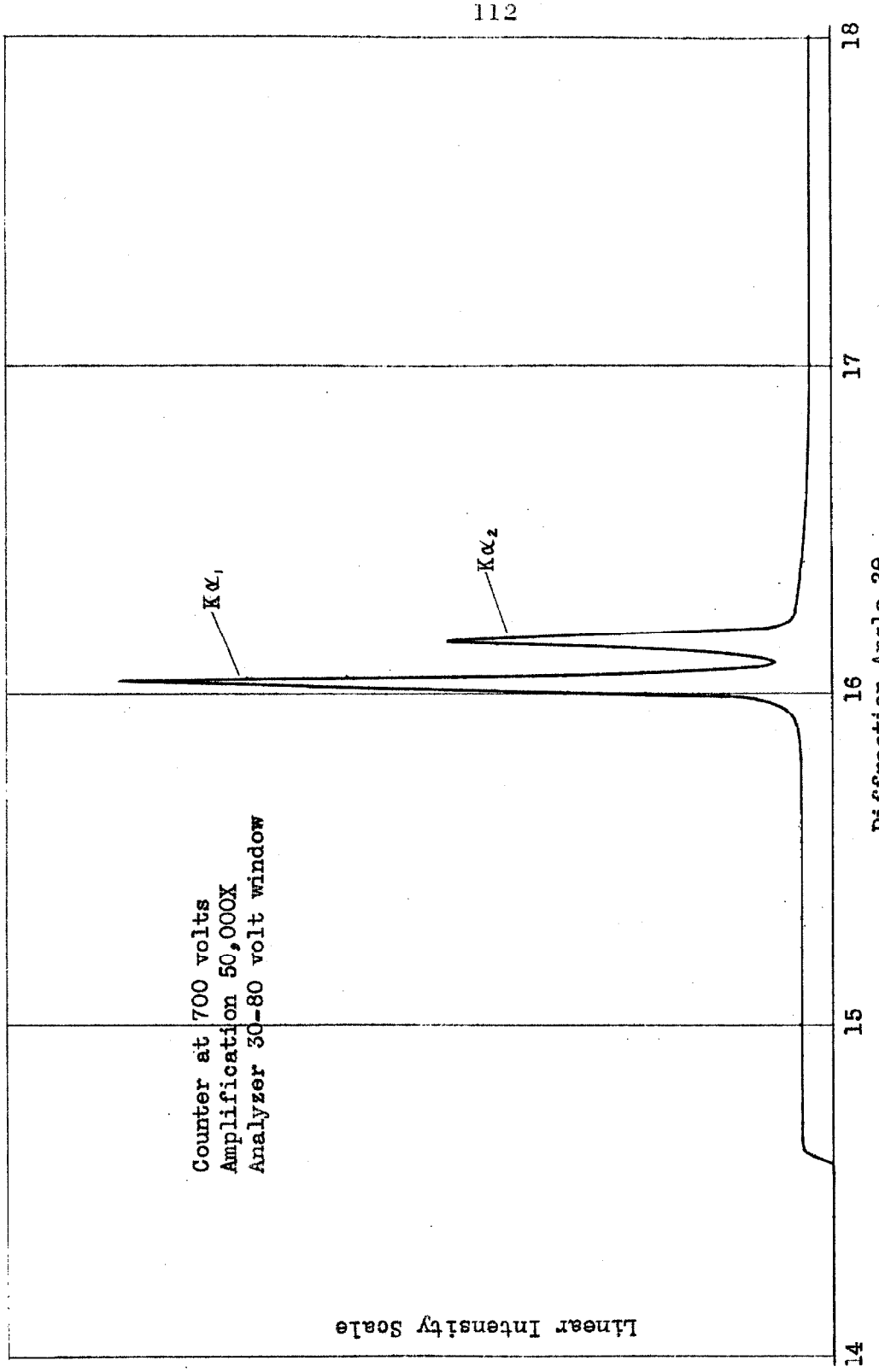

Figure 7. LiF-crystal spectrum of incident radiation.

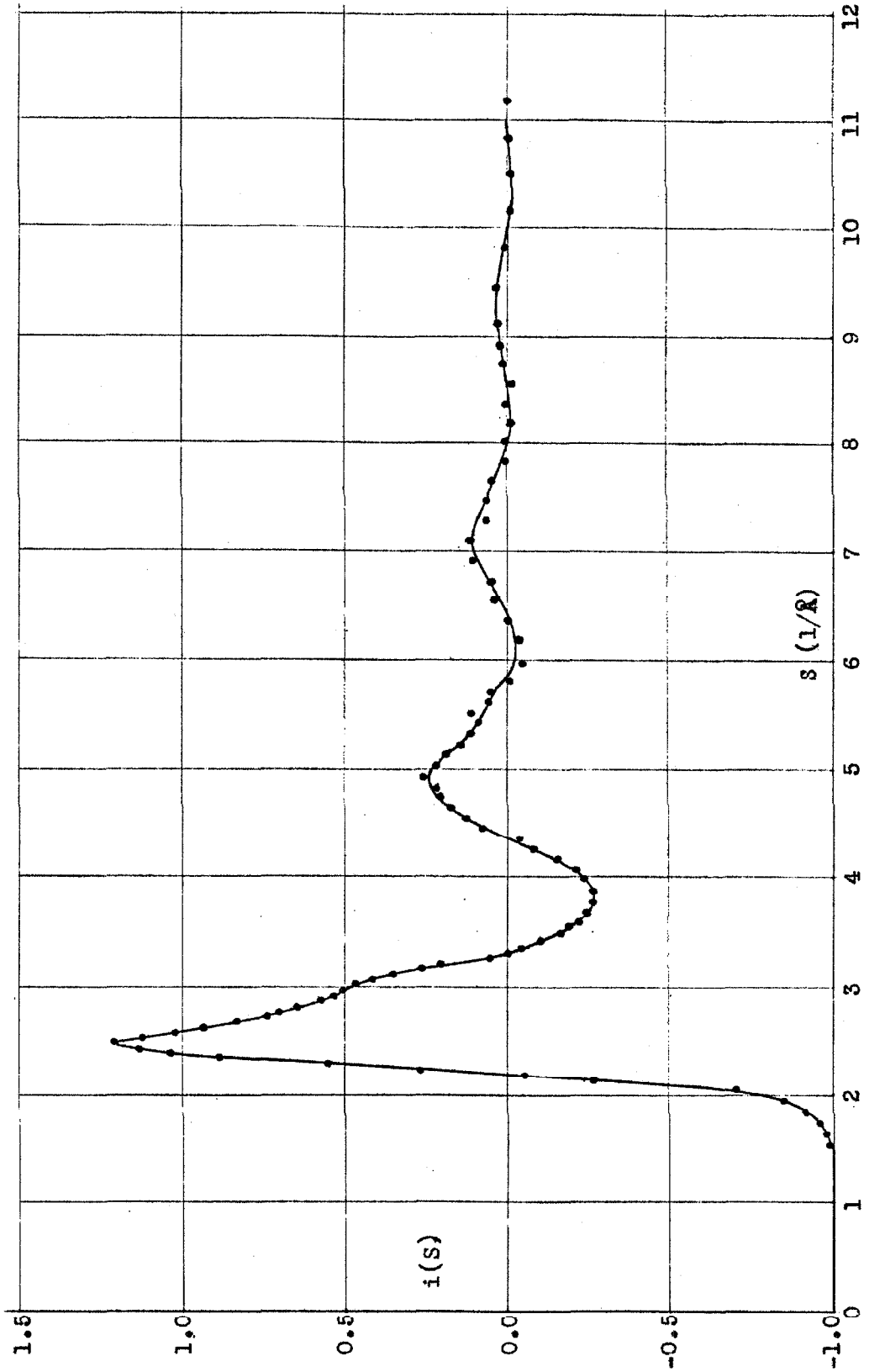

Figure 8. Scattering function data and approximation at 0.0 °C.

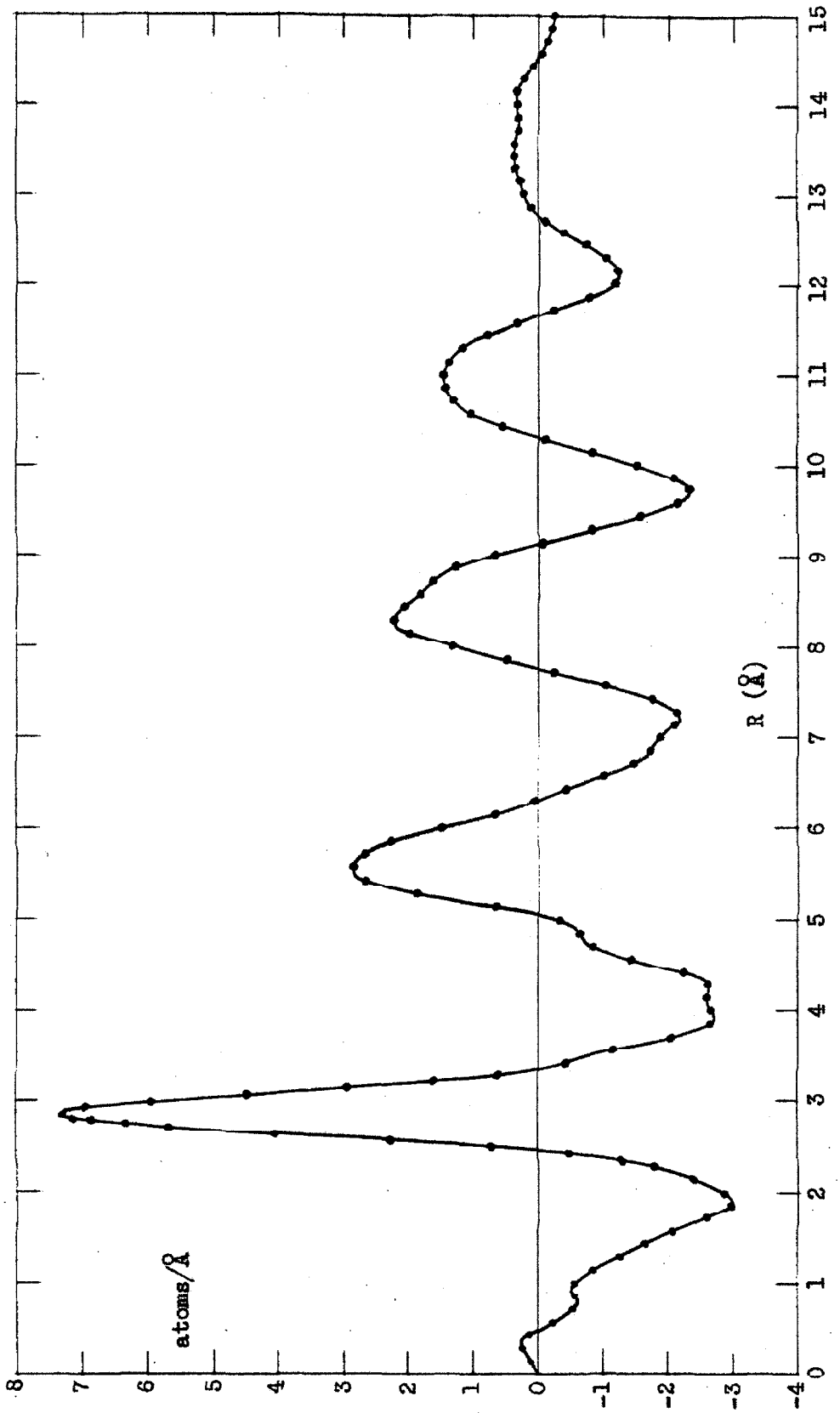

Figure 9. Inversion for $4\pi R^2[\rho(R)-\rho_o]$ distribution at 0.0 °C.

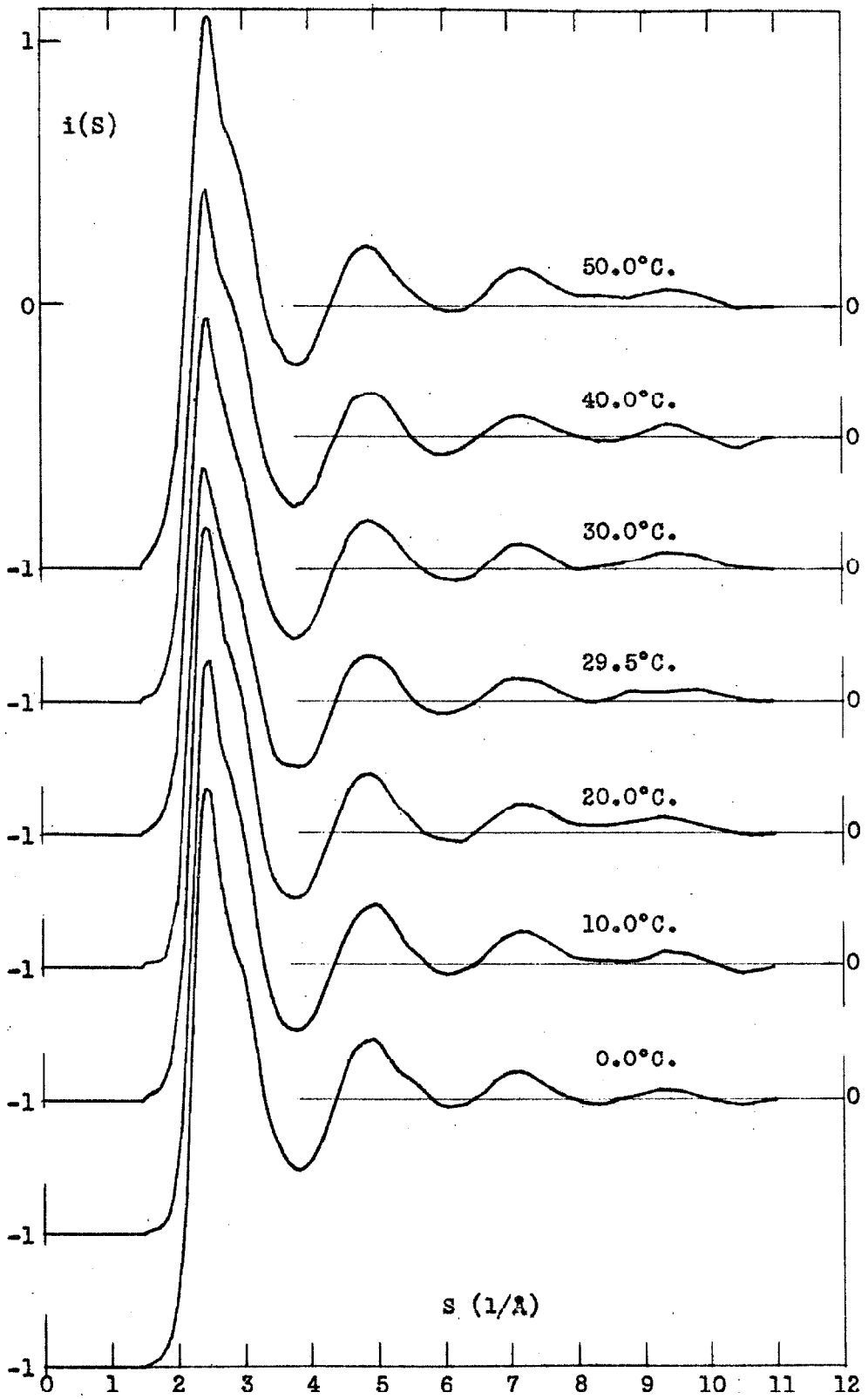

Figure 10. Approximations to scattering functions.

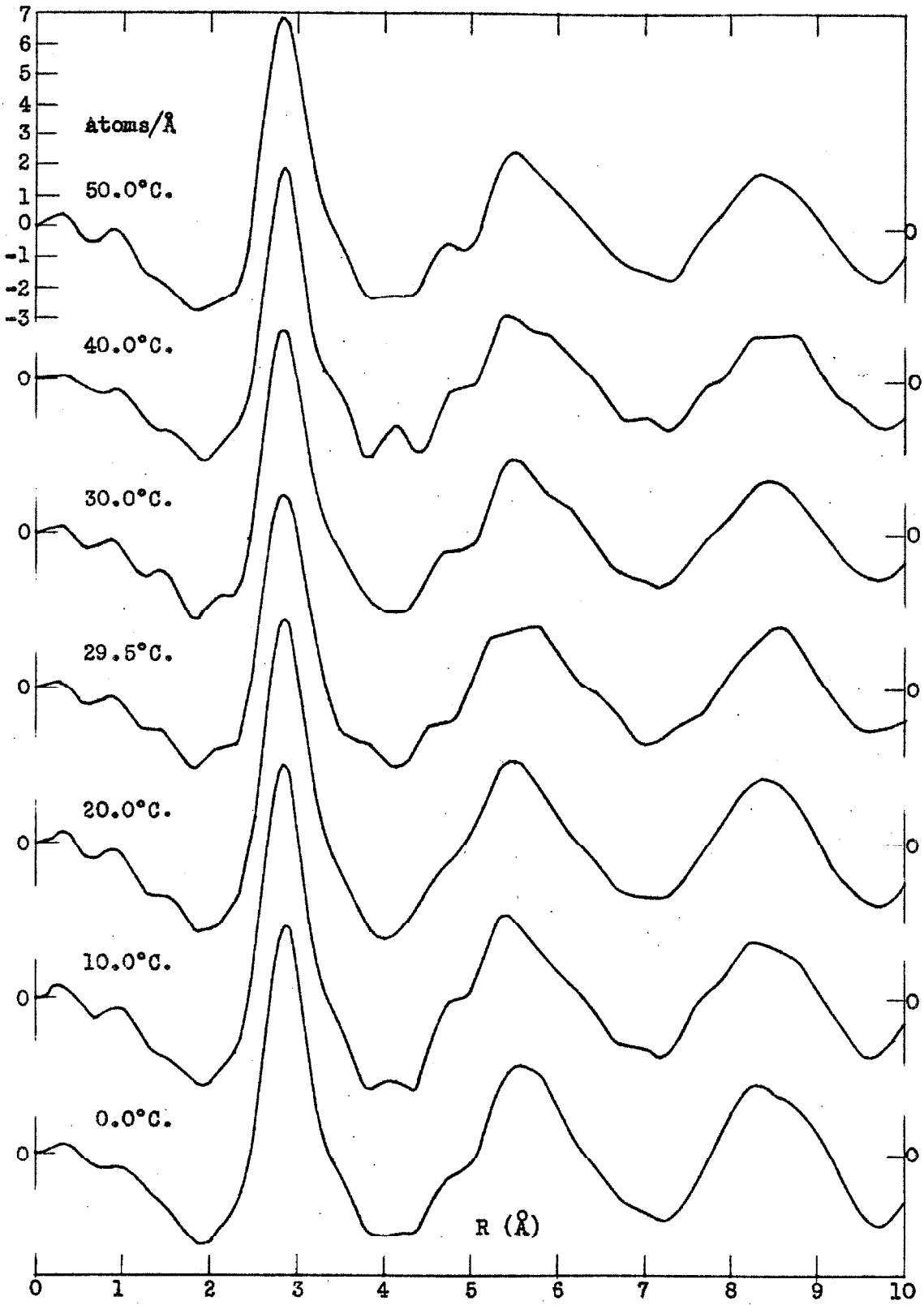

Figure 11. $4\pi R^2[\rho(R)-\rho_o]$ inversions.

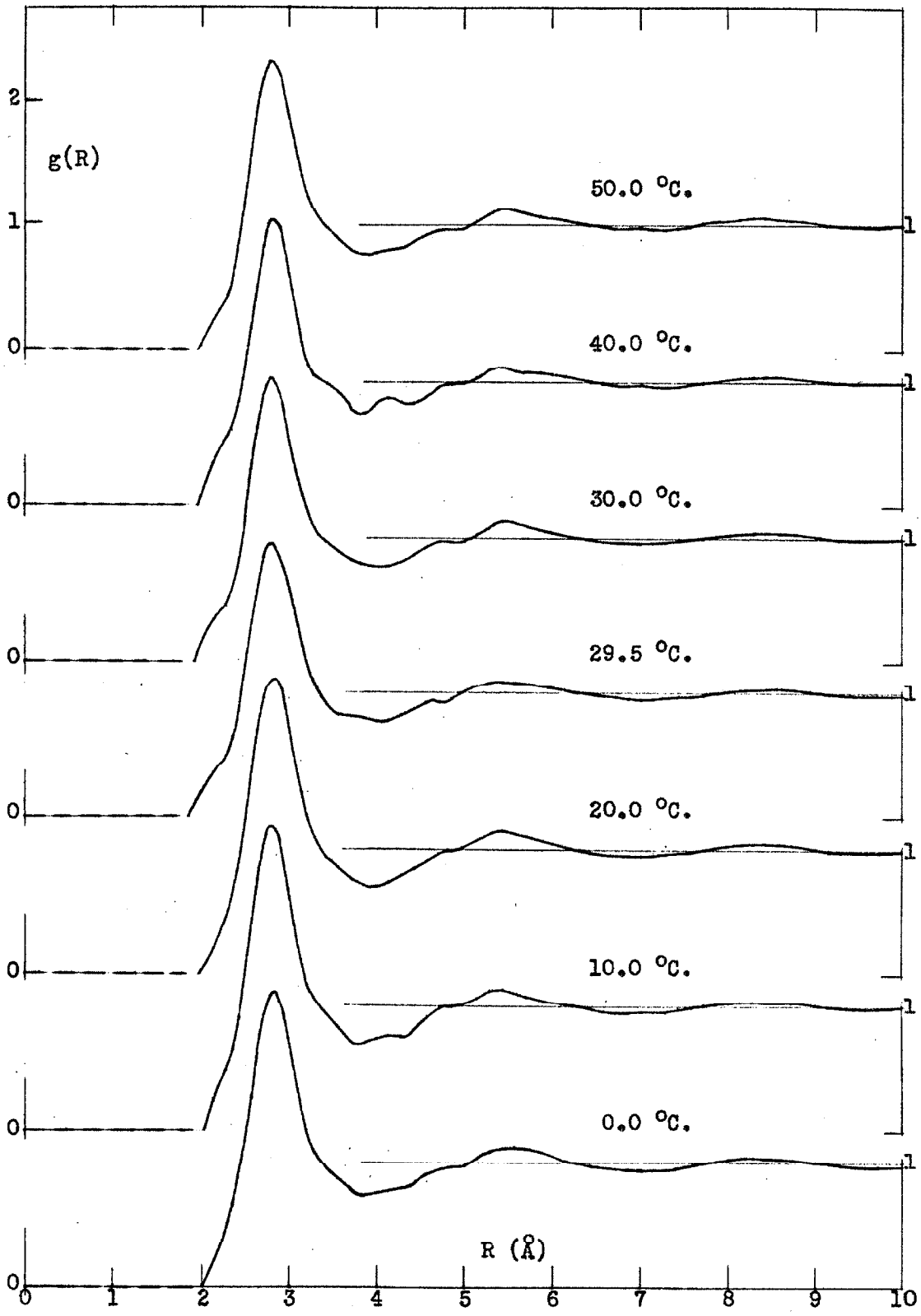

Figure 12. Radial distribution functions.

TABLE I

Special values used in calculations

$\lambda = 0.5608$ Å	Weighted average of Ag K-alpha lines from reference 37.
$\alpha = 4.80^{\circ}$	Measured.
$a = 2.74$	Absorption coefficients from ref. 38. Exponents for variation in absorption with wavelength estimated from coefficients for Ag and Rh K-alpha radiation. Beta filter thickness of no more than 0.0035 inches.
$b = 2.65$	
$\mu_D t = 1.41$	

$\rho_o = 0.0525$ atoms/Å^3 at 0°C.	Estimated from liquid densities in reference 3.
$\rho_o = 0.0528$ atoms/Å^3 at 50°C.	

TABLE II

Scanning plan

Approx. 2θ range	2θ increment	Scatter slits (in.)	Relative Power	Angular resolution	Counting mode
8°-13°	0.50°	0.002 0.001	0.11	0.12°	1000.0 secs.
11°-18°	0.25°	0.002 0.003	0.33	0.18°	10/1200.0 secs.
16°-30°	0.50°	0.003 0.007	1.0	0.40°	15/1600.0 secs.
26°-46°	1.00°	0.007 0.009	4.1	0.53°	4,000 counts
40°-64°	2.00°	0.009 0.021	12	1.25°	10,000 counts
55°-up	3.00°	0.021 0.021	29	1.25°	10,000 counts

TABLE III

Independent scatter data

$\frac{\sin\theta}{\lambda}$	f (Ga) ref. 41	F_M (Cu) ref. 44	F_M (Ge) ref. 45	F_M (Ga) interp.
0	31	0	0	0
0.1	28.31	1.99	1.59	1.72
0.2	24.49	5.26	4.75	4.92
0.3	20.96	8.15	7.39	7.64
0.4	17.73	10.70	10.02	10.25
0.5	14.90	12.90	12.54	12.66
0.6	12.57	14.82	14.73	14.76
0.7	10.74	16.46	16.59	16.55
0.8	9.36			
0.9	8.35	19.02	19.59	19.40
1.0	7.59			
1.1	7.03	20.80	21.90	21.53
1.3	6.22			
1.5	5.59			
1.7	4.99			
1.9	4.43			

Dispersion corrections(43): $\Delta f'_K = 0.38$, $\Delta f''_K = 1.16$

TABLE IV

Summary information

Temperature (°C.)		50.0	40.0	30.0	29.5	20.0	10.0	00.0
i(S)								
1st max.	S(Å^{-1})	2.51	2.49	2.51	2.47	2.50	2.51	2.48
	i(S)	1.10	0.94	0.95	0.88	1.17	1.16	1.18
Shoulder	S(Å^{-1})	3.10	3.06	3.10	2.99	3.10	3.12	3.08
	i(S)	0.42	0.36	0.31	0.32	0.41	0.39	0.41
2nd max.	S(Å^{-1})	4.90	4.96	4.92	4.85	4.92	5.00	4.94
	i(S)	0.23	0.17	0.19	0.18	0.23	0.24	0.24
3rd max.	S(Å^{-1})	7.22	7.23	7.19	7.12	7.23	7.19	7.08
	i(S)	0.14	0.08	0.10	0.09	0.12	0.14	0.11
g(R)								
1st max.	R(Å)	2.81	2.82	2.80	2.80	2.82	2.81	2.83
	g(R)	2.39	2.29	2.26	2.19	2.36	2.43	2.36
2nd max.	R(Å)	5.47	5.43	5.47	5.48	5.45	5.39	5.52
	g(R)	1.12	1.11	1.12	1.09	1.14	1.14	1.14
3rd max.	R(Å)	8.33	8.35	8.41	8.52	8.36	8.28	8.27
	g(R)	1.04	1.03	1.04	1.04	1.04	1.04	1.05
$4\pi R^2\rho(R)$								
Zero	R(Å)	1.99	1.96	1.94	1.90	2.03	2.01	2.03
1st max.	R(Å)	2.85	2.87	2.86	2.87	2.88	2.86	2.89
	(atoms/Å)	12.2	12.3	12.0	11.7	12.6	12.9	12.8
Coordination number (atoms)	A	8.00	8.42	8.42	8.74	9.00	8.86	9.20
	B	10.8	10.7	10.8	10.7	11.0	11.0	11.1
	C	10.6	10.6	10.7	10.6	10.8	10.6	10.8

Table V-A

Diffraction data for 50.0 °C.

TEMPERATURE 50.0 °C.
NORMAL FACTOR A = 8440.74 SEC/CTS
BACKGROUND E_B = 0.048-0.048 CTS/SEC
CCUNTING FOR 1000.0 SECONDS

2θ(o)	COUNTS	S(1/Å)	AE_{XC}	I_{coh}/NI_o	i(S)
7.00	98	1.368	25.95	23.98	-0.970
7.50	80	1.465	17.81	15.62	-0.980
8.00	105	1.563	33.89	31.46	-0.959
8.50	150	1.661	64.51	61.83	-0.918
9.00	184	1.758	91.18	88.26	-0.881
9.50	247	1.855	141.01	137.85	-0.810
10.00	347	1.953	223.33	219.91	-0.690
10.50	537	2.050	384.04	380.37	-0.452
11.00	657	2.148	501.78	497.85	-0.266
11.50	983	2.245	806.61	802.43	0.212
12.00	1299	2.342	1127.89	1123.45	0.737
12.50	1485	2.439	1351.72	1347.03	1.133
13.00	1407	2.537	1331.67	1326.73	1.152

Table V-A

(Continued)

TEMPERATURE 50.0 °C.
NORMAL FACTOR A = 2614.87 SEC/CTS
BACKGROUND E_B = 0.040-0.040 CTS/SEC
COUNTING FOR 1000.0 SECONDS

2θ(°)	COUNTS	S(1/Å)	AE_{XC}	I_{coh}/NI_o	i(S)
11.00	2252	2.148	564.62	560.69	-0.173
11.25	2740	2.196	705.37	701.31	0.046
11.50	3268	2.245	862.70	858.51	0.296
11.75	3846	2.294	1040.08	1035.77	0.582
12.00	4196	2.342	1160.79	1156.35	0.788
12.25	4409	2.391	1246.69	1242.13	0.944
12.50	4347	2.439	1255.09	1250.40	0.980
12.75	4604	2.488	1357.69	1352.87	1.169
13.00	4245	2.537	1276.48	1271.54	1.063
13.25	4039	2.585	1238.33	1233.28	1.023
13.50	3683	2.634	1150.35	1145.20	0.901
13.75	3510	2.682	1116.98	1111.72	0.866
14.00	3171	2.731	1027.08	1021.71	0.735
14.25	2944	2.779	970.49	965.02	0.658
14.50	3006	2.828	1009.51	1003.93	0.745
14.75	2655	2.876	906.22	900.53	0.583
15.00	2550	2.925	885.39	879.60	0.565
15.25	2408	2.973	850.02	844.12	0.519
15.50	2346	3.022	842.13	836.13	0.522
15.75	2179	3.070	794.50	788.41	0.452
16.00	2006	3.118	742.56	736.36	0.373
16.25	1897	3.167	713.05	706.75	0.333
16.50	1638	3.215	623.66	617.26	0.178
16.75	1583	3.264	611.93	605.44	0.169
17.00	1376	3.312	538.30	531.70	0.039
17.25	1277	3.360	506.26	499.56	-0.012
17.50	1142	3.409	458.02	451.23	-0.097
17.75	1160	3.457	472.65	465.76	-0.057
18.00	1076	3.505	443.83	436.84	-0.105

Table V-A

(Continued)

TEMPERATURE 50.0 °C.
NORMAL FACTOR A = 960.30 SEC/CTS
BACKGROUND E_B = 0.047-0.104 CTS/SEC
COUNTING FOR 1600.0 SECONDS

2θ(°)	COUNTS	S(1/Å)	AE_{XC}	I_{coh}/NI_o	i(S)
16.00	8571	3.118	736.52	730.33	0.361
16.50	7286	3.215	645.66	639.26	0.220
17.00	6055	3.312	552.45	545.86	0.067
17.50	5101	3.409	478.58	471.79	-0.056
18.00	4611	3.505	444.82	437.83	-0.103
18.50	4073	3.602	403.37	396.18	-0.168
19.00	3839	3.698	390.48	383.10	-0.176
19.50	3428	3.795	357.26	349.69	-0.230
20.00	3299	3.891	352.71	344.94	-0.221
20.50	3248	3.987	356.26	348.30	-0.194
21.00	3207	4.083	360.70	352.55	-0.164
21.50	3198	4.179	368.75	360.41	-0.124
22.00	3251	4.275	384.38	375.85	-0.063
22.50	3296	4.371	399.38	390.66	-0.002
23.00	3401	4.467	422.43	413.52	0.083
23.50	3393	4.563	431.29	422.19	0.134
24.00	3345	4.659	434.75	425.46	0.172
24.50	3262	4.754	433.12	423.65	0.197
25.00	3081	4.850	417.15	407.51	0.181
25.50	3157	4.945	437.23	427.41	0.270
26.00	2879	5.040	405.52	395.52	0.205
26.50	2646	5.136	378.83	368.66	0.153
27.00	2566	5.231	374.28	363.93	0.167
27.50	2365	5.326	350.15	339.63	0.117
28.00	2233	5.421	335.83	325.14	0.097
28.50	2141	5.515	327.23	316.37	0.095
29.00	1990	5.610	308.14	297.11	0.055
29.50	1844	5.705	288.89	277.71	0.012
30.00	1797	5.799	285.97	274.62	0.026
30.50	1679	5.894	270.09	258.58	-0.009
31.00	1650	5.988	269.58	257.91	0.014

Table V-A

(Continued)

TEMPERATURE 50.0 °C.
NORMAL FACTOR A = 209.17 SEC/CTS
BACKGROUND E_B = 0.082-0.060 CTS/SEC
COUNTING 4000 COUNTS

2θ(°)	SECONDS	S(1/Å)	AE_{XC}	I_{coh}/NI_o	i(S)
26.00	500.1	5.040	407.88	397.88	0.213
27.00	568.8	5.231	374.09	363.74	0.166
28.00	652.8	5.421	339.51	328.82	0.110
29.00	742.5	5.610	310.54	299.52	0.064
30.00	862.9	5.799	277.55	266.20	-0.005
31.00	951.5	5.988	261.37	249.71	-0.018
32.00	1040.4	6.176	248.00	236.03	-0.023
33.00	1124.5	6.364	237.89	225.63	-0.018
34.00	1170.1	6.551	237.02	224.47	0.027
35.00	1221.9	6.738	235.12	222.30	0.068
36.00	1272.0	6.924	233.81	220.72	0.114
37.00	1332.9	7.110	230.80	217.45	0.152
38.00	1500.4	7.295	211.55	197.96	0.100
39.00	1590.6	7.480	206.08	192.25	0.120
40.00	1790.1	7.664	188.64	174.58	0.065
41.00	1902.5	7.847	183.04	168.77	0.078
42.00	2146.0	8.030	166.90	152.42	0.018
43.00	2285.6	8.212	161.39	146.71	0.024
44.00	2395.4	8.394	158.61	143.74	0.048
45.00	2540.9	8.575	153.85	138.80	0.055
46.00	2896.4	8.755	138.36	123.14	-0.024

Table V-A

(Continued)

TEMPERATURE 50.0 °C.
NORMAL FACTOR A = 74.90 SEC/CTS
BACKGROUND E_B = 0.072-0.082 CTS/SEC
COUNTING 10000 COUNTS

2θ(°)	SECONDS	S(1/Å)	AE_{XC}	I_{coh}/NI_o	i(S)
40.00	1612.1	7.664	191.04	176.98	0.080
42.00	1930.6	8.030	169.61	155.13	0.036
44.00	2259.9	8.394	153.72	138.85	0.012
46.00	2508.0	8.755	146.75	131.53	0.042
48.00	2839.8	9.114	136.97	121.42	0.042
50.00	3104.5	9.469	132.23	116.38	0.077
52.00	3552.4	9.822	121.56	105.44	0.048
54.00	4059.9	10.172	111.63	95.27	0.013
56.00	4513.5	10.519	105.23	88.66	0.003
58.00	4956.2	10.863	100.24	83.48	0.002
60.00	5485.6	11.203	94.48	77.55	-0.017
62.00	5907.6	11.540	91.42	74.33	-0.007
64.00	6280.6	11.874	89.44	72.23	0.014

Table V-A

(Continued)

TEMPERATURE 50.0 °C.
NORMAL FACTOR A = 27.76 SEC/CTS
BACKGROUND E_B = 0.048-0.048 CTS/SEC
COUNTING 10000 COUNTS

2θ(°)	SECONDS	S(1/Å)	AE_{XC}	I_{coh}/NI_o	i(S)
55.00	1634.4	10.346	108.04	91.57	0.005
58.00	1917.8	10.863	99.04	82.28	-0.013
61.00	2170.6	11.372	93.74	76.73	-0.001
64.00	2397.4	11.874	90.51	73.30	0.029
67.00	2760.8	12.367	83.35	65.98	-0.009
70.00	3084.3	12.852	78.72	61.22	-0.022
73.00	3420.5	13.328	74.44	56.85	-0.041
76.00	3696.9	13.795	71.80	54.15	-0.040
79.00	3958.9	14.252	69.43	51.74	-0.039
82.00	4206.7	14.700	67.17	49.47	-0.041
85.00	4449.1	15.138	64.80	47.10	-0.050
88.00	4642.6	15.565	62.87	45.20	-0.055
91.00	4799.9	15.982	61.09	43.45	-0.059
94.00	4818.3	16.387	60.70	43.10	-0.036
97.00	4856.9	16.782	59.58	42.04	-0.030
100.00	4917.2	17.165	57.77	40.30	-0.042

Table V-B

Diffraction data for 40.0 °C.

TEMPERATURE 40.0 °C.
NORMAL FACTOR A = 7817.63 SEC/CTS
BACKGROUND E_B = 0.050-0.050 CTS/SEC
COUNTING FOR 1000.0 SECONDS

2θ(°)	COUNTS	S(1/Å)	AE_{XC}	I_{coh}/NI_o	i(S)
8.00	80	1.563	16.52	14.09	-0.982
8.50	90	1.661	23.43	20.76	-0.973
9.00	132	1.758	50.92	48.00	-0.935
9.50	175	1.855	82.04	78.87	-0.891
10.00	269	1.953	151.50	148.08	-0.791
10.50	461	2.050	298.95	295.28	-0.575
11.00	691	2.148	489.16	485.23	-0.284
11.50	1097	2.245	836.56	832.37	0.257
12.00	1340	2.342	1077.19	1072.75	0.659
12.50	1414	2.439	1188.34	1183.64	0.875
13.00	1312	2.537	1145.33	1140.40	0.850
13.50	1150	2.634	1038.46	1033.31	0.715
14.00	987	2.731	918.94	913.57	0.551

Table V-B

(Continued)

TEMPERATURE 40.0 °C.
NORMAL FACTOR A = 2508.35 SEC/CTS
BACKGROUND E_B = 0.050-0.050 CTS/SEC
COUNTING FOR 1200.0 SECONDS

2θ(°)	COUNTS	S(1/Å)	AE_{XC}	I_{coh}/NI_o	i(S)
11.00	2594	2.148	517.05	513.12	-0.243
11.25	3200	2.196	655.75	651.69	-0.028
11.50	3702	2.245	778.07	773.89	0.168
11.75	4340	2.294	934.97	930.66	0.422
12.00	4749	2.342	1046.92	1042.48	0.612
12.25	5034	2.391	1134.59	1130.02	0.768
12.50	5304	2.439	1221.57	1216.88	0.927
12.75	5254	2.488	1235.13	1230.31	0.972
13.00	4841	2.537	1160.17	1155.23	0.874
13.25	4490	2.585	1096.59	1091.54	0.791
13.50	4127	2.634	1026.60	1021.45	0.695
13.75	4012	2.682	1016.93	1011.67	0.698
14.00	3658	2.731	943.50	938.13	0.593
14.25	3554	2.779	933.41	927.94	0.594
14.50	3441	2.828	919.90	914.32	0.589
14.75	3112	2.876	845.47	839.79	0.477
15.00	3108	2.925	859.47	853.68	0.519
15.25	2813	2.973	789.97	784.07	0.411
15.50	2673	3.022	762.81	756.81	0.378
15.75	2564	3.070	743.49	737.39	0.358
16.00	2404	3.118	707.72	701.52	0.308
16.25	2116	3.167	631.08	624.78	0.178
16.50	1987	3.215	601.19	594.79	0.135
16.75	1783	3.264	546.24	539.74	0.042
17.00	1643	3.312	509.86	503.26	-0.017
17.25	1563	3.360	491.72	485.02	-0.041
17.50	1429	3.409	454.85	448.05	-0.103
17.75	1349	3.457	434.84	427.95	-0.133
18.00	1302	3.505	425.34	418.35	-0.143
18.25	1232	3.553	407.38	400.29	-0.170
18.50	1179	3.602	394.72	387.53	-0.187
18.75	1070	3.650	361.48	354.20	-0.247
19.00	1013	3.698	346.01	338.64	-0.272
19.25	1024	3.746	355.01	347.54	-0.244
19.50	1038	3.795	365.26	357.69	-0.212

Table V-B

(Continued)

TEMPERATURE 40.0 °C.
NORMAL FACTOR A = 821.57 SEC/CTS
BACKGROUND E_B = 0.050-0.050 CTS/SEC
COUNTING FOR 1600.0 SECONDS

2θ(°)	COUNTS	S(1/Å)	ΔE_{XC}	I_{coh}/NI_o	i(S)
16.00	9496	3.118	698.37	692.18	0.290
16.50	8157	3.215	619.01	612.61	0.169
17.00	6611	3.312	516.74	510.14	-0.003
17.50	5559	3.409	447.18	440.38	-0.119
18.00	4882	3.505	403.98	396.99	-0.186
18.50	4566	3.602	388.72	381.53	-0.199
19.00	4178	3.698	365.50	358.13	-0.230
19.50	3872	3.795	347.90	340.33	-0.250
20.00	3599	3.891	331.89	324.13	-0.268
20.50	3683	3.987	349.13	341.17	-0.211
21.00	3542	4.083	344.47	336.32	-0.202
21.50	3591	4.179	358.54	350.19	-0.149
22.00	3583	4.275	366.95	358.42	-0.107
22.50	3703	4.371	389.13	380.41	-0.028
23.00	3656	4.467	393.63	384.72	0.008
23.50	3745	4.563	413.28	404.18	0.086
24.00	3697	4.659	417.65	408.37	0.125
24.50	3624	4.754	418.87	409.41	0.156
25.00	3481	4.850	411.30	401.66	0.164
25.50	3329	4.945	401.90	392.07	0.165
26.00	3241	5.040	399.80	389.80	0.188
26.50	3034	5.136	381.90	371.72	0.162
27.00	2713	5.231	347.83	337.48	0.082
27.50	2673	5.326	349.92	339.40	0.117
28.00	2346	5.421	312.28	301.59	0.018
28.50	2244	5.515	304.47	293.61	0.016
29.00	2204	5.610	305.01	293.99	0.044
29.50	1907	5.705	267.72	256.53	-0.065
30.00	1912	5.799	273.85	262.51	-0.019
30.50	1817	5.894	264.82	253.31	-0.029
31.00	1767	5.988	262.25	250.59	-0.014

Table V-B

(Continued)

TEMPERATURE 40.0 °C.
NORMAL FACTOR A = 199.90 SEC/CTS
BACKGROUND E_B = 0.048-0.048 CTS/SEC
COUNTING 4000 COUNTS

2θ(°)	SECONDS	S(1/Å)	AE_{XC}	I_{coh}/NI_o	i(S)
26.00	494.7	5.040	395.76	385.76	0.176
27.00	566.4	5.231	360.72	350.37	0.124
28.00	649.5	5.421	327.83	317.14	0.070
29.00	749.4	5.610	295.71	284.69	0.011
30.00	868.7	5.799	265.16	253.82	-0.051
31.00	954.9	5.988	250.60	238.94	-0.060
32.00	1043.9	6.176	237.92	225.95	-0.065
33.00	1123.1	6.364	229.35	217.08	-0.055
34.00	1140.7	6.551	234.19	221.64	0.014
35.00	1200.1	6.738	230.56	217.74	0.046
36.00	1283.0	6.924	223.16	210.07	0.060
37.00	1403.2	7.110	210.90	197.55	0.046
38.00	1434.7	7.295	213.30	199.71	0.110
39.00	1618.9	7.480	194.99	181.16	0.055
40.00	1771.6	7.664	183.76	169.71	0.036
41.00	1970.1	7.847	170.23	155.96	-0.004
42.00	1999.3	8.030	173.08	158.60	0.060
43.00	2287.1	8.212	155.53	140.85	-0.017
44.00	2393.3	8.394	153.05	138.18	0.007
45.00	2637.4	8.575	142.71	127.65	-0.029
46.00	2708.8	8.755	143.00	127.78	0.013
47.00	2879.6	8.935	138.22	122.83	0.013
48.00	3009.0	9.114	135.92	120.37	0.033

Table V-B

(Continued)

TEMPERATURE 40.0 °C.
NORMAL FACTOR A = 65.21 SEC/CTS
BACKGROUND E_B.= 0.048-0.048 CTS/SEC
COUNTING 10000 COUNTS

2θ(°)	SECONDS	S(1/Å)	AE_{XC}	I_{coh}/NI_o	i(S)
40.00	1467.5	7.664	183.55	169.49	0.034
42.00	1733.9	8.030	165.37	150.89	0.008
44.00	1982.0	8.394	153.70	138.83	0.012
46.00	2293.2	8.755	140.82	125.60	-0.005
48.00	2501.4	9.114	136.67	121.12	0.039
50.00	2805.0	9.469	128.74	112.89	0.045
52.00	3210.6	9.822	118.53	102.42	0.018
54.00	3725.9	10.172	107.39	91.04	-0.032
56.00	4074.4	10.519	103.16	86.59	-0.020
58.00	4425.4	10.863	99.59	82.82	-0.006
60.00	4852.8	11.203	95.00	78.07	-0.010
62.00	5394.9	11.540	89.17	72.08	-0.037
64.00	5651.8	11.874	88.75	71.54	0.004

Table V-B

(Continued)

TEMPERATURE 40.0 °C.
NORMAL FACTOR A = 27.88 SEC/CTS
BACKGROUND E_B = 0.048-0.048 CTS/SEC
COUNTING 10000 COUNTS

2θ(°)	SECONDS	S(1/Å)	AE_{XC}	I_{coh}/Nf_0	i(S)
55.00	1634.7	10.346	108.46	91.99	0.009
58.00	1910.9	10.863	99.80	83.04	-0.003
61.00	2174.4	11.372	93.95	76.94	0.002
64.00	2459.5	11.874	88.56	71.34	0.001
67.00	2769.6	12.367	83.42	66.05	-0.006
70.00	3132.0	12.852	77.81	60.31	-0.037
73.00	3410.6	13.328	74.96	57.37	-0.032
76.00	3718.9	13.795	71.66	54.00	-0.043
79.00	4068.6	14.252	67.79	50.10	-0.070
82.00	4212.2	14.700	67.35	49.65	-0.038
85.00	4415.0	15.138	65.57	47.87	-0.035
88.00	4619.3	15.565	63.45	45.78	-0.043
91.00	4780.6	15.982	61.59	43.95	-0.049
94.00	4849.2	16.387	60.54	42.95	-0.040
97.00	4869.8	16.782	59.65	42.11	-0.028
100.00	4827.5	17.165	59.11	41.63	-0.010

Table V-C

Diffraction data for 30.0 °C.

TEMPERATURE 30.0 °C.
NORMAL FACTOR A = 7043.09 SEC/CTS
BACKGROUND E_B = 0.050-0.050 CTS/SEC
COUNTING FOR 1000.0 SECONDS

2θ(°)	COUNTS	S(1/Å)	AE_{XC}	I_{coh}/NI_o	i(S)
8.00	74	1.563	11.91	9.47	-0.988
8.50	91	1.661	21.64	18.96	-0.975
9.00	139	1.758	49.79	46.87	-0.937
9.50	173	1.855	72.73	69.56	-0.904
10.00	273	1.953	138.98	135.56	-0.809
10.50	413	2.050	237.88	234.21	-0.663
11.00	726	2.148	464.76	460.83	-0.320
11.50	1121	2.245	770.95	766.77	0.158
12.00	1472	2.342	1069.77	1065.33	0.647
12.50	1607	2.439	1222.09	1217.39	0.928
13.00	1500	2.537	1185.57	1180.64	0.915
13.50	1331	2.634	1089.52	1084.36	0.800

Table V-C

(Continued)

TEMPERATURE 30.0 °C.
NORMAL FACTOR A = 2743.01 SEC/CTS
BACKGROUND E_B = 0.050-0.050 CTS/SEC
COUNTING FOR 1100.0 SECONDS

2θ(°)	COUNTS	S(1/Å)	AE_{XC}	I_{coh}/NI_o	i(S)
11.00	2231	2.148	529.68	525.75	-0.225
11.25	2667	2.196	650.74	646.69	-0.035
11.50	3122	2.245	781.67	777.48	0.174
11.75	3638	2.294	933.75	929.43	0.420
12.00	3912	2.342	1027.34	1022.90	0.582
12.25	4236	2.391	1137.74	1133.17	0.773
12.50	4410	2.439	1210.25	1205.55	0.909
12.75	4340	2.488	1215.60	1210.78	0.941
13.00	4234	2.537	1209.78	1204.84	0.954
13.25	3885	2.585	1131.01	1125.97	0.847
13.50	3522	2.634	1044.03	1038.87	0.724
13.75	3410	2.682	1029.90	1024.64	0.720
14.00	3253	2.731	1000.43	995.06	0.690
14.25	2980	2.779	932.19	926.72	0.592
14.50	2874	2.828	915.00	909.42	0.581
14.75	2713	2.876	878.42	872.73	0.534
15.00	2455	2.925	807.34	801.55	0.426
15.25	2415	2.973	807.87	801.98	0.443
15.50	2263	3.022	768.96	762.97	0.389
15.75	2104	3.070	725.79	719.70	0.326
16.00	2023	3.118	708.85	702.66	0.310
16.25	1825	3.167	648.14	641.84	0.211
16.50	1663	3.215	598.47	592.07	0.130
16.75	1495	3.264	544.61	538.11	0.039
17.00	1387	3.312	511.81	505.21	-0.013
17.25	1288	3.360	481.23	474.53	-0.062
17.50	1228	3.409	464.93	458.14	-0.083
17.75	1129	3.457	432.23	425.33	-0.139
18.00	1046	3.505	404.87	397.88	-0.185
18.25	1024	3.553	401.82	394.73	-0.181
18.50	956	3.602	379.15	371.96	-0.219
18.75	855	3.650	341.57	334.29	-0.290
19.00	875	3.698	355.18	347.80	-0.252
19.25	885	3.746	364.65	357.17	-0.223

Table V-C

(Continued)

TEMPERATURE 30.0 °C.
NORMAL FACTOR A = 852.28 SEC/CTS
BACKGROUND E_B = 0.050-0.050 CTS/SEC
COUNTING FOR 1600.0 SECONDS

2θ(°)	COUNTS	S(1/Å)	AE_{XC}	I_{coh}/Nf_0	i(S)
16.00	9204	3.118	702.01	695.81	0.297
16.50	7752	3.215	609.94	603.54	0.152
17.00	6289	3.312	509.62	503.02	-0.017
17.50	5406	3.409	450.94	444.14	-0.111
18.00	4782	3.505	410.35	403.36	-0.173
18.50	4261	3.602	375.83	368.64	-0.226
19.00	3867	3.698	350.39	343.01	-0.262
19.50	3701	3.795	344.62	337.05	-0.257
20.00	3637	3.891	348.01	340.25	-0.232
20.50	3439	3.987	337.65	329.69	-0.237
21.00	3432	4.083	345.99	337.84	-0.199
21.50	3472	4.179	359.33	350.99	-0.147
22.00	3542	4.275	376.21	367.68	-0.084
22.50	3549	4.371	386.52	377.79	-0.035
23.00	3709	4.467	414.39	405.48	0.062
23.50	3646	4.563	417.14	408.04	0.096
24.00	3578	4.659	419.00	409.72	0.129
24.50	3568	4.754	427.66	418.20	0.181
25.00	3437	4.850	421.15	411.51	0.192
25.50	3213	4.945	402.03	392.21	0.165
26.00	3075	5.040	392.97	382.97	0.167
26.50	2891	5.136	376.99	366.82	0.147
27.00	2778	5.231	369.74	359.39	0.153
27.50	2587	5.326	350.96	340.44	0.120
28.00	2330	5.421	321.66	310.97	0.049
28.50	2220	5.515	312.34	301.49	0.044
29.00	2118	5.610	303.60	292.58	0.039
29.50	1917	5.705	279.24	268.05	-0.023
30.00	1958	5.799	291.22	279.87	0.046
30.50	1775	5.894	268.07	256.57	-0.016
31.00	1692	5.988	259.96	248.29	-0.024

Table V-C

(Continued)

TEMPERATURE 30.0 °C.
NORMAL FACTOR A = 213.67 SEC/CTS
BACKGROUND E_B = 0.050-0.050 CTS/SEC
COUNTING 4000 COUNTS

2θ(°)	SECONDS	S(1/Å)	AE_{XC}	I_{coh}/NI_o	i(S)
26.00	519.4	5.040	402.69	392.69	0.197
27.00	599.8	5.231	363.85	353.50	0.134
28.00	686.1	5.421	331.46	320.77	0.083
29.00	797.1	5.610	296.88	285.86	0.015
30.00	888.1	5.799	277.05	265.71	-0.007
31.00	1008.1	5.988	253.44	241.77	-0.049
32.00	1082.8	6.176	244.92	232.95	-0.036
33.00	1198.3	6.364	229.42	217.15	-0.055
34.00	1226.1	6.551	232.50	219.95	0.006
35.00	1295.2	6.738	227.94	215.11	0.034
36.00	1374.0	6.924	222.33	209.24	0.056
37.00	1409.4	7.110	224.26	210.92	0.117
38.00	1565.5	7.295	208.44	194.85	0.083
39.00	1737.8	7.480	193.71	179.88	0.048
40.00	1876.8	7.664	185.00	170.94	0.043
41.00	2109.5	7.847	169.46	155.19	-0.009
42.00	2102.6	8.030	175.50	161.02	0.076
43.00	2444.4	8.212	155.05	140.37	-0.020
44.00	2463.8	8.394	158.57	143.71	0.048
45.00	2699.0	8.575	148.73	133.68	0.017

Table V-C

(Continued)

TEMPERATURE 30.0 °C.
NORMAL FACTOR A = 69.68 SEC/CTS
BACKGROUND E_B = 0.050-0.050 CTS/SEC
COUNTING 10000 COUNTS

2θ(°)	SECONDS	S(1/Å)	$AE_{\&C}$	I_{coh}/NI_o	i(S)
40.00	1522.9	7.664	188.88	174.82	0.067
42.00	1820.4	8.030	168.17	153.69	0.027
44.00	2150.8	8.394	151.15	136.28	-0.007
46.00	2407.0	8.755	143.20	127.98	0.014
48.00	2656.1	9.114	137.35	121.80	0.045
50.00	2916.2	9.469	132.16	116.31	0.076
52.00	3358.9	9.822	120.89	104.77	0.041
54.00	3792.1	10.172	112.62	96.27	0.023
56.00	4200.9	10.519	106.75	90.18	0.020
58.00	4691.6	10.863	100.14	83.38	0.001
60.00	5140.9	11.203	95.58	78.65	-0.003
62.00	5431.4	11.540	94.51	77.43	0.034
64.00	5914.3	11.874	90.40	73.18	0.027

Table V-C

(Continued)

TEMPERATURE 30.0 °C.
NORMAL FACTOR A = 29.44 SEC/CTS
BACKGROUND E_B = 0.050-0.050 CTS/SEC
COUNTING 10000 COUNTS

2θ(°)	SECONDS	S(1/Å)	AE_{XC}	I_{coh}/NI_o	i(S)
55.00	1709.3	10.346	109.47	93.00	0.020
58.00	1993.6	10.863	100.95	84.18	0.010
61.00	2257.7	11.372	95.48	78.47	0.022
64.00	2562.8	11.874	89.66	72.45	0.017
67.00	2878.5	12.367	84.67	67.30	0.011
70.00	3260.0	12.852	78.85	61.35	-0.020
73.00	3507.6	13.328	76.89	59.30	0.000
76.00	3916.9	13.795	71.72	54.07	-0.042
79.00	4142.4	14.252	70.23	52.54	-0.024
82.00	4429.0	14.700	67.51	49.81	-0.035
85.00	4671.3	15.138	65.31	47.61	-0.040
88.00	4915.2	15.565	62.82	45.15	-0.056
91.00	4964.5	15.982	62.52	44.88	-0.028
94.00	5054.1	16.387	61.22	43.63	-0.024
97.00	5054.7	16.782	60.58	43.04	-0.007
100.00	5124.4	17.165	58.66	41.19	-0.021
103.00	5065.2	17.536	57.88	40.47	-0.009
106.00	5011.5	17.895	56.67	39.33	-0.011
109.00	4895.4	18.242	55.86	38.60	-0.003
112.00	4764.4	18.576	54.96	37.78	0.001
115.00	4554.6	18.898	54.78	37.68	0.023
118.00	4323.8	19.206	54.74	37.72	0.049
121.00	4167.7	19.502	53.62	36.69	0.045
124.00	3933.6	19.784	53.47	36.61	0.067
127.00	3756.0	20.053	52.50	35.73	0.064
130.00	3592.1	20.307	51.30	34.61	0.052
133.00	3374.7	20.548	50.90	34.28	0.063

Table V-D

Diffraction data for 29.5 °C.

TEMPERATURE 29.5 °C.
NORMAL FACTOR A = 6344.92 SEC/CTS
BACKGROUND E_B = 0.045-0.045 CTS/SEC
COUNTING FOR 1000.0 SECONDS

2θ(°)	COUNTS	S(1/Å)	AE_{XC}	I_{coh}/NI_o	i(S)
8.00	75	1.563	13.41	10.98	-0.986
8.50	83	1.661	18.06	15.39	-0.980
9.00	91	1.758	23.18	20.27	-0.973
9.50	113	1.855	36.22	33.05	-0.954
10.00	210	1.953	92.64	89.22	-0.874
10.50	371	2.050	192.46	188.78	-0.728
11.00	711	2.148	412.50	408.57	-0.397
11.50	1125	2.245	700.36	696.18	0.051
12.00	1536	2.342	1010.49	1006.05	0.556
12.50	1758	2.439	1211.25	1206.56	0.911
13.00	1744	2.537	1251.46	1246.52	1.022
13.50	1423	2.634	1055.84	1050.69	0.744
14.00	1278	2.731	981.44	976.07	0.658

Table V-D

(Continued)

TEMPERATURE 29.5 °C.
NORMAL FACTOR A = 2549.09 SEC/CTS
BACKGROUND E_B = 0.045-0.045 CTS/SEC
COUNTING FOR 1200.0 SECONDS

2θ(°)	COUNTS	S(1/Å)	AE_{XC}	I_{coh}/NI_o	i(S)
11.00	2443	2.148	495.38	491.45	-0.275
11.25	3014	2.196	628.20	624.14	-0.069
11.50	3485	2.245	744.90	740.72	0.118
11.75	4155	2.294	910.42	906.10	0.384
12.00	4570	2.342	1024.68	1020.24	0.577
12.25	4933	2.391	1131.00	1126.43	0.763
12.50	5099	2.439	1194.30	1189.61	0.884
12.75	4942	2.488	1181.24	1176.42	0.886
13.00	4587	2.537	1117.86	1112.92	0.805
13.25	4382	2.585	1088.74	1083.70	0.778
13.50	4160	2.634	1053.28	1048.13	0.740
13.75	3753	2.682	967.29	962.02	0.615
14.00	3780	2.731	992.93	987.56	0.677
14.25	3403	2.779	909.21	903.73	0.553
14.50	3195	2.828	868.48	862.90	0.500
14.75	3113	2.876	861.16	855.49	0.504
15.00	3066	2.925	863.12	857.33	0.525
15.25	2814	2.973	804.84	798.95	0.438
15.50	2610	3.022	758.29	752.29	0.370
15.75	2412	3.070	711.51	705.42	0.300
16.00	2257	3.118	675.95	669.75	0.248
16.25	2086	3.167	633.85	627.55	0.184
16.50	1975	3.215	609.05	602.65	0.150
16.75	1788	3.264	558.65	552.15	0.066
17.00	1719	3.312	544.98	538.38	0.052
17.25	1496	3.360	479.43	472.73	-0.065
17.50	1377	3.409	446.70	439.91	-0.120
17.75	1270	3.457	416.88	409.99	-0.170
18.00	1218	3.505	405.11	398.11	-0.184
18.25	1144	3.553	385.03	377.95	-0.216
18.50	1135	3.602	387.51	380.32	-0.202
18.75	1096	3.650	378.99	371.71	-0.210

Table V-D

(Continued)

TEMPERATURE 29.5 °C.
NORMAL FACTOR A = 795.78 SEC/CTS
BACKGROUND E_B = 0.045-0.045 CTS/SEC
COUNTING FOR 1600.0 SECONDS

2θ(°)	COUNTS	S(1/Å)	AE_{XC}	I_{coh}/Nb	i(S)
16.00	9696	3.118	691.39	685.19	0.277
16.50	8148	3.215	599.50	593.10	0.132
17.00	6871	3.312	521.05	514.45	0.005
17.50	5725	3.409	446.90	440.10	-0.119
18.00	5196	3.505	417.53	410.54	-0.159
18.50	4485	3.602	370.39	363.20	-0.238
19.00	4269	3.698	362.58	355.20	-0.236
19.50	4060	3.795	354.39	346.82	-0.236
20.00	3725	3.891	333.71	325.95	-0.264
20.50	3669	3.987	337.61	329.64	-0.237
21.00	3621	4.083	342.04	333.89	-0.208
21.50	3629	4.179	351.83	343.49	-0.165
22.00	3797	4.275	377.96	369.42	-0.079
22.50	3813	4.371	389.19	380.46	-0.028
23.00	3884	4.467	406.43	397.52	0.041
23.50	3783	4.563	405.32	396.23	0.064
24.00	3807	4.659	417.73	408.45	0.125
24.50	3780	4.754	424.50	415.03	0.172
25.00	3669	4.850	421.35	411.70	0.193
25.50	3328	4.945	390.12	380.29	0.130
26.00	3281	5.040	393.13	383.13	0.168
26.50	3054	5.136	373.42	363.24	0.136
27.00	3037	5.231	379.39	369.04	0.184
27.50	2721	5.326	346.25	335.73	0.104
28.00	2516	5.421	326.24	315.55	0.065
28.50	2310	5.515	304.99	294.14	0.018
29.00	2228	5.610	299.89	288.87	0.026
29.50	2001	5.705	273.79	262.60	-0.043
30.00	1951	5.799	272.06	260.71	-0.026
30.50	1913	5.894	271.86	260.36	-0.002
31.00	1743	5.988	251.61	239.94	-0.056

Table V-D

(Continued)

TEMPERATURE 29.5 °C.
NORMAL FACTOR A = 204.20 SEC/CTS
BACKGROUND E_B = 0.045-0.045 CTS/SEC
COUNTING 4000 COUNTS

2θ(°)	SECONDS	S(1/Å)	AE_{XC}	I_{coh}/NI_o	i(S)
26.00	491.6	5.040	407.00	397.00	0.210
27.00	582.4	5.231	358.45	348.11	0.116
28.00	675.7	5.421	321.97	311.28	0.050
29.00	784.9	5.610	288.46	277.44	-0.015
30.00	857.2	5.799	274.72	263.38	-0.016
31.00	968.8	5.988	252.47	240.80	-0.053
32.00	1045.2	6.176	242.93	230.96	-0.044
33.00	1104.2	6.364	238.55	226.29	-0.015
34.00	1174.2	6.551	232.52	219.97	0.006
35.00	1202.6	6.738	235.24	222.42	0.069
36.00	1292.6	6.924	226.47	213.38	0.077
37.00	1405.6	7.110	215.30	201.95	0.070
38.00	1476.5	7.295	211.85	198.26	0.102
39.00	1678.2	7.480	192.25	178.43	0.039
40.00	1751.8	7.664	190.14	176.09	0.075
41.00	1972.9	7.847	173.91	159.64	0.020
42.00	2122.5	8.030	166.56	152.08	0.016
43.00	2297.1	8.212	158.45	143.77	0.004
44.00	2476.1	8.394	151.25	136.38	-0.006
45.00	2580.3	8.575	149.41	134.36	0.022
46.00	2664.8	8.755	148.88	133.66	0.059
47.00	2815.8	8.935	144.82	129.43	0.068
48.00	3122.5	9.114	133.93	118.38	0.016

Table V-D

(Continued)

TEMPERATURE 29.5 °C.
NORMAL FACTOR A = 67.12 SEC/CTS
BACKGROUND E_B = 0.045-0.045 CTS/SEC
COUNTING 10000 COUNTS

2θ(°)	SECONDS	S(1/Å)	AE_{XC}	I_{coh}/NI_o	i(S)
40.00	1469.4	7.664	188.75	174.70	0.066
42.00	1739.3	8.030	169.76	155.28	0.037
44.00	2054.3	8.394	152.67	137.80	0.004
46.00	2309.5	8.755	144.00	128.78	0.021
48.00	2655.6	9.114	132.51	116.96	0.004
50.00	2882.1	9.469	129.02	113.17	0.047
52.00	3233.2	9.822	121.25	105.14	0.045
54.00	3645.4	10.172	113.15	96.79	0.029
56.00	4067.9	10.519	106.48	89.91	0.017
58.00	4539.0	10.863	100.01	83.25	-0.001
60.00	4904.6	11.203	96.87	79.93	0.014
62.00	5257.8	11.540	94.38	77.30	0.033
64.00	5785.2	11.874	89.34	72.13	0.012

Table V-D

(Continued)

TEMPERATURE 29.5 °C.
NORMAL FACTOR A = 27.80 SEC/CTS
BACKGROUND E_B = 0.045-0.045 CTS/SEC
COUNTING 10000 COUNTS

2θ(°)	SECONDS	S(1/Å)	AE_{XC}	I_{coh}/NI_o	i(S)
55.00	1620.6	10.346	109.15	92.68	0.017
58.00	1915.1	10.863	99.36	82.59	-0.009
61.00	2181.2	11.372	93.45	76.44	-0.005
64.00	2417.3	11.874	89.93	72.71	0.021
67.00	2810.7	12.367	82.02	64.64	-0.029
70.00	3051.5	12.852	79.74	62.24	-0.006
73.00	3410.4	13.328	74.83	57.24	-0.034
76.00	3719.3	13.795	71.52	53.87	-0.045
79.00	4006.6	14.252	68.75	51.06	-0.052
82.00	4242.3	14.700	66.76	49.05	-0.049
85.00	4516.3	15.138	63.97	46.28	-0.067
88.00	4660.9	15.565	62.78	45.11	-0.057
91.00	4742.5	15.982	62.01	44.37	-0.039
94.00	4743.9	16.387	61.83	44.24	-0.011
97.00	4914.8	16.782	59.01	41.47	-0.043
100.00	4896.1	17.165	58.18	40.71	-0.032

Table V-E

Diffraction data for 20.0 °C.

TEMPERATURE 20.0 °C.
NORMAL FACTOR A = 8027.60 SEC/CTS
BACKGROUND E_B = 0.048-0.048 CTS/SEC
COUNTING FOR 1000.0 SECONDS

2θ(°)	COUNTS	S(1/Å)	AE_{XC}	I_{coh}/NI_o	i(S)
7.00	73	1.368	12.34	10.37	-0.987
7.50	75	1.465	14.30	12.10	-0.985
8.00	83	1.563	19.79	17.36	-0.978
8.50	95	1.661	28.27	25.60	-0.966
9.00	115	1.758	42.72	39.80	-0.946
9.50	160	1.855	75.48	72.31	-0.900
10.00	268	1.953	156.28	152.86	-0.785
10.50	388	2.050	253.95	250.28	-0.639
11.00	696	2.148	507.79	503.86	-0.257
11.50	1096	2.245	859.85	855.66	0.292
12.00	1313	2.342	1084.69	1080.25	0.670
12.50	1526	2.439	1322.24	1317.55	1.087
13.00	1323	2.537	1188.21	1183.27	0.919

Table V-E

(Continued)

TEMPERATURE 20.0 °C.
NORMAL FACTOR A = 2478.50 SEC/CTS
BACKGROUND E_B = 0.050-0.073 CTS/SEC
COUNTING FOR 1200.0 SECONDS

2θ(°)	COUNTS	S(1/Å)	AE_{XC}	I_{coH}/NI_o	i(S)
11.00	2136	2.148	418.56	414.63	-0.389
11.25	2785	2.196	562.12	558.06	-0.167
11.50	3728	2.245	773.92	769.73	0.162
11.75	4485	2.294	954.55	950.23	0.452
12.00	5164	2.342	1125.21	1120.77	0.733
12.25	5672	2.391	1263.85	1259.29	0.971
12.50	5850	2.439	1331.44	1326.75	1.101
12.75	5796	2.488	1346.28	1341.46	1.150
13.00	5546	2.537	1313.64	1308.71	1.123
13.25	5329	2.585	1286.73	1281.69	1.103
13.50	4815	2.634	1183.70	1178.54	0.956
13.75	4581	2.682	1146.93	1141.67	0.917
14.00	4182	2.731	1065.18	1059.81	0.800
14.25	3985	2.779	1032.92	1027.45	0.765
14.50	3688	2.828	971.90	966.32	0.679
14.75	3572	2.876	957.55	951.87	0.674
15.00	3350	2.925	912.57	906.78	0.613
15.25	3099	2.973	857.22	851.33	0.532
15.50	3019	3.022	848.76	842.77	0.534
15.75	2804	3.070	799.93	793.83	0.462
16.00	2565	3.118	741.84	735.64	0.371
16.25	2369	3.167	694.45	688.15	0.298
16.50	2056	3.215	609.06	602.66	0.150
16.75	1910	3.264	572.89	566.39	0.094
17.00	1793	3.312	544.51	537.91	0.051
17.25	1615	3.360	495.25	488.55	-0.034
17.50	1503	3.409	465.88	459.08	-0.081
17.75	1319	3.457	411.39	404.50	-0.181
18.00	1323	3.505	418.67	411.68	-0.156
18.25	1293	3.553	414.32	407.24	-0.155
18.50	1222	3.602	395.39	388.20	-0.185

Table V-E

(Continued)

TEMPERATURE 20.0 °C.
NORMAL FACTOR A = 841.73 SEC/CTS
BACKGROUND E_B = 0.057-0.074 CTS/SEC
COUNTING FOR 1600.0 SECONDS

2θ(°)	COUNTS	S(1/Å)	AE_{XC}	I_{coh}/NI_o	i(S)
16.00	9873	3.118	743.31	737.11	0.374
16.50	8104	3.215	629.08	622.68	0.188
17.00	6577	3.312	525.60	519.00	0.014
17.50	5688	3.409	467.76	460.96	-0.078
18.00	4941	3.505	417.68	410.68	-0.158
18.50	4486	3.602	389.73	382.54	-0.197
19.00	4200	3.698	374.93	367.55	-0.210
19.50	3785	3.795	346.56	338.99	-0.253
20.00	3665	3.891	344.58	336.81	-0.240
20.50	3727	3.987	360.09	352.12	-0.185
21.00	3661	4.083	362.92	354.77	-0.159
21.50	3525	4.179	358.14	349.80	-0.150
22.00	3782	4.275	394.86	386.33	-0.037
22.50	3758	4.371	402.11	393.38	0.005
23.00	3763	4.467	412.56	403.65	0.057
23.50	3902	4.563	438.58	429.48	0.154
24.00	3767	4.659	433.01	423.73	0.167
24.50	3758	4.754	442.02	432.56	0.222
25.00	3660	4.850	440.02	430.37	0.247
25.50	3429	4.945	420.67	410.85	0.221
26.00	3260	5.040	408.11	398.11	0.213
26.50	3103	5.136	396.22	386.05	0.207
27.00	2841	5.231	369.28	358.93	0.151
27.50	2616	5.326	345.99	335.47	0.104
28.00	2583	5.421	348.53	337.84	0.140
28.50	2341	5.515	320.81	309.95	0.073
29.00	2111	5.610	293.45	282.43	0.003
29.50	2041	5.705	288.78	277.60	0.011
30.00	2016	5.799	290.62	279.27	0.044

Table V-E

(Continued)

TEMPERATURE 20.0 °C.
NORMAL FACTOR A = 203.07 SEC/CTS
BACKGROUND E_b = 0.073-0.082 CTS/SEC
COUNTING 4000 COUNTS

2θ(°)	SECONDS	S(1/A)	AE_{XC}	I_{coh}/NI_o	i(S)
26.00	483.5	5.040	410.16	400.16	0.220
27.00	550.1	5.231	376.05	365.70	0.173
28.00	639.1	5.421	337.08	326.39	0.102
29.00	736.8	5.610	304.09	293.07	0.041
30.00	843.5	5.799	275.92	264.58	-0.011
31.00	916.6	5.988	263.67	252.00	-0.009
32.00	1039.1	6.176	241.06	229.09	-0.052
33.00	1079.5	6.364	240.67	228.40	-0.006
34.00	1139.6	6.551	236.18	223.63	0.023
35.00	1191.1	6.738	233.96	221.13	0.063
36.00	1259.1	6.924	228.91	215.82	0.089
37.00	1325.9	7.110	224.68	211.33	0.119
38.00	1432.6	7.295	214.62	201.03	0.117
39.00	1574.5	7.480	201.28	187.45	0.092
40.00	1704.9	7.664	191.52	177.47	0.083
41.00	1878.5	7.847	178.83	164.56	0.051
42.00	2040.3	8.030	169.33	154.85	0.035
43.00	2173.8	8.212	163.46	148.79	0.039
44.00	2367.0	8.394	154.12	139.25	0.015
45.00	2493.6	8.575	150.33	135.28	0.029
46.00	2612.6	8.755	147.39	132.16	0.047
47.00	2808.0	8.935	140.56	125.17	0.033

Table V-E

(Continued)

TEMPERATURE 20.0 °C.
NORMAL FACTOR A = 62.73 SEC/CTS
BACKGROUND E_B = 0.068-0.117 CTS/SEC
COUNTING 1C000 COUNTS

2θ(°)	SECONDS	S(1/Å)	AE_{XC}	I_{coh}/NI_o	i(S)
40.00	1359.6	7.664	190.16	176.10	0.075
42.00	1627.8	8.030	168.88	154.40	0.031
44.00	1868.5	8.394	156.12	141.26	0.030
46.00	2095.1	8.755	147.46	132.24	0.048
48.00	2308.4	9.114	141.47	125.92	0.081
50.00	2652.1	9.469	129.76	113.91	0.054
52.00	2972.1	9.822	121.80	105.68	0.050
54.00	3372.7	10.172	112.58	96.23	0.023
56.00	3844.7	10.519	103.31	86.73	-0.018
58.00	4145.9	10.863	100.17	83.40	0.001
60.00	4548.8	11.203	95.15	78.21	-0.008
62.00	4876.5	11.540	92.36	75.28	0.006
64.00	5079.8	11.874	92.19	74.97	0.052
66.00	5430.2	12.204	89.29	71.96	0.058
68.00	5830.2	12.530	85.83	68.41	0.050

Table V-E

(Continued)

TEMPERATURE 20.0 °C.
NORMAL FACTOR A = 26.21 SEC/CTS
BACKGROUND E_B = 0.048-0.048 CTS/SEC
COUNTING 10000 COUNTS

2θ(°)	SECONDS	S(1/Å)	AE_{XC}	I_{coh}/NI_o	i(S)
55.00	1541.6	10.346	108.19	91.72	0.006
58.00	1765.5	10.863	101.64	84.88	0.019
61.00	2029.4	11.372	94.72	77.71	0.012
64.00	2257.1	11.874	90.82	73.61	0.033
67.00	2610.4	12.367	83.29	65.91	-0.010
70.00	2896.7	12.852	79.20	61.70	-0.015
73.00	3281.7	13.328	73.30	55.71	-0.060
76.00	3522.9	13.795	71.19	53.54	-0.051
79.00	3799.8	14.252	68.34	50.65	-0.060
82.00	4076.1	14.700	65.49	47.78	-0.074
85.00	4288.3	15.138	63.52	45.82	-0.076
88.00	4432.7	15.565	62.23	44.55	-0.068
91.00	4515.1	15.982	61.40	43.76	-0.053
94.00	4635.0	16.387	59.62	42.03	-0.060
97.00	4574.1	16.782	59.80	42.26	-0.025
100.00	4615.7	17.165	58.19	40.71	-0.032

Table V-F

Diffraction data for 10.0 °C.

TEMPERATURE 10.0 °C.
NORMAL FACTOR A = 7535.19 SEC/CTS
BACKGROUND E_B = 0.050-0.050 CTS/SEC
COUNTING FOR 10C0.0 SECONDS

2θ(°)	COUNTS	S(1/Å)	AE_{XC}	I_{coh}/NI_o	i(S)
8.00	79	1.563	15.39	12.96	-0.983
8.50	75	1.661	14.11	11.44	-0.985
9.00	95	1.758	26.93	24.02	-0.968
9.50	124	1.855	46.81	43.64	-0.940
10.00	201	1.953	100.68	97.26	-0.863
10.50	331	2.050	197.01	193.34	-0.721
11.00	609	2.148	411.17	407.24	-0.399
11.50	1031	2.245	755.51	751.32	0.134
12.00	1419	2.342	1101.86	1097.42	0.697
12.50	1644	2.439	1338.54	1333.85	1.113
13.00	1580	2.537	1338.39	1333.45	1.163

Table V-F

(Continued)

TEMPERATURE 10.0 °C.
NORMAL FACTOR A = 2187.54 SEC/CTS
BACKGROUND E_β = 0.040-0.040 CTS/SEC
COUNTING FOR 1000.0 SECONDS

2θ(°)	COUNTS	S(1/Å)	AE_{XC}	I_{coh}/NI_o	i(S)
11.00	2430	2.148	510.36	506.43	-0.253
11.25	2852	2.196	614.57	610.52	-0.089
11.50	3353	2.245	740.72	736.53	0.112
11.75	4012	2.294	908.06	903.74	0.381
12.00	4582	2.342	1061.29	1056.85	0.634
12.25	5023	2.391	1189.53	1184.96	0.854
12.50	5399	2.439	1306.44	1301.75	1.062
12.75	5440	2.488	1343.86	1339.04	1.147
13.00	5264	2.537	1326.65	1321.72	1.144
13.25	4960	2.585	1274.55	1269.50	1.083
13.50	4513	2.634	1181.62	1176.47	0.953
13.75	4268	2.682	1138.57	1133.31	0.903
14.00	3977	2.731	1080.43	1075.06	0.826
14.25	3857	2.779	1067.15	1061.67	0.824
14.50	3601	2.828	1013.95	1008.37	0.753
14.75	3413	2.876	977.87	972.19	0.709
15.00	3181	2.925	926.91	921.12	0.638
15.25	2857	2.973	845.94	840.05	0.512
15.50	2814	3.022	847.49	841.49	0.532
15.75	2701	3.070	826.87	820.77	0.512
16.00	2433	3.118	756.13	749.93	0.398
16.25	2222	3.167	700.92	694.62	0.310
16.50	1992	3.215	637.32	630.92	0.204
16.75	1819	3.264	590.23	583.73	0.127
17.00	1714	3.312	564.26	557.66	0.090
17.25	1432	3.360	476.60	469.90	-0.071
17.50	1422	3.409	480.53	473.73	-0.052
17.75	1349	3.457	462.14	455.24	-0.078
18.00	1208	3.505	418.61	411.62	-0.156
18.25	1131	3.553	396.87	389.78	-0.192
18.50	1032	3.602	366.20	359.02	-0.246

Table V-F

(Continued)

TEMPERATURE 10.0 °C.
NORMAL FACTOR A = 755.93 SEC/CTS
BACKGROUND E_B = 0.050-0.050 CTS/SEC
COUNTING FOR 1500.0 SECONDS

2θ(°)	COUNTS	S(1/Å)	AE_{XC}	I_{coh}/NI_o	i(S)
16.00	10461	3.118	756.02	749.82	0.398
16.50	8559	3.215	638.13	631.73	0.206
17.00	7185	3.312	552.11	545.51	0.066
17.50	5987	3.409	473.57	466.77	-0.066
18.00	5125	3.505	416.96	409.97	-0.160
18.50	4675	3.602	391.20	384.01	-0.194
19.00	4391	3.698	377.80	370.43	-0.203
19.50	4056	3.795	358.46	350.89	-0.227
20.00	3772	3.891	342.21	334.44	-0.245
20.50	3777	3.987	352.07	344.10	-0.204
21.00	3807	4.083	364.45	356.29	-0.155
21.50	3782	4.179	371.53	363.18	-0.117
22.00	3801	4.275	383.07	374.53	-0.067
22.50	3894	4.371	402.57	393.85	0.006
23.00	3943	4.467	417.87	408.96	0.071
23.50	3898	4.563	423.09	413.99	0.112
24.00	3892	4.659	432.56	423.28	0.166
24.50	3817	4.754	434.07	424.60	0.199
25.00	3711	4.850	431.56	421.92	0.222
25.50	3620	4.945	430.37	420.55	0.250
26.00	3373	5.040	409.39	399.39	0.217
26.50	3283	5.136	407.04	396.86	0.241
27.00	2887	5.231	364.58	354.23	0.136
27.50	2831	5.326	365.01	354.49	0.166
28.00	2619	5.421	344.09	333.40	0.125
28.50	2390	5.515	319.67	308.81	0.069
29.00	2290	5.610	312.18	301.16	0.070
29.50	2152	5.705	298.70	287.51	0.048
30.00	1943	5.799	274.05	262.71	-0.018

Table V-F

(Continued)

TEMPERATURE 10.0 °C.
NORMAL FACTOR A = 188.93 SEC/CTS
BACKGROUND E_B = 0.050-0.058 CTS/SEC
COUNTING 4000 COUNTS

2θ(°)	SECONDS	S(1/Å)	AE_{XC}	I_{coh}/NI_o	i(S)
26.00	445.6	5.040	415.41	405.41	0.236
27.00	506.9	5.231	381.10	370.75	0.189
28.00	608.3	5.421	330.85	320.16	0.080
29.00	675.6	5.610	310.12	299.10	0.062
30.00	764.4	5.799	284.97	273.62	0.023
31.00	866.8	5.988	260.97	249.31	-0.020
32.00	942.6	6.176	249.07	237.10	-0.019
33.00	1013.4	6.364	240.25	227.99	-0.008
34.00	1055.6	6.551	239.09	226.54	0.036
35.00	1120.3	6.738	233.29	220.46	0.059
36.00	1163.1	6.924	232.58	219.49	0.108
37.00	1222.0	7.110	228.93	215.59	0.142
38.00	1328.3	7.295	217.52	203.93	0.133
39.00	1485.2	7.480	200.66	186.83	0.088
40.00	1612.5	7.664	190.59	176.53	0.077
41.00	1770.2	7.847	178.85	164.58	0.051
42.00	1884.7	8.030	173.07	158.59	0.059
43.00	2104.3	8.212	159.36	144.69	0.010
44.00	2157.6	8.394	160.10	145.23	0.059
45.00	2388.9	8.575	148.48	133.43	0.015
46.00	2507.6	8.755	145.42	130.19	0.032

Table V-F

(Continued)

TEMPERATURE 10.0 °C.
NORMAL FACTOR A = 55.62 SEC/CTS
BACKGROUND E_B = 0.050-0.050 CTS/SEC
COUNTING 10000 COUNTS

2θ(°)	SECONDS	S(1/Å)	AE_{XC}	I_{coh}/NI_o	i(S)
40.00	1180.2	7.664	194.89	180.84	0.104
42.00	1438.2	8.030	170.25	155.77	0.041
44.00	1666.9	8.394	156.07	141.20	0.029
46.00	1951.1	8.755	141.35	126.13	-0.000
48.00	2127.1	9.114	137.28	121.73	0.045
50.00	2374.1	9.469	129.94	114.10	0.056
52.00	2691.8	9.822	120.83	104.71	0.041
54.00	3100.6	10.172	110.34	93.99	-0.001
56.00	3491.5	10.519	102.90	86.33	-0.023
58.00	3788.3	10.863	99.46	82.69	-0.008
60.00	4084.2	11.203	96.56	79.63	0.010
62.00	4523.9	11.540	91.00	73.92	-0.012
64.00	4839.3	11.874	88.68	71.46	0.003

Table V-F

(Continued)

TEMPERATURE 10.0 °C.
NORMAL FACTOR A = 25.45 SEC/CTS
BACKGROUND E_B = 0.050-0.050 CTS/SEC
COUNTING 10000 COUNTS

2θ(°)	SECONDS	S(1/Å)	AE_{XC}	I_{coH}/NI_o	i(S)
55.00	1467.8	10.346	110.33	93.86	0.030
58.00	1750.0	10.863	99.53	82.77	-0.007
61.00	1967.3	11.372	94.86	77.85	0.014
64.00	2245.3	11.874	88.61	71.40	0.002
67.00	2497.6	12.367	84.52	67.15	0.009
70.00	2790.0	12.852	79.83	62.33	-0.005
73.00	3098.4	13.328	75.40	57.81	-0.025
76.00	3400.4	13.795	71.61	53.96	-0.044
79.00	3577.0	14.252	70.51	52.82	-0.019
82.00	3848.6	14.700	67.36	49.66	-0.038
85.00	4026.7	15.138	65.71	48.01	-0.032
88.00	4166.9	15.565	64.31	46.63	-0.025
91.00	4280.7	15.982	62.90	45.26	-0.020
94.00	4443.0	16.387	60.39	42.80	-0.043
97.00	4537.2	16.782	58.49	40.95	-0.055
100.00	4416.2	17.165	59.06	41.58	-0.011

Table V-G

Diffraction data for 0.0 °C.

TEMPERATURE 0.0 °C.
NORMAL FACTOR A = 7339.16 SEC/CTS
BACKGROUND E_B = 0.044-0.048 CTS/SEC
COUNTING FOR 1000.0 SECONDS

2θ(°)	COUNTS	S(1/Å)	AE_{XC}	I_{coh}/NI_o	i(S)
7.00	115	1.368	32.04	30.07	-0.963
7.50	71	1.465	12.91	10.71	-0.986
8.00	65	1.563	10.51	8.08	-0.990
8.50	81	1.661	19.80	17.12	-0.977
9.00	105	1.758	34.78	31.86	-0.957
9.50	154	1.855	66.75	63.58	-0.912
10.00	216	1.953	110.40	106.98	-0.849
10.50	360	2.050	214.19	210.52	-0.697
11.00	675	2.148	450.15	446.22	-0.342
11.50	1159	2.245	834.11	829.93	0.253
12.00	1601	2.342	1217.96	1213.52	0.876
12.50	1798	2.439	1431.59	1426.89	1.260
13.00	1646	2.537	1361.51	1356.57	1.200

Table V-G

(Continued)

TEMPERATURE 0.0 °C.
NORMAL FACTOR A = 2413.12 SEC/CTS
BACKGROUND E_B = 0.060-0.166 CTS/SEC
COUNTING FOR 1000.0 SECONDS

2θ(°)	COUNTS	S(1/Å)	AE_{XC}	I_{coh}/Nf_o	i(S)
10.00	713	1.953	139.44	136.02	-0.808
10.25	890	2.002	181.11	177.56	-0.747
10.50	1157	2.050	244.91	241.23	-0.652
10.75	1545	2.099	339.45	335.65	-0.511
11.00	2203	2.148	501.86	497.93	-0.266
11.25	2726	2.196	638.99	634.93	-0.053
11.50	3513	2.245	847.02	842.83	0.273
11.75	4138	2.294	1022.93	1018.61	0.556
12.00	4836	2.342	1224.61	1220.17	0.887
12.25	5042	2.391	1304.54	1299.97	1.034
12.50	5102	2.439	1347.53	1342.84	1.127
12.75	5131	2.488	1382.71	1377.89	1.209
13.00	4790	2.537	1314.59	1309.65	1.124
13.25	4419	2.585	1234.08	1229.04	1.017
13.50	4120	2.634	1170.40	1165.25	0.934
13.75	3790	2.682	1094.15	1088.89	0.828
14.00	3518	2.731	1031.73	1026.36	0.743
14.25	3347	2.779	997.39	991.92	0.704
14.50	3161	2.828	956.40	950.82	0.652
14.75	2935	2.876	900.50	894.82	0.573
15.00	2795	2.925	870.03	864.24	0.537
15.25	2672	2.973	843.58	837.68	0.508
15.50	2540	3.022	812.68	806.69	0.469
15.75	2394	3.070	775.47	769.37	0.417
16.00	2245	3.118	735.52	729.32	0.359
16.25	2046	3.167	676.13	669.83	0.263
16.50	1904	3.215	634.95	628.55	0.199
16.75	1655	3.264	552.95	546.45	0.055
17.00	1539	3.312	517.48	510.88	-0.002
17.25	1455	3.360	492.73	486.03	-0.039
17.50	1336	3.409	453.55	446.75	-0.106
17.75	1323	3.457	454.24	447.34	-0.094
18.00	1226	3.505	421.55	414.55	-0.150
18.25	1163	3.553	401.33	394.24	-0.182
18.50	1099	3.602	379.94	372.75	-0.218

Table V-G

(Continued)

TEMPERATURE 0.0 °C.
NORMAL FACTOR A = 722.47 SEC/CTS
BACKGROUND E_B = 0.048-0.058 CTS/SEC
COUNTING FOR 1500.0 SECONDS

2θ(°)	COUNTS	S(1/Å)	AE_{XC}	I_{coh}/NI_o	i(S)
16.00	10594	3.118	732.02	725.82	0.353
16.50	9027	3.215	643.71	637.31	0.216
17.00	7097	3.312	521.29	514.69	0.006
17.50	6081	3.409	459.91	453.11	-0.093
18.00	5258	3.505	409.07	402.07	-0.176
18.50	4695	3.602	375.54	368.35	-0.227
19.00	4379	3.698	360.06	352.68	-0.242
19.50	4081	3.795	344.68	337.11	-0.257
20.00	3881	3.891	336.59	328.83	-0.258
20.50	3814	3.987	339.68	331.72	-0.233
21.00	3736	4.083	341.47	333.32	-0.210
21.50	3797	4.179	356.25	347.90	-0.154
22.00	3929	4.275	378.35	369.82	-0.078
22.50	3919	4.371	386.87	378.15	-0.034
23.00	4161	4.467	421.42	412.51	0.081
23.50	4129	4.563	428.27	419.17	0.126
24.00	4113	4.659	436.75	427.47	0.177
24.50	4003	4.754	434.80	425.34	0.201
25.00	3862	4.850	428.84	419.19	0.214
25.50	3818	4.945	433.46	423.64	0.259
26.00	3461	5.040	400.80	390.79	0.191
26.50	3307	5.136	390.93	380.76	0.190
27.00	2984	5.231	359.38	349.03	0.119
27.50	2857	5.326	350.97	340.45	0.120
28.00	2671	5.421	334.30	323.61	0.092
28.50	2604	5.515	332.39	321.53	0.113
29.00	2451	5.610	318.58	307.55	0.092
29.50	2267	5.705	299.71	288.52	0.051
30.00	2064	5.799	277.21	265.86	-0.006

Table V-G

(Continued)

TEMPERATURE 0.0 °C.
NORMAL FACTOR A = 179.33 SEC/CTS
BACKGROUND E_B = 0.058-0.052 CTS/SEC
COUNTING 4000 COUNTS

2θ(°)	SECONDS	S(1/Å)	AE_{XC}	I_{coh}/NI_o	i(S)
26.00	418.8	5.040	419.32	409.32	0.248
27.00	488.3	5.231	375.26	364.91	0.170
28.00	571.0	5.421	334.39	323.70	0.092
29.00	658.1	5.610	301.96	290.94	0.033
30.00	754.8	5.799	273.69	262.34	-0.020
31.00	847.8	5.988	253.07	241.41	-0.051
32.00	911.0	6.176	244.50	232.53	-0.038
33.00	954.9	6.364	242.02	229.75	-0.000
34.00	997.5	6.551	240.20	227.65	0.041
35.00	1076.3	6.738	230.50	217.68	0.046
36.00	1100.9	6.924	233.36	220.27	0.112
37.00	1180.5	7.110	225.04	211.69	0.121
38.00	1332.8	7.295	205.77	192.18	0.068
39.00	1435.6	7.480	197.24	183.42	0.068
40.00	1570.5	7.664	185.97	171.92	0.049
41.00	1758.8	7.847	171.07	156.79	0.002
42.00	1886.8	8.030	164.32	149.84	0.001
43.00	2038.4	8.212	156.60	141.93	-0.009
44.00	2119.6	8.394	155.14	140.27	0.023
45.00	2336.9	8.575	144.62	129.57	-0.015
46.00	2407.5	8.755	144.50	129.27	0.025
47.00	2565.8	8.935	139.33	123.94	0.023

Table V-G

(Continued)

TEMPERATURE 0.0 °C.
NORMAL FACTOR A = 58.22 SEC/CTS
BACKGROUND E_B = 0.052-0.044 CTS/SEC
COUNTING 10000 COUNTS

2θ(°)	SECONDS	S(1/Å)	AE_{XC}	I_{coh}/NI_o	i(S)
40.00	1291.0	7.664	186.33	172.28	0.051
42.00	1533.5	8.030	167.01	152.53	0.019
44.00	1805.0	8.394	150.73	135.86	-0.010
46.00	2036.5	8.755	141.69	126.46	0.002
48.00	2261.5	9.114	135.08	119.53	0.026
50.00	2530.7	9.469	127.54	111.69	0.034
52.00	2902.8	9.822	117.22	101.10	0.005
54.00	3266.5	10.172	109.63	93.28	-0.009
56.00	3623.3	10.519	103.85	87.27	-0.012
58.00	3958.0	10.863	99.72	82.95	-0.004
60.00	4321.7	11.203	95.60	78.66	-0.002
62.00	4671.9	11.540	92.40	75.32	0.006
64.00	5059.0	11.874	88.96	71.75	0.007

Table V-G

(Continued)

TEMPERATURE 0.0 °C.
NORMAL FACTOR A = 25.13 SEC/CTS
BACKGROUND E_B = 0.048-0.048 CTS/SEC
COUNTING 100000 COUNTS

2θ(°)	SECONDS	S(1/Å)	AE_{XC}	I_{coh}/NI_o	i(S)
55.00	1467.5	10.346	108.98	92.51	0.015
58.00	1725.6	10.863	99.71	82.94	-0.005
61.00	2000.8	11.372	92.11	75.09	-0.022
64.00	2209.1	11.874	88.98	71.76	0.007
67.00	2480.9	12.367	84.06	66.68	0.002
70.00	2811.9	12.852	78.24	60.74	-0.030
73.00	3088.1	13.328	74.74	57.15	-0.036
76.00	3280.7	13.795	73.37	55.72	-0.012
79.00	3624.0	14.252	68.75	51.06	-0.052
82.00	3815.9	14.700	67.14	49.44	-0.042
85.00	4033.5	15.138	64.81	47.11	-0.050
88.00	4196.5	15.565	63.09	45.41	-0.050
91.00	4375.4	15.982	60.78	43.14	-0.066
94.00	4371.1	16.387	60.68	43.09	-0.037
97.00	4463.2	16.782	58.78	41.24	-0.048
100.00	4462.2	17.165	57.74	40.27	-0.042

Table VI-A

Approximation to i(S) for 50.0 °C.

TEMPERATURE 50.0 °C.

BOUNDARIES S_1-S_2(1/Å)	COEFFICIENTS OF i(S) IN ($S-S_1$) POWER 0	POWER 1	POWER 2	POWER 3	RMS DEV
0. - 1.50	-1.0000	0.	0.	0.	0.
1.50- 1.85	-1.0000	0.7699	-2.4635	5.0252	0.001
1.85- 2.14	-0.8169	0.9649	3.2305	3.2533	0.010
2.14- 2.29	-0.1860	3.9846	9.5319	-25.6279	0.016
2.29- 2.43	0.5396	4.9856	-16.7839	36.4768	0.031
2.43- 2.58	1.0088	1.8966	-8.2684	-18.8145	0.041
2.58- 2.73	1.0437	-1.2787	-10.9147	38.5525	0.024
2.73- 2.90	0.7364	-1.6562	11.4013	-35.0855	0.042
2.90- 3.10	0.6120	-1.2816	4.0672	-12.5936	0.028
3.10- 3.30	0.4176	-1.4910	-1.8087	4.4797	0.018
3.30- 3.50	0.0829	-1.3891	2.3914	-1.6035	0.023
3.50- 3.80	-0.1121	-0.4948	0.1152	1.1267	0.016
3.80- 4.20	-0.2197	-0.1839	1.6349	-1.1465	0.007
4.20- 4.60	-0.1051	0.5856	0.6908	-1.3847	0.006
4.60- 5.00	0.1511	0.4179	-0.2541	-0.9215	0.023
5.00- 5.40	0.2186	-0.1095	-1.3146	2.1019	0.023
5.40- 5.80	0.0990	-0.3018	0.2218	-0.0343	0.013
5.80- 6.50	0.0116	-0.1721	0.2150	0.0372	0.009
6.50- 7.20	0.0093	0.2048	0.1735	-0.2883	0.016
7.20- 7.90	0.1387	-0.0270	-0.2711	0.1840	0.016
7.90- 8.60	0.0501	-0.0864	0.1938	-0.1576	0.016
8.60- 9.40	0.0305	-0.0215	0.1739	-0.1165	0.015
9.40-10.50	0.0649	0.0213	-0.1678	0.0831	0.006
10.50-11.30	-0.0041	-0.0186	0.0744	-0.1037	0.004

Table VI-B

Approximation to i(S) for 40.0 °C.

TEMPERATURE 40.0 °C.

BOUNDARIES S_1-S_2 (1/Å)	COEFFICIENTS OF i(S) IN $(S-S_1)$ POWER 0	POWER 1	POWER 2	POWER 3	RMS DEV
0. - 1.50	-1.0000	0.	0.	0.	0.
1.50- 1.85	-1.0000	0.2949	-1.0742	3.1726	0.004
1.85- 2.14	-0.8924	0.6874	3.2521	5.7796	0.005
2.14- 2.29	-0.2786	4.0135	6.1493	-20.4183	0.010
2.29- 2.43	0.3929	4.6258	-6.0828	-11.8736	0.012
2.43- 2.58	0.8887	2.2581	-26.9568	54.6439	0.018
2.58- 2.73	0.8053	-1.5976	1.1309	7.2351	0.021
2.73- 2.90	0.6156	-1.1052	7.3637	-25.5173	0.029
2.90- 3.10	0.5151	-0.9073	0.5069	-6.2114	0.030
3.10- 3.30	0.3043	-1.3393	-3.4360	13.3003	0.017
3.30- 3.50	0.0054	-1.3112	3.8662	-6.0632	0.011
3.50- 3.80	-0.1507	-0.4945	-0.0446	1.6364	0.014
3.80- 4.20	-0.2589	-0.0131	0.8949	-0.3142	0.014
4.20- 4.60	-0.1411	0.5586	0.4015	-0.7854	0.008
4.60- 5.00	0.0963	0.5045	-1.0437	0.6431	0.006
5.00- 5.40	0.1723	-0.0469	-0.7504	0.4770	0.014
5.40- 5.80	0.0640	-0.3323	-0.1250	0.7158	0.021
5.80- 6.50	-0.0431	-0.1617	0.3595	-0.0886	0.022
6.50- 7.20	-0.0106	0.1949	-0.0132	-0.1109	0.018
7.20- 7.90	0.0813	0.0049	-0.2816	0.1903	0.022
7.90- 8.60	0.0120	-0.0598	0.0135	0.0435	0.017
8.60- 9.40	-0.0083	0.0044	0.2271	-0.1755	0.010
9.40-10.50	0.0507	-0.0199	-0.1362	0.0859	0.015
10.50-11.30	-0.0216	0.0168	0.0280	-0.0355	0.016

Table VI-C

Approximation to i(S) for 30.0 °C.

TEMPERATURE 30.0 °C.

BOUNDARIES S_1-S_2 (1/Å)	COEFFICIENTS OF i(S) IN ($S-S_1$) POWER 0	POWER 1	POWER 2	POWER 3	RMS DEV
0. - 1.50	-1.0000	0.	0.	0.	0.
1.50- 1.85	-1.0000	0.2470	-0.8322	2.6691	0.005
1.85- 2.14	-0.9010	0.4664	2.3271	10.8075	0.026
2.14- 2.29	-0.3065	4.5793	4.4045	-25.9277	0.021
2.29- 2.43	0.3920	4.4586	-4.5091	-19.3945	0.015
2.43- 2.58	0.8746	2.1049	-14.3483	1.4174	0.012
2.58- 2.73	0.8723	-2.0398	6.8686	-17.0823	0.028
2.73- 2.90	0.6632	-1.0724	-0.1796	2.5647	0.024
2.90- 3.10	0.4883	-1.0656	3.1940	-11.4095	0.019
3.10- 3.30	0.3117	-1.2821	-4.0066	13.0345	0.011
3.30- 3.50	-0.0007	-1.2659	3.8180	-7.1652	0.009
3.50- 3.80	-0.1585	-0.7103	1.4837	-0.6493	0.022
3.80- 4.20	-0.2556	-0.0112	0.9168	-0.3627	0.013
4.20- 4.60	-0.1366	0.6192	0.4104	-0.9308	0.011
4.60- 5.00	0.1172	0.3938	-0.4353	-0.3684	0.011
5.00- 5.40	0.1815	-0.1023	-0.3859	0.1000	0.011
5.40- 5.80	0.0852	-0.3388	0.2853	-0.0666	0.015
5.80- 6.50	-0.0089	-0.1340	0.0808	0.1240	0.016
6.50- 7.20	-0.0206	0.1826	0.2497	-0.3754	0.013
7.20- 7.90	0.1008	-0.0102	-0.3466	0.2565	0.026
7.90- 8.60	0.0118	-0.0777	0.2622	-0.1977	0.023
8.60- 9.40	0.0181	0.0063	0.1852	-0.1420	0.006
9.40-10.50	0.0690	0.0148	-0.1378	0.0685	0.009
10.50-11.30	0.0097	-0.0244	0.0476	-0.0532	0.006

Table VI-D

Approximation to i(S) for 29.5 °C.

TEMPERATURE 29.5 °C.

BOUNDARIES S_1-S_2 (1/Å)	COEFFICIENTS OF i(S) IN $(S-S_1)$ POWER 0	POWER 1	POWER 2	POWER 3	RMS DEV
0. - 1.50	-1.0000	0.	0.	0.	0.
1.50- 1.85	-1.0000	0.3878	-2.3528	4.6458	0.003
1.85- 2.14	-0.9533	0.3043	2.5878	11.8478	0.026
2.14- 2.29	-0.3585	4.6135	3.6726	-17.5717	0.025
2.29- 2.43	0.3569	4.9387	-5.8929	-27.4651	0.010
2.43- 2.58	0.8574	1.4347	-23.5314	67.3629	0.012
2.58- 2.73	0.7705	-0.9248	0.4509	-4.6794	0.034
2.73- 2.90	0.6262	-0.6324	-3.3959	13.2633	0.038
2.90- 3.10	0.4857	-0.4748	-4.3589	7.2471	0.021
3.10- 3.30	0.2743	-1.1771	0.2421	-2.4683	0.010
3.30- 3.50	0.0289	-1.3537	0.4664	4.2217	0.012
3.50- 3.80	-0.1894	-0.4669	1.4248	-1.4585	0.013
3.80- 4.20	-0.2407	-0.1021	0.7484	0.1944	0.012
4.20- 4.60	-0.1493	0.6432	0.2178	-0.6344	0.013
4.60- 5.00	0.1022	0.4471	-0.6244	-0.1539	0.022
5.00- 5.40	0.1713	-0.0825	-0.2140	-0.4275	0.020
5.40- 5.80	0.0767	-0.4153	0.3701	0.0183	0.018
5.80- 6.50	-0.0290	-0.0908	0.1438	0.0660	0.016
6.50- 7.20	0.0006	0.1883	0.0784	-0.2304	0.013
7.20- 7.90	0.0918	-0.0161	-0.2195	0.1524	0.017
7.90- 8.60	0.0252	-0.1261	0.1938	-0.0309	0.008
8.60- 9.40	0.0213	0.0946	-0.1491	0.0725	0.017
9.40-10.50	0.0386	0.0602	-0.1248	0.0437	0.004
10.50-11.30	0.0121	-0.0595	0.0015	0.1217	0.003

Table VI-E

Approximation to i(S) for 20.0 °C.

TEMPERATURE 20.0 °C.

BOUNDARIES $S_1 - S_2$ (1/Å)	COEFFICIENTS OF i(S) IN $(S-S_1)$ POWER 0	POWER 1	POWER 2	POWER 3	RMS DEV
0. - 1.50	-1.0000	0.	0.	0.	0.
1.50- 1.85	-1.0000	0.4853	-2.5451	5.5675	0.001
1.85- 2.14	-0.9032	0.6724	1.9466	6.1925	0.014
2.14- 2.29	-0.3935	4.0748	13.0194	-26.9834	0.021
2.29- 2.43	0.4196	5.9687	0.1333	-59.4214	0.010
2.43- 2.58	1.0948	2.1172	-17.7439	20.7745	0.017
2.58- 2.73	1.0833	-1.4302	-8.0299	35.9839	0.021
2.73- 2.90	0.8095	-1.7164	8.7926	-26.4004	0.013
2.90- 3.10	0.6421	-0.8079	-1.9940	0.7501	0.018
3.10- 3.30	0.4068	-1.8346	-1.9402	9.7178	0.010
3.30- 3.50	0.0400	-1.4337	1.4796	2.9040	0.019
3.50- 3.80	-0.1644	-0.4725	0.6430	0.4109	0.024
3.80- 4.20	-0.2371	-0.0602	1.2938	-0.7681	0.018
4.20- 4.60	-0.1034	0.5991	0.4621	-0.8982	0.018
4.60- 5.00	0.1527	0.5536	-1.0878	0.4273	0.013
5.00- 5.40	0.2275	-0.1968	-0.5678	0.7519	0.014
5.40- 5.80	0.1060	-0.3169	-0.0344	0.4240	0.015
5.80- 6.50	0.0009	-0.1213	0.0969	0.1156	0.013
6.50- 7.20	0.0032	0.2122	0.0908	-0.2198	0.008
7.20- 7.90	0.1208	-0.0006	-0.3300	0.2474	0.004
7.90- 8.60	0.0436	-0.0975	0.1941	-0.1032	0.006
8.60- 9.40	0.0351	0.0611	-0.0183	-0.0185	0.012
9.40-10.50	0.0628	-0.0500	-0.0441	0.0346	0.010
10.50-11.30	0.0004	-0.0002	0.1424	-0.2260	0.009

Table VI-F

Approximation to i(S) for 10.0 °C.

TEMPERATURE 10.0 °C.

BOUNDARIES S_1-S_2 (1/Å)	COEFFICIENTS OF i(S) IN $(S-S_1)$ POWER 0	POWER 1	POWER 2	POWER 3	RMS DEV
0. - 1.50	-1.0000	0.	0.	0.	0.
1.50- 1.85	-1.0000	0.2959	-1.6703	3.7191	0.003
1.85- 2.14	-0.9416	0.3583	2.6698	10.6340	0.035
2.14- 2.29	-0.3538	4.3381	2.4889	1.1396	0.029
2.29- 2.43	0.3567	5.4346	0.0817	-36.7289	0.008
2.43- 2.58	1.0184	3.3504	-22.0624	19.7618	0.006
2.58- 2.73	1.0913	-1.7732	-6.7880	45.1957	0.015
2.73- 2.90	0.8251	-1.0077	6.3075	-30.8729	0.015
2.90- 3.10	0.6844	-1.2174	-0.0019	-2.0441	0.035
3.10- 3.30	0.4245	-1.6406	-0.8823	0.4497	0.022
3.30- 3.50	0.0647	-1.4620	2.8700	-3.9121	0.024
3.50- 3.80	-0.1442	-0.8041	2.2299	-1.7740	0.017
3.80- 4.20	-0.2327	-0.1159	1.5278	-1.0644	0.008
4.20- 4.60	-0.1027	0.5419	0.5664	-1.0207	0.005
4.60- 5.00	0.1394	0.4692	-0.5186	-0.0430	0.008
5.00- 5.40	0.2413	-0.0510	-0.9791	0.8301	0.014
5.40- 5.80	0.1174	-0.3049	0.0827	0.0631	0.013
5.80- 6.50	0.0127	-0.2269	0.4390	-0.1492	0.007
6.50- 7.20	0.0178	0.2006	0.1785	-0.3144	0.006
7.20- 7.90	0.1379	-0.0166	-0.2972	0.1956	0.012
7.90- 8.60	0.0477	-0.1146	0.2258	-0.1617	0.012
8.60- 9.40	0.0227	-0.0450	0.2270	-0.1461	0.005
9.40-10.50	0.0571	0.0016	-0.1217	0.0614	0.013
10.50-11.30	-0.0066	-0.0490	0.0228	0.1187	0.016

Table VI-G

Approximation to i(S) for 0.0 °C.

TEMPERATURE 0.0 °C.

BOUNDARIES S_1-S_2 (1/Å)	COEFFICIENTS OF i(S) IN $(S-S_1)$ POWER 0	POWER 1	POWER 2	POWER 3	RMS DEV
0. - 1.50	-1.0000	0.	0.	0.	0.
1.50- 1.85	-1.0000	0.1512	-0.3166	1.5913	0.002
1.85- 2.14	-0.9176	0.3861	1.4395	13.9719	0.022
2.14- 2.29	-0.3439	4.9429	9.4389	-19.1013	0.019
2.29- 2.43	0.5455	6.0552	-10.3014	-18.5622	0.028
2.43- 2.58	1.1404	1.9033	-24.3672	48.6174	0.019
2.58- 2.73	1.0417	-2.0393	-2.9935	23.5257	0.007
2.73- 2.90	0.7478	-1.3312	2.0019	-2.7979	0.012
2.90- 3.10	0.5656	-0.9222	2.4506	-12.1388	0.006
3.10- 3.30	0.3821	-1.4941	-4.6729	15.7969	0.016
3.30- 3.50	0.0228	-1.4912	5.5809	-11.2123	0.016
3.50- 3.80	-0.1420	-0.6341	0.4630	0.9668	0.014
3.80- 4.20	-0.2644	-0.0821	1.3198	-0.7979	0.007
4.20- 4.60	-0.1371	0.6814	0.6269	-1.3542	0.011
4.60- 5.00	0.1490	0.4595	-0.3740	-0.6294	0.010
5.00- 5.40	0.2327	-0.1806	-1.3971	2.5129	0.008
5.40- 5.80	0.0978	-0.1958	0.1395	-0.4330	0.017
5.80- 6.50	0.0141	-0.2612	0.3042	-0.1897	0.019
6.50- 7.20	0.0133	0.1996	0.0608	-0.2234	0.017
7.20- 7.90	0.1062	-0.0976	-0.1676	0.1540	0.013
7.90- 8.60	0.0085	-0.1023	0.1811	-0.0676	0.010
8.60- 9.40	0.0021	0.0260	0.0973	-0.0957	0.007
9.40-10.50	0.0361	-0.0138	-0.0743	0.0450	0.011
10.50-11.30	-0.0091	-0.0150	0.0241	0.0186	0.010

Proposition on the virial-theorem equation of state

The magnitude of fluctuations in the equation of state for an ideal gas may be estimated from the virial theorem.

The virial theorem provides a brief and direct derivation of a general equation of state for a substance composed of molecules having only translational degrees of freedom. This derivation predicts that the average conditions of the system over some period of time may be expressed in the form:

$$PV + \emptyset = NkT + \frac{m}{\Delta t} \Delta\left(\sum_{1}^{N} \bar{r}_i \cdot \bar{v}_i\right)$$

where P, V, and T are the equilibrium pressure, total volume, and temperature of the system; $\emptyset$ is a function of the intermolecular potential; N is the total number of molecules; k is Boltzmann's constant; m is the mass of a molecule; $\bar{r}_i$ and $\bar{v}_i$ are the position and velocity vectors of a molecule at any time; Δ indicates an increment over the period of time Δt. PV and $\emptyset$ respectively represent the interactions of the molecules with the containing walls and with each other averaged over the time interval. NkT is proportional to the total kinetic energy which remains constant. The above relation constitutes a time-independent equation of state because the last term must be negli-

gible for a sufficiently long period of time Δt. This conclusion follows from the fact that the quantities $(\bar{r}_i \cdot \bar{v}_i)$ are bounded for a finite system and hence their ratio to Δt must decrease as the latter increases. However, neither the $(\bar{r}_i \cdot \bar{v}_i)$ nor their sum can be expected to remain precisely constant over a period of time but rather to oscillate about the value zero. Correspondingly, the system departs temporarily from its equilibrium equation of state and a question arises as to the possible magnitude of these deviations.

It may be deduced that for the large number of molecules of small mass associated with actual substances these fluctuations must be generally insignificant. Their probable magnitude is largely controlled by the frequency of interactions between the molecules and the confining walls and by the duration of these interactions. In comparison with the pressure and temperature terms in the equation of state these deviations would be most important for very low concentrations of molecules, corresponding to ideal gas behavior, and for interactions with the wall which consist of instantaneous contact collisions. For this case, using the average molecular velocity given by the Maxwell distribution, the average value of the deviation term is calculated to be

$$\frac{m}{\Delta t}\,\Delta\Big(\sum_{1}^{N} r_i \cdot v_i\Big) = \frac{m}{\Delta t}\,\frac{3V}{A}\,(\pi kT/2m)^{1/2}$$

where A is the area of the walls. This result shows that the term is entirely negligible with respect to the other energy terms in the ideal gas equation for all but exaggeratedly low molecular concentrations.

Proposition on the measurement of reaction rates

Rates of reaction may be determined by subjecting reactions at equilibrium to a measurable heat input of limited duration.

A method for investigating reaction rates can consist of disturbing the equilibrium of a reaction by adding heat to the system in a known manner to give a temporary rise in the temperature of the system. The reaction will proceed to some extent in the endothermic direction before eventually returning to equilibrium. The temperature variation occurring in the system will be determined in part by the heat of reaction and the relative effects of changes in temperature and composition on the forward and reverse reaction mechanisms. With data or assumptions about these pertinent effects the forward rate of reaction can be obtained by analysis of the temperature history of the system according to a suitable differential energy balance relation. The applicability of the method would depend on experimental design factors such as the means utilized to provide the heat impulse.

The theoretical analysis required for the proposed method, involving changes in both temperature and composition, is more complex than for the usual investigation of reactions by mixing reactants under isothermal conditions. However, the heat-impulse

method provides a different experimental approach which may have some useful variations. For instance, the same system contents could be used to establish a series of initial equilibrium conditions of varying temperature and composition. Further, the response of the system could be observed for the same initial equilibrium conditions but with variations in the time form and/or magnitude of the heat input. This procedure may provide a check on the reliability of the determination or permit extrapolation of the behavior into a range where simplified theoretical analysis is possible.

Assuming a small disturbance from equilibrium, simple rate expressions for the forward and reverse reactions, and Arrhenius-type functions of temperature for the reaction rate constants, the initial transient behavior of the temperature is described by:

$$mC \frac{dt}{d\theta} + \frac{r_0(\Delta E_a)(\Delta Q)}{RT_0^2} t = \dot{q}$$

where t is the temperature rise in the reaction phase, θ is the time, m and C are respectively the weight and heat capacity of the reaction phase, r_0 is the forward rate of reaction at initial equilibrium conditions, ΔE_a is the difference between the activation energies for the forward and reverse reaction rate constants, ΔQ is the heat absorbed by the reaction, R is

the universal gas constant, T_0 is the initial equilibrium temperature, and $\dot{q}$ is the net rate of heat input to the reaction phase. This equation indicates a temperature maximum which is inversely proportional to the forward reaction rate at equilibrium. Such features may reduce the necessity for accurate time determination during the temperature transient.

Proposition on laminar flow in porous media

The Kozeny equation for laminar flow in porous media can be extended to the general case of anisotropic permeability. This development prescribes that the "constant" factor in the equation must depend in general on the direction of flow, and indicates the probable magnitude of this factor for the special case of isotropic media.

The permeability of porous media for laminar flow is often correlated to the porosity by means of the Kozeny equation. Such correlations are largely limited to unconsolidated beds of about 25 to 50% porosity which consist of well sorted and uniformly shaped non-hollow particles. The Kozeny equation may be given as:

$$K = \frac{1}{C} \frac{\phi^3}{(1-\phi)^2 S^2}$$

where K is the permeability, ϕ is the porosity, S is the ratio of surface area to volume for the solids in the porous material, and C is a dimensionless factor. Values of C determined experimentally vary appreciably in the approximate range of 4 to 6. This equation is derived by assuming that laminar flow in porous media is equivalent to flow in an assembly of capillary channels.

The value of C may be said to result from two contributions. Firstly, C depends on the characteristic shape of the channel cross sections. The average velocity in a channel is expressed as:

$$U = k \frac{r_h^2}{u} (dp/dx)$$

where r_h is the hydraulic radius of the channel, u is the fluid viscosity, (dp/dx) is the pressure gradient along the channel, and k is a dimensionless factor. The value of the factor k depends rigorously on the shape of flow cross section offered by the channel. Secondly, C depends on what has been termed the tortuosity of the porous media. The equivalent flow channels are not straight but winding or indirect thus diminishing the effective pressure gradient and net velocity of flow.

In attempting to relate porosity and permeability by means of the Kozeny equation it is implicitly assumed that there is some natural average for the factor C, that is, an average effect of tortuosity and shape of flow section for all porous media. However, neither the derivation of the equation nor the usual experimental determination of the factor C take into account the possible significance of anisotropy in the porous media. This omission seems fundamentally wrong because the tortuosity of the flow channel is related to the fact that a porous medium has permeability in all directions. It is proposed that the

model of equivalent flow channels may be extended to the anisotropic case with the assumption that the relative number of channels and their shape, or value of k, vary with orientation. Consequently, the value of C depends in general on the direction of flow since C results as an average effect from the distribution of channels and corresponding coefficients k considered in relation to a particular direction of flow.

The approach proposed here yields the value $C = 3/k$ for the limiting case of isotropic media for which the distribution of channels is presumably uniform with orientation. For the isotropic case the average channel cross section probably corresponds to some regular shape. Hence, the likely values of C are between 5 for an equilateral triangular cross section ($k=0.6$) and 6 for a circular section ($k=0.5$). The generally accepted value of $C = 5$ may correspond to some natural average since the equilateral triangle is the simplest possible regular area. This viewpoint differs from that of Carman(1) who explained $C = 5$ with a tortuosity factor of 2 and $k = 0.4$ corresponding to a rectangular flow section. Pursuing the present interpretation, experimental values of C very different from 5 would indicate anisotropy to some extent. Thus, in the determination by Ergun(2) giving $36C = 150$ the experimental porous beds were probably anisotropic. These beds were deposited under flow conditions which may have enhanced permeability in

the flow direction.

Variations in the value of C with grain shape and porosity such as reported by Coulson(3) are also partly attributable to anisotropy. With particles of reduced symmetry and/or marked angularity, like cylinders, plates, and cubes, anisotropy can result from preferential orientation of the particles thus giving an improved or impaired permeability for the chosen direction of flow. Further, the extent of this anisotropy will probably be affected by the relative density of packing and hence will vary with the porosity. Thus, it may be expected that the flow characteristics for any one direction will fail to correlate according to the ordinary form of the Kozeny equation.

The natural or most likely value of C, if such exists, cannot be determined by measurements of permeability limited to a single direction of flow unless experimental conditions guarantee an isotropic bed in every case. Otherwise, a proper test of the Kozeny equation must include measurements in more than one direction without disturbing the porous medium. A result of the general approach proposed above is that the arithmetic average value of 1/C for any three mutually perpendicular directions is a unique scalar property of the porous medium. Experimental tests of the Kozeny equation should be based on such a spatial average, thus eliminating apparent deviations which are due to anisotropic permeability.

References:

1. P. C. Carman, Trans. Inst. Chem. Eng. 15, 150 (1937).

2. S. Ergun, Chem. Eng. Prog. 48, 89 (1952).

3. J. M. Coulson, Trans. Inst. Chem. Eng. 27, 237 (1949).

Proposition on incoherent X-ray scattering

An approximation to incoherent X-ray scattering is improved by allowing in a simple way for the different angular dependence of individual electronic scattering factors.

The incoherent or modified part of the X-ray intensity scattered by an atom, neglecting exchange terms, is given by

$$I_{inc} = Z - \sum_{1}^{Z} f_K^2 \qquad (1)$$

where Z is the atomic number and f_k is the scattering factor corresponding to individual electronic wave functions. Both f_k and I_{inc} will be functions of $\frac{\sin \theta}{\lambda}$ where 2θ is the angle of scatter and λ the radiation wavelength. f_k is unity at zero angle of scatter and decays to oscillations about zero for increasing $\frac{\sin \theta}{\lambda}$.

James (1,p.462) has suggested that, lacking other information, the individual electronic factors may be replaced by

$$f_k = \frac{f}{Z} \qquad (2)$$

where

$$f = \sum_{1}^{Z} f_k \qquad (3)$$

is the total or atomic scattering factor. Thus, it is

assumed that the electronic factors are all equal to the average, and the incoherent scatter becomes

$$I_{inc} = Z - \frac{f^2}{Z} \qquad (4)$$

a form which is used in practice(2).

It is proposed that this sort of approximation should try to take into account the general angular dependence of the factors f_k. Equations (2) and (4) imply that all f_k contribute equally to f for all angles of scatter. However, electronic scattering factors are markedly affected by the spread of the electronic charge distribution (1,pp.125-129). The more concentrated the charge distribution, the more slowly will f_k decrease as $\frac{\sin \theta}{\lambda}$ increases. Furthermore, once an f_k has fallen to zero, it never regains appreciable positive or negative values. Hence, the decline of the total factor f does not result from equal electronic contributions. Rather, the f_k of outer electrons decay early to zero while the contribution from inner electrons falls off very slowly.

It is proposed that a better approximation would assign the entire decrease in atomic factor f to the outer electrons. The f_k for outer electrons is assumed to be zero as required by the f decline while the f_k of inner electrons remains at unity. This assignment implies that electronic scattering factors

behave as step functions, being unity up to some value of $\frac{\sin \theta}{\lambda}$ and then dropping abruptly to zero. The actual behavior is not so abrupt but this picture leads to an approximation which does reflect the characteristics of the f_k. For this purpose, the concept of discrete electronic orbitals in the summations of equations (1) and (3) is discarded. It is merely required that (3) be satisfied by f_k that are either 0 or 1. There follows that only a number f of electrons (generally a non-integral value) have the f_k of unity. Hence, equation (1) gives

$$I_{inc} = Z - f \tag{5}$$

This approximation is even simpler numerically than equation (4).

This proposed alternative approximation can be given additional logical support. It is apparent that approximations (4) and (5) are extrema of a more general case. Equations (4) and (5) give respectively the maximum and minimum incoherent scatter under the condition that the atomic scattering factor of (3) be satisfied by electronic factors which are zero for some electrons and uniform at one or less for the rest. The original equation (1) already gives too large an estimate for I_{inc} due to neglect of exchange terms (1,p.116). Therefore, considering (4) and (5) as extreme forms of the same approach, equation (5) has the correct trend.

The approximation proposed in equation (5) may be expected to work best for the larger atomic number Z which imply greater differences among the electronic f_k and more important exchange terms. As examples are taken oxygen of relatively small Z = 8 and germanium with Z = 32. Tabulated below for some values of $\frac{\sin\theta}{\lambda}$ are values of f and I_{inc} including exchange, plus the approximate I_{inc} values given by equations (4) and the proposed equation (5).

Z = 8

$\frac{\sin\theta}{\lambda}$	f ref. 3	I_{inc} ref. 4	I_{inc} eq. 4	I_{inc} eq. 5
0	8	0	0	0
0.2	5.630	2.797	4.038	2.370
0.4	3.008	5.271	6.869	4.992
0.7	1.714	6.417	7.633	6.286
1.1	1.294	7.036	7.791	6.706

Z = 32

$\frac{\sin\theta}{\lambda}$	f ref. 5	I_{inc} ref. 4	I_{inc} eq. 4	I_{inc} eq. 5
0	32	0	0	0
0.2	25.09	4.75	13.33	6.91
0.4	18.53	10.02	21.28	13.47
0.7	11.34	16.59	27.98	20.66
1.1	7.24	21.90	30.36	24.76

The proposed equation (5) approximation appears superior in both cases. For the light oxygen atom the minimizing effect of equation (5) is too large and the estimated I_{inc} falls below the accurate value. By Z = 32 for germanium the effect is already reversed, with the actual I_{inc} being less than that given by either approximation. Thus, the new approximation is particularly better for heavier elements where it is most often required.

An improved approximation to incoherent scatter, when only the atomic scattering factor is known, has been proposed.

References:

1. R. W. James, The Optical Principles of the Diffraction of X-Rays, G. Bell and Sons, London (1958).
2. K. Furukawa, B. R. Orton, J. Hamor, G. I. Williams, Phil. Mag. 8, 141 (1963).
3. A. J. Freeman, Acta Cryst. 12, 261 (1959).
4. A. J. Freeman, Acta Cryst. 12, 929 (1959).
5. J. Berghuis, I. J. M. Haanappel, M. Potters, B. O. Loopstra, C. H. MacGillavry, A. L. Veenendaal, Acta Cryst. 8, 478 (1955).

Proposition on the interpretation of diffraction data.

Truncation errors in the determination of liquid structure by X-ray diffraction can be eliminated in the mathematical sense. The analysis is based on a structural model which recognizes the limited resolution of the determination.

X-ray intensity scattered by a liquid may be related to the structure of the liquid by

$$Si(S) = \int_0^\infty 4\pi R^2 [\rho(R) - \rho_o] \frac{\sin(SR)}{SR} dR \qquad (1)$$

where $S = \frac{4\pi \sin\theta}{\lambda}$, 2θ is the angle of scatter and λ the radiation wavelength. i(S) is a function of the coherent scattered intensity and independent scattering properties of the atoms. R is radial distance from any reference atom. $\rho(R)$ is the density of neighboring atoms at distance R. ρ_o is the average atom density of the liquid. Equation (1) transforms by the Fourier integral theorem to give the distribution of neighbors

$$4\pi R^2 [\rho(R) - \rho_o] = \frac{2}{\pi} \int_0^{S_m} Si(S)\sin(RS)\, d(RS) . \qquad (2)$$

The limit is S_m rather than infinity because the function i(S) is only evaluated to some finite S_m in practice. Thus, the

function i(S) is truncated to zero value for all S greater than S_m and a corresponding "truncation error" occurs in the inversion, i.e. equation (2) is wrong.

It is proposed that the truncation error in equation (2) is not a purely mathematical or numerical shortcoming but represents an experimental limitation which can be recognized beforehand in the analysis. The absence of high-S information for i(S) means that high-frequency components are missing in the spectrum of the atom distribution. Specifically, there is an unknown contribution from sine terms of period smaller than $2\pi/S_m$. Consequently, with S_m finite, it is impossible to resolve the atom distribution in infinitesimal detail. Instead, the distribution can only be resolved coarsely to reveal density variations occurring over radial increments of π/S_m and larger. Therefore, the truncation at S_m represents a basic physical limitation of this experimental tool for structural investigation. From this point of view the incorrectness of equation (2) arises from an over-zealous insistence in evaluating the density $\rho(R)$ at each and every value of R, as imagined in equation (1).

It is proposed that this lack of resolution can be deliberately taken into account in the diffraction analysis. For this purpose, the environment of an atom is considered as a sequence of spherical shells of finite thickness for each of

which the total number of atoms contained but not their exact distribution is known or determinable. This model of structure is less ambitious than the concept of a continuous atom distribution implied by equations (1) and (2) but it is more general since the continuous case is included as a limit for shells of infinitesimal thickness.

The space about an origin or reference atom is subdivided by spheres of radii R_k ($k = 0,1,2,\ldots$) where $R_o = 0$ but the intervals are otherwise arbitrary. The scattering function $i(S)$ will then be given by

$$i(S) = \sum_{k=1}^{\infty} \frac{4\pi}{S^3} \left(\overline{\rho}_k - \overline{\rho}_{k+1} \right) f(R_k S) \tag{3}$$

where $$f(R_k S) = \sin(R_k S) - R_k S \cos(R_k S) \tag{4}$$

and $\overline{\rho}_k$ is the average density of atoms in the kth shell between R_{k-1} and R_k. This relation is obtained by integration of (1) for the individual shells assuming that the continuous density within each shell can be replaced by a uniform average density for the shell. This assumption is probabilistic rather than physical. There is no implication that the atoms within the shell are uniformly distributed in reality. However, it is stipulated that the exact distribution within the shell is not known or determinable and, for lack of further information, it

is assumed that the atoms could be anywhere within the shell with equal probability. This procedure is somewhat analogous to the integration with respect to direction which leads to equation (1). That integration needs to assume that atoms are found in any direction with equal probability because the investigation cannot provide information on the angular dependence of the density distribution.

The function i(S) is presumably known in the range 0 to S_m from experiment. Equation (3) may be inverted for the shell density increments by using the orthogonal properties of the function $f(R_k S)/S$. With the characteristic values

$$R_k = \frac{k\pi}{S_m} \tag{5}$$

the functions $f(R_k S)/S$ are orthogonal in 0 to S_m:

$$\int_0^{S_m} \frac{1}{S^2} f(R_k S) f(R_n S)\, dS = 0 \qquad (n \neq k) \tag{6}$$

$$\int_0^{S_m} \frac{1}{S^2} f^2(R_k S)\, dS = R_k^2 S_m/2 \tag{7}$$

Hence, equation (3) may be inverted in the usual manner to give

$$4\pi R^2 (\overline{\rho}_k - \overline{\rho}_{k+1}) = \frac{2}{S_m} \int_0^{S_m} Si(S) f(R_k S)\, d(R_k S) \tag{8}$$

This relation plus the fact that $\rho(R)$ goes to ρ_o at large R and hence $\overline{\rho}_k$ goes to ρ_o at large k (or preferably, $\rho(R)-\rho_o$ and $\overline{\rho}_k-\rho_o$ go to zero) leads to evaluation of all the average shell densities $\overline{\rho}_k$. The numerical approach and properties of this solution will not be discussed here.

The important fact is that the proposed inversion is analytically exact whatever the value of S_m, in contrast with equation (2). Shell thicknesses are obtained naturally as a function of the truncation limit S_m. For the solution adopted here the shells are of equal thickness, from equation (5)

$$R_k - R_{k-1} = \pi/S_m \tag{9}$$

Thus, the larger the experimental limit S_m, the thinner the shells or better the resolution; the description of atomic distribution gains detail as S_m increases. It can be shown that in the limit of infinite S_m the distribution becomes exactly that given by equation (2).

This proposition points out that loss of structural resolution due to truncation of diffraction data is a general physical limitation of the experimental method. However, this limitation need not turn up as a mathematical surprise but may be allowed for in the fundamental analysis.